catalysts

MDPI

Review

Recent Advances on Fine-Tuning Engineering Strategies of CeO_2-Based Nanostructured Catalysts Exemplified by CO_2 Hydrogenation Processes

Georgios Varvoutis [1,*], Maria Lykaki [2], George E. Marnellos [1,3] and Michalis Konsolakis [2,*]

[1] Department of Mechanical Engineering, University of Western Macedonia, 50100 Kozani, Greece
[2] School of Production Engineering and Management, Technical University of Crete, 73100 Chania, Greece
[3] Chemical Process and Energy Resources Institute, Centre for Research and Technology Hellas, 57001 Thessaloniki, Greece
* Correspondence: gvarvoutis@uowm.gr (G.V.); mkonsolakis@tuc.gr (M.K.)

Abstract: Ceria-based oxides have been extensively involved in a wide range of catalytic applications due to their intriguing properties, related mostly to their superior redox features in conjunction with peculiar metal-support interaction phenomena. Most importantly, the fine-tuning of key interrelated factors, such as the size, morphology and electronic state of the catalyst's counterparts, can exert a profound influence on the intrinsic characteristics and interfacial reactivity with pronounced implications in catalysis. The present review, while also elaborating our recent efforts in the field, aims to provide key fundamental and practical aspects in relation to the rational design and functionalization strategies of ceria-based catalysts, exemplified by the CO_2 hydrogenation processes, namely, CO_2 methanation and reverse water–gas shift (rWGS) reactions. Firstly, a description of the most prominent catalytically relevant features of cerium oxide is provided, focusing on reducibility and metal-support interaction phenomena, followed by a brief overview of the current status of ceria-based catalysts for various energy and environmental applications. Then, the main implications of fine-tuning engineering via either appropriate synthesis routes or aliovalent doping on key activity descriptors are thoroughly discussed and exemplified by state-of-the-art ceria-based catalysts for CO_2 hydrogenation. It is clearly revealed that highly active and cost-efficient ceria-based catalytic materials can be obtained on the grounds of the proposed functionalization strategy, with comparable or even superior reactivity to that of noble metal catalysts for both the studied reactions. In a nutshell, it can be postulated that the dedicated fabrication of CeO_2-based systems with augmented redox capabilities and, thus, oxygen vacancies abundance can greatly enhance the activation of gas-phase CO_2 towards CO or CH_4. Besides, the morphology-engineering of CeO_2-based catalysts can notably affect the CO_2 hydrogenation performance, by means of an optimum metal-ceria interphase based on the exposed facets, whereas doping and promotion strategies can effectively shift the reaction pathway towards the selective production of either CO or CH_4. The conclusions derived from the present work can provide design and fine-tuning principles for cost-efficient, highly active and earth-abundant metal oxide systems, not only for the CO_2 hydrogenation process but for various other energy and environmental applications.

Keywords: CO_2 hydrogenation; CeO_2-based catalysts; size/shape/electronic functionalization; rational design; metal-support interactions; reverse water–gas shift; methanation reactions

Citation: Varvoutis, G.; Lykaki, M.; Marnellos, G.E.; Konsolakis, M. Recent Advances on Fine-Tuning Engineering Strategies of CeO_2-Based Nanostructured Catalysts Exemplified by CO_2 Hydrogenation Processes. *Catalysts* **2023**, *13*, 275. https://doi.org/10.3390/catal13020275

Academic Editor: Avelina García-García

Received: 21 December 2022
Revised: 22 January 2023
Accepted: 24 January 2023
Published: 26 January 2023

1. Introduction

Cerium oxide, symbolized as CeO_2 and also known as ceria, has attracted a lot of scientific attention in the last decades, having been established by now as a widely used material due to its intriguing properties pertaining to a wide array of technological applications [1,2], as seen in Figure 1. Besides its well-established role in the field of catalysis, CeO_2 exhibits, for instance, superior polishing properties compared to the conventional

anhydrous ferric oxide particles and is thus extensively used as a polishing agent for glasses (mirrors, plates, ophthalmic lenses and precision optics) [3]. Ceria is also able to prevent glass solarization and discoloration, mainly by preventing the formation of Fe^{2+} [4]. Moreover, it has been shown that the addition of CeO_2 nanoparticles into automotive fuels can significantly contribute to the mitigation of particle emissions. Notably, CeO_2 nanoparticles have been recently shown to be promising materials in the fields of sensor technology [5] as well as biomedicine and pharmaceutics via their beneficial effect on biological systems on the protection against oxidative stress and other unfavorable factors, as antioxidants in biological systems, in regenerative medicine as spinal healing agents and UV light sorbents [6]. Moreover, ceria is widely used in electrochemical applications as electrolyte material in solid-oxide fuel cells (SOFCs) due to its high ionic conductivity [7,8].

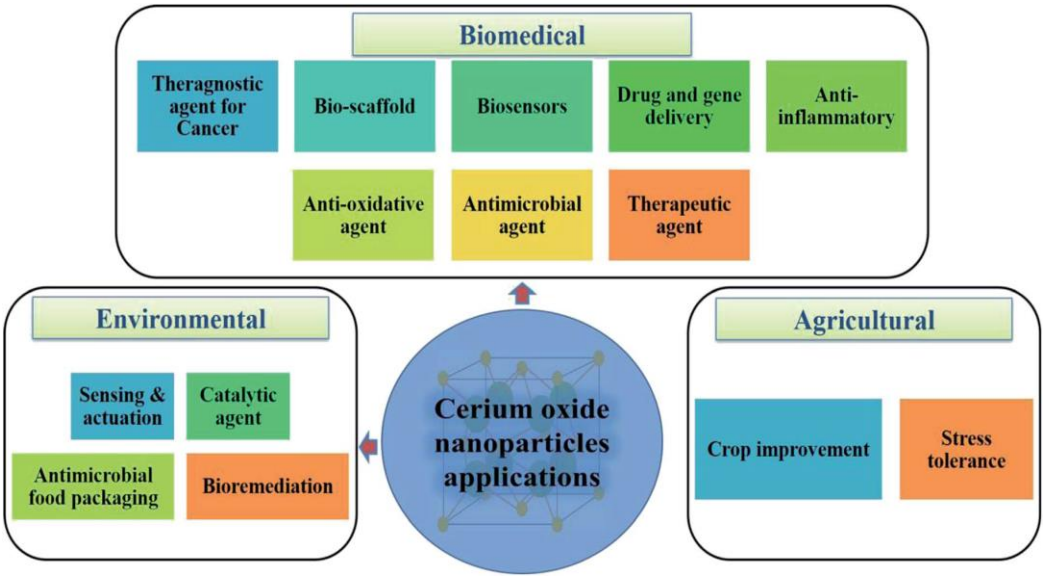

Figure 1. The uses of ceria in various fields. Reproduced with permission from Ref. [9]. Copyright© 2020, Royal Society of Chemistry.

Naturally occurring cerium is a mixture of four isotopes, with cerium-140 and secondarily cerium-142 being by far the most common, as seen by the relative abundance of each of the following isotopes: ^{140}Ce (88.5%), ^{142}Ce (11.0%), ^{138}Ce (0.3%), ^{136}Ce (0.2%) [10]. Cerium is found in various minerals (i.e., in carbonates, silicates, phosphates and oxides), the most common being monazite, bastnaesite, cerite and allanite (also known as orthite). Monazite, which is a cerium phosphate containing thorium and other light rare earth metals, is the principal source of cerium. Its most important deposits are located in the United States, Australia, Brazil, India and South Africa. Bastnaesite, a rare earth fluorocarbonate, is the second most used source and its major reserves are situated in Southern California. Cerite, which is a calcium-iron-rare earth silicate, is widely found in the United States, Sweden, Germany, Greenland, Madagascar, Russia and Scandinavia [11,12]. The commercial production of cerium is realized by electrolysis of fused chlorides or molten cerium oxide or by reduction of the fused fluoride with Ca. Cerium oxide is produced by heating bastnaesite and subsequently treating it with HCl [13].

As for its physicochemical properties, elemental cerium is the most abundant of the rare earth metals (its mass fraction is approximately 0.0046% of the Earth's crust) and belongs to the lanthanide series in the periodic table (atomic number 58), being the most reactive element among them. It has an atomic mass of 140.12, and its atomic radius is 1.81 Å (Figure 2). Based on known reserves, it is almost as abundant as zinc and more abundant than tin or lead [2]. Cerium, as a typical 4f metal, is characterized by a variable electronic configuration in which the energy of the inner 4f orbital is nearly the same as that of the 6s orbital, allowing variable occupancy of both. The stable oxidation states of

cerium are Ce^{3+} and Ce^{4+}, presenting in the two respective oxides named cerium dioxide or ceria (CeO_2) and cerium sesquioxide (Ce_2O_3). The 4+ oxidation state of cerium is considered more stable due to the fact that its electronic structure is identical to a noble-gas configuration (i.e., [Xe] $4f^0$) compared to the electronic configuration [Xe] $4f^1$ for Ce^{3+} [14].

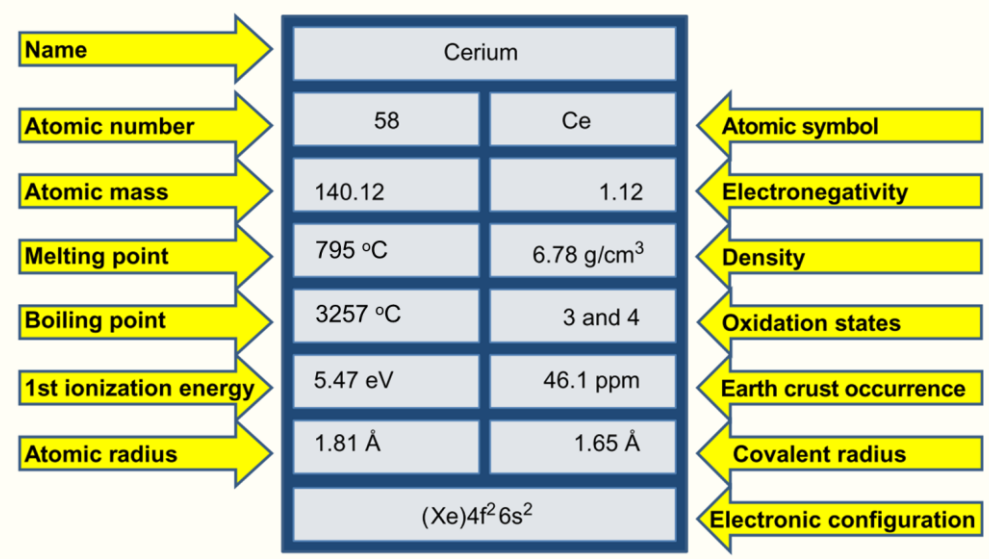

Figure 2. The main properties of elemental Ce. Reproduced with permission from Ref. [2]. Copyright© 2020, Elsevier.

In this regard, a recent soar in the market and, in turn, the recently developed technology of ceria nanoparticle production have boosted their production (Figure 3). For instance, it is forecasted that the global CeO_2 market will almost triple, from 218.8 million USD in 2017 to 630.2 million USD in 2022, due to both increasing demand and government investments in many industrial applications [2]. At the same time, the general trend regarding the price of CeO_2 in the global market is a steadily decreasing one, projected to reach a value of ca. USD 3300 per metric ton in the year 2025 and is notably different from the one for most of the other rare earth elements, being cheaper than e.g., lanthanum oxide. With the eventual scope of an environmentally friendly process, the aim is to prepare fewer toxic materials in a sustainable and cost-effective manner. So far, ceria-based materials have shown adequate performance with regard to their sustainability, regeneration (mostly via thermal reduction) and, finally, reusability [15]. Additionally, from a geopolitical perspective, cerium and, in turn, cerium-based materials can be considered as markedly exploitable, with a high potential in the short-to-medium term and thus deserving even more research attention, from lab- to industrial-scale works.

Despite the use of ceria in a wide range of technological fields, the most common application of ceria remains its use as a component in heterogeneous catalytic systems. Indeed, CeO_2 is more or less a platform component in a variety of state-of-the-art catalytic composites for various environmentally relevant reactions involving, among others, CO_2 hydrogenation to value-added products [16–21]. At the same time, intensified research attention is constantly attracted toward the further optimization of ceria-based catalysts. This is due to the intriguing characteristics and augmented tunability of the surface chemistry, structure and electronic properties of ceria, which, in turn, offer a wide margin for the design of optimal catalysts, depending on the application [14,22]. Therefore, the fine-tuning of CeO_2-based catalysts through a rational design methodology employing both theoretical and experimental studies exploring the underlying phenomena that govern their catalytic behavior can potentially lead to highly active and cost-effective materials that can be scaled up for widespread use.

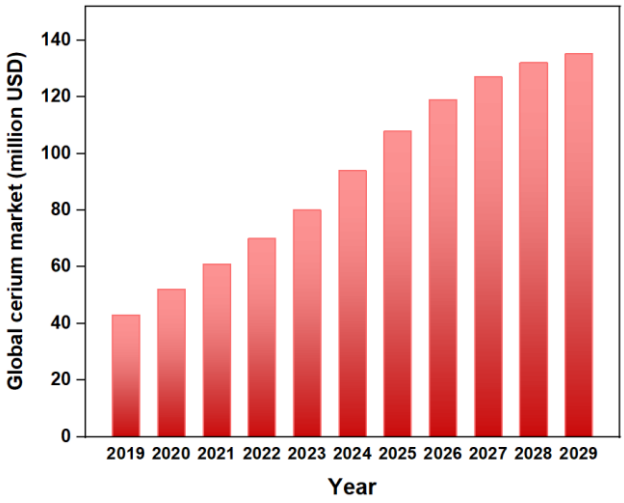

Figure 3. Current and future trends in the global cerium market.

In light of the above, the present review aims to provide key fundamental and practical aspects in relation to the rational design and surface-structure functionalization of ceria-based catalysts, also considering our recent efforts in the field. Firstly, a description of the most prominent catalytically relevant features of cerium oxide is provided, focused on reducibility and metal-support interaction phenomena, followed by a brief overview of the current status of ceria-based catalysts for various energy and environmental applications (e.g., three-way catalysis, catalytic combustion processes, water–gas shift and preferential oxidation of CO). Next, key fundamental aspects of fine-tuning engineering strategies are elaborated, with particular emphasis on the size, shape and electronic engineering of CeO_2-based oxides at the nanoscale through appropriate synthesis and modification routes. Lastly, the aforementioned discussion is exemplified by the implications of fine-tuning approaches on the key features and catalytic performance of state-of-the-art CeO_2-based materials for CO_2 hydrogenation to CO or CH_4.

2. Catalytic Features of CeO_2-Based Materials

The scientific interest regarding ceria-containing catalysts, either as active phase, support or as a promoter, has skyrocketed in the last decades, providing along the way a very good level of accumulated fundamental knowledge of their catalytic behavior and intrinsic properties, documented by the great number of seminal reviews and books published from 2010, summarized recently by Huang et al. [19]. The oxide of cerium has by now been established as an incredibly unique compound, predominantly due to its versatile chemical structure, in addition to its abundance and cost-effectiveness, even though it contains a rare earth metal. Specifically, CeO_2 can be thought of as a very good case study for the understanding of complex catalytic phenomena, as it is associated with all of the following intriguing characteristics pertaining to the field of heterogeneous catalysis [23];

- Complex electronic structure;
- Oxygen transport ability;
- Enhanced reducibility;
- Marked size- and shape-sensitivity;
- Combination of acid/base and redox chemistry;
- Facile chemistry modification via doping/promotion.

The above features can be better comprehended by considering the general scheme of reactivity pillars pioneeringly proposed by Grasselli [24] and further discussed in the context of CeO_2-based catalysts by Capdevila-Cortada et al. [23]. Indeed, as is the case in any heterogeneous catalytic system, the total (or apparent) activity of a ceria-based catalyst

is practically never solely ascribed to an individual property but is rather a synergistic combination of a plethora of descriptors. This is schematically shown in Figure 4.

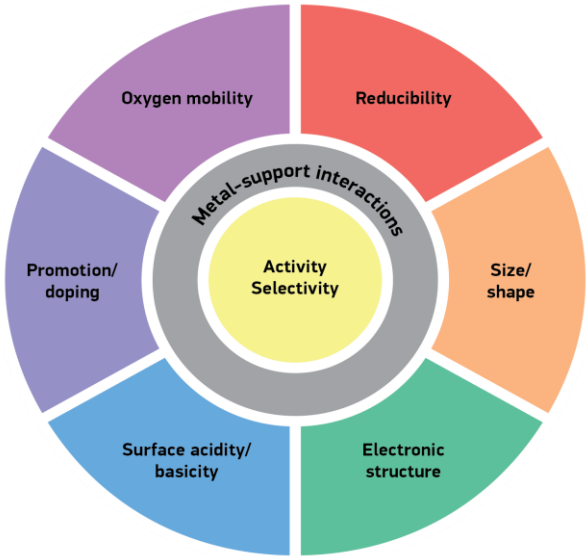

Figure 4. Interrelated and catalytically relevant performance descriptors of ceria-based materials.

Most importantly, in the case of ceria-based oxides consisting of two or more single oxides at a specific composition, completely different features—reflected in the catalytic efficiency—can be obtained, arising mainly from the synergistic interactions between the different counterparts. These synergistic interactions, thoroughly discussed in several relevant articles [25–31], can notably affect the physical-chemical characteristics of parent oxides through geometric/electronic interactions, offering, in addition, interfacial sites of unique reactivity. In view of this fact, the modulation of various parameters, involving mainly the size, shape and electronic state of parent oxides, can put forward a profound impact on the interfacial area and metal-support interactions with direct implications in catalysis (Figure 4).

Collectively, it can be reasoned that the detailed roles of CeO_2-based materials in a specific reaction are typically complicated, and they need to be meticulously studied in order to further optimize their activity on a large scale. In any case, the two most prominent categories of catalytic features of ceria-based catalysts, i.e., redox properties and metal-support interactions, are elaborated next.

2.1. Redox Properties and Oxygen Storage Capacity

Typically, ceria adopts a fluorite-type, face-centered cubic (FCC) lattice crystal structure (CaF_2, FCC, space group Fm3m) with an average lattice constant equal to 5.41134 Å. In the unit cell of the FCC structure, each cerium atom is attached to eight oxygen atoms (the coordination number, CN, of cerium atoms is equal to 8), whereas the CN value for an oxygen atom is 4 (Figure 5). The overall crystal structure can be thus regarded either as a combination of CeO_8 cubes or, equivalently, as a reconstruction of several OCe_4 tetrahedra. As for the fully reduced sesquioxide, Ce_2O_3, its stable form is hexagonal, in the space group $P3^{-}mL$. In this structure, Ce cations are coordinated into seven O anions, with four of the oxygen anions being closer than the other three [14]. Arising from its rather unique electron configuration ([Xe] $4f^1 5d^1 6s^2$) and upon exposure to reducing conditions (e.g., reaction with H_2 or CO), it is easier for cerium atoms to transition reversibly between the two states of Ce^{4+} and Ce^{3+}, while upon exposure to an oxidizing atmosphere (e.g., reaction with H_2O or CO_2), the reduced oxide takes up oxygen, restoring the fully stoichiometric phase of CeO_2 [32]. Albeit reduction typically requires high temperatures, re-oxidation is a rapid process and can also occur at ambient conditions [16].

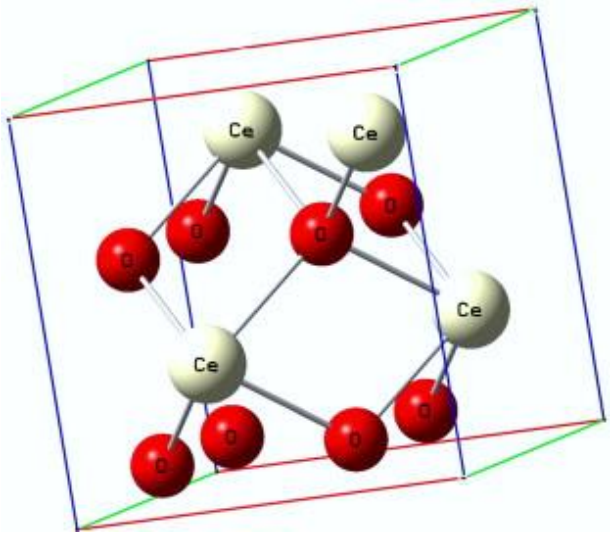

Figure 5. The FCC-CaF_2 crystallographic structure of the cerium oxide unit cell. Reproduced with permission from Ref. [33]. Copyright© 2009, Elsevier.

In essence, the interchangeability of the two Ce oxidation states refers to the creation of a non-stoichiometric cerium oxide phase, denoted as CeO_{2-x}, where x is a number between 0 and 0.5, representing the reduction degree of cerium and is a measure of the deviation from the stoichiometric CeO_2 (Equation (1)). As a result of charge balance, Ce^{3+} formation is accompanied by the creation of oxygen vacancies both on the surface and in the bulk. During this reversible process, the atoms of Ce and O maintain the CaF_2 FCC arrangement, at least for typical values of $x < 0.25$ that are observed in catalytic applications, despite the symmetry changes due to oxygen vacancies formation. Notably, since the size of a Ce^{3+} cation is larger than Ce^{4+}, the generation of an oxygen vacancy would induce lattice distortion, affecting the corresponding charge distribution on the surface or in the bulk [34]. The crystal structure of defective CeO_{2-x} is known as the most energetically favorable for the arrangement of oxygen vacancies. Moreover, the two electrons associated with a missing oxygen atom upon the formation of an oxygen vacancy fully localize on two Ce^{4+} sites, forming a tetrahedron around the vacancy site, as shown in another equation with the use of the Kröger–Vink notation (Equation (2)). In this expression, Ce_{Ce} and Ce'_{Ce} stand for either a Ce^{4+} or Ce^{3+} cation on a Ce lattice site, respectively, O_o denotes an O^{2-} anion on an O lattice site and V_o'' represents a neutral oxygen vacancy site [35].

$$2CeO_2 \leftrightarrow 2CeO_{2-x} + xO_2(g),\ 0 \leq x \leq 0.5 \quad (1)$$

$$2O_o + 4Ce_{Ce} \leftrightarrow O_2 + 2V_o'' + 4Ce'_{Ce} \quad (2)$$

The defects induced by oxygen vacancy and Ce^{3+} formation in CeO_{2-x} can improve gas-phase oxygen adsorption and activation as well as oxygen self-diffusion in its lattice, significantly contributing to a high performance in redox processes and catalytic reactions. Moreover, structural defects such as oxygen vacancies resulting from the substitution of other valence elements are intricately linked to oxygen ion diffusion, having a key role in determining the reactivity of cerium-based oxides for thermal catalysis and electrochemical purposes. In fact, the catalytic performance of CeO_2-based catalysts in numerous reactions relies to a great extent on its redox properties and oxygen storage capacity; in other words, the catalytic behavior is highly dependent on the effectiveness and degree of interchangeability between the $Ce^{3+} \leftrightarrow Ce^{4+}$ redox cycles. In turn, the ability of ceria nanoparticles to shift between the different oxidation states is largely determined by the Ce^{3+}/Ce^{4+} ratio and oxygen vacancy concentration [36].

In light of the above, it has been established from early works that partially reduced CeO_{2-x} is associated with significantly different surface properties than fully oxidized CeO_2. In particular, the associated changes in the coordination number (CN) of Ce and in its oxidation state lead to higher affinity and stability for the adsorption of reactant gaseous molecules, in essence, facilitating the selective formation of products containing more or less oxygen compared to the reactants, accordingly [14]. In other words, the transition between $Ce^{3+} \leftrightarrow Ce^{4+}$ is suggestive of the capability of ceria to switch between the release and storage of oxygen from and in its lattice. This surface property is commonly referred to in the scientific literature as oxygen storage capacity or OSC, which can be used to quantitatively or semi-quantitatively evaluate the capability of ceria-based catalysts in releasing and storing oxygen, a very helpful descriptor in redox chemical reactions. It becomes evident that OSC is augmented in elevated temperatures due to the increased mobility of oxygen moieties induced by the provision of thermal energy. The oxygen storage capacity of ceria at a given temperature can be further divided into total and dynamic OSC, the former referring to the thermodynamically allowed amount of transferable oxygen and the latter to labile oxygen moieties, i.e., surface oxygen species and oxygen vacancies [37]. In practical terms, however, dynamic OSC is a more relevant indicator of catalytic activity in redox reactions [38,39].

Generally, a material with high OSC values, such as CeO_2, is associated with the following properties: (i) the redox cycle between the oxidized and reduced forms is energetically favored or, equivalently, the vacancy formation energy is low; (ii) the vacancies (and as a consequence the O atoms) are highly mobile and can thus easily migrate between the surface and the bulk and deep inside the bulk; (iii) facile transformation between the crystal structures of the oxidized (CeO_2) and reduced (Ce_2O_3) forms or, at least, a facile alignment of the vacancies through defect lines [23]. The OSC has been instrumental to understand ceria chemistry in many oxidation reactions, be it as a standalone catalyst or support [17]. Supported metals greatly promote the OSC of ceria by directly participating through metal/metal oxide redox cycles and activating oxygen species of the support [40]. In this sense, a summary of the analytical techniques that can be used for the characterization of structural defects in CeO_{2-x} can be found in the recent review by Xu et al. [22].

2.2. Strong Metal-Support Interactions (SMSI)

Along with the key role of redox properties, the indispensable role of metal-support interactions on the catalytic performance of supported systems has been well documented. Ever since the first report on the so-called SMSI (strong metal-support interaction) effect by Tauster in 1978 [41], its implications in heterogeneous catalysis have been widely examined in various works. Essentially, the original description of the SMSI effect can be summarized by the following features [42]:

- It is practically associated with reducible supporting materials;
- It is induced by high-temperature reduction procedures, typically above 500 °C;
- The chemical properties of the dispersed metal nanoparticles are heavily disturbed by strong inhibition of its chemisorption properties and/or significant changes in catalytic behavior;
- It is reversible, which means that upon re-oxidation at a temperature higher than ca. 500 °C, followed by mild reduction, the conventional behavior of the supported metal phase may revert to its starting behavior in terms of catalytic activity.

In the general category of a catalytic composite consisting of a metal active phase supported on a metallic oxide, the interactions between the two phases have a pivotal role and exert a strong impact on the performance of heterogeneous catalysts in any reaction. Specific sites at the metal-support interface can provide remarkably high reactivity, and the optimization of the metal-support interfacial phenomena is crucial in the development of selective and active catalytic materials. For typically reducible oxide supports such as TiO_2, CeO_2 or Nb_2O_5, these interactions can have different origins. For example, encapsulation of

the dispersed metal nanoparticles by a layer of the supporting oxide via several processes such as reduction, oxidation or reactant adsorption is referred to as an SMSI. Moreover, at high reduction temperatures, the chemisorption ability of metal particles is reduced or even vanished due to the support-induced decorating effects [42]. Besides, charge transfer to or from the metal nanoparticles, the restructuring of metallic nanoparticles induced by the presence of the support and formation of specific metal-support interfaces can also contribute to these phenomena. Whereas SMSI are often associated with a decrease in the active metal surface area, this effect is largely counterbalanced by the peculiar properties arising in the vicinity of the metal and the support that increase the catalytic performance [43].

However, it is now widely accepted that many mechanisms may occur exactly because of metal-support interactions (MSIs), and they cannot be fully elucidated by simply considering the SMSI effect. These mechanisms involve primarily the electronic interactions between the support and the metal active phase, the unique activity of interfacial sites and a variety of geometric effects involving the alteration of the structure of metal sites via their interaction with the supporting material [44,45]. Thus, in the seminal work by Campbell [46], the term EMSI (electronic metal-support interactions) was introduced in order to holistically describe the origin of the outstanding catalytic activity in some materials, which stems directly from the contact between highly dispersed metal nanoparticles and reducible oxides such as CeO_2. In the concept of EMSI, the alteration of the chemical properties of metal sites can be thought of as the outcome of perturbations in their electronic properties via bonding interaction with the highly reducible ceria or any other oxide, for that matter.

Particularly, ceria-based catalysts differ from other widely used supports since, on top of decoration or alloying effects, electronic phenomena also contribute to the SMSIs. Moreover, in conjunction with their reducible nature, metal/ceria catalysts were included among the candidate systems exhibiting strong metal/support interaction effects from as early as the 1980s [47,48]. Although the abovementioned EMSI concept has been mainly adopted for the interpretation of the interactions in noble metal phases supported on ceria, recent studies have established that the same phenomena are demonstrated for 3D transition metal catalysts as well, particularly Ni/CeO_2 [49] and Cu/CeO_2 [30,50]. It should be emphasized, however, although the terms SMSI and EMSI are usually used to denote the pronounced synergistic interactions that lead to enhanced catalytic performance, this is not always the case, as the overall activity is dependent on the nature and local geometry of catalytic sites, as well as on the reaction environment and is therefore not entirely analogous with the extent of metal-support interactions. In any case, the fine-tuning and control of MSIs is the key factor in regulating the interfacial sites and their local surface chemistry. To this end, the strengthening or weakening of MSIs can be used as a regulating tool for interfacial reactivity, which, in turn, can determine the bonding and, eventually, the activation of the reactant molecules [51–53]. In this regard, MSIs tuning strategies by means of advanced synthetic, compositional and promotional means have received particular attention in heterogeneous catalysis. In light of these, in the section below indicative applications of CeO_2-based catalysts are discussed from the viewpoint of the aforementioned redox and interfacial properties. The key role of fine-tuning strategies is clearly revealed, which is elaborated on in the upcoming section.

3. Applications of CeO_2-Based Catalysts

On the basis of the unique surface properties of CeO_2, a plethora of ceria-based catalysts have been explored and developed recently in several chemical reactions (Figure 6). For metal oxide catalysts with CeO_2 as the supporting material, the active phases (predominantly transition metals) can be highly dispersed on the surface. Because of its excellent redox ability, high OSC, appropriate surface acidity and augmented Ce^{4+}/Ce^{3+} interchangeability, ceria can exert a strong interaction with the active phase, thus affecting the performance of catalysts via the abovementioned metal-support interactions. Nonetheless, even though ceria has been widely applied as a catalyst constituent, herein, an overview

of the most significant and essentially environmentally relevant applications of ceria-containing heterogeneous catalytic materials are elaborated from the viewpoint of redox and interfacial properties.

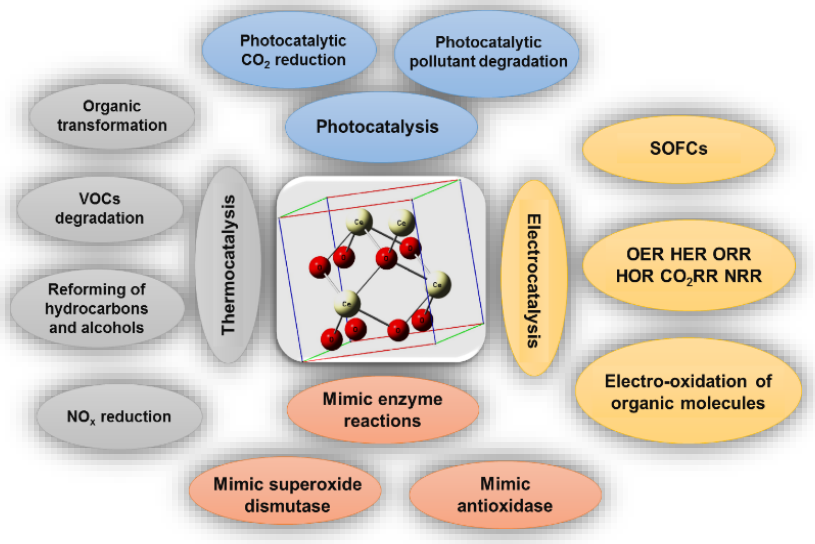

Figure 6. Overview of catalytic applications of CeO_2-based materials. Adapted from Ref. [19]. Copyright© 2021, American Chemical Society.

3.1. Three-Way Catalysis

The first application of ceria as a catalyst was as an oxygen storage component in three-way catalytic converters (TWCs) used for the treatment of exhaust gases in automobiles. Undoubtedly, the utilization of CeO_2 as a key component in TWCs remains its most important technological application and has stimulated an increased research effort in this area. In order to improve the TWCs performance by maintaining the control of the gas mixture composition around the stoichiometric ratio, the introduction of a component that could act as an oxygen buffer during the excursion of the air-to-fuel ratio in the lean and rich composition side was necessary [54,55]. Thus, given the already discussed $Ce^{3+} \leftrightarrow Ce^{4+}$ transition in ceria, this material enables the simultaneous provision of oxygen in the rich part of the oxidation cycle of the unburned species by being reduced (Equations (3)–(5)) while storing oxygen under lean conditions and reverting to CeO_2 (Equations (6)–(8)). Furthermore, the OSC ability directly affects the activity in both CO oxidation [56] and WGS [57]. In addition to OSC, the presence of ceria induces an enhancement of the dispersion of the noble metal particles and the formation of active sites at their interface [26,58].

$$CeO_2 + xCO \rightarrow CeO_{2-x} + xCO_2 \quad (3)$$

$$CeO_2 + C_xH_y \rightarrow CeO_{2-(2x+0.5y)} + xCO_2 + 0.5yH_2O \quad (4)$$

$$CeO_2 + xH_2 \rightarrow CeO_{2-x} + xH_2O \quad (5)$$

$$CeO_{2-x} + xNO \rightarrow CeO_2 + 0.5xN_2 \quad (6)$$

$$CeO_{2-x} + xH_2O \rightarrow CeO_2 + xH_2 \quad (7)$$

$$CeO_{2-x} + 0.5xO_2 \rightarrow CeO_2 \quad (8)$$

A further enhanced low-temperature oxygen availability and higher resistance to high-temperature excursion can be obtained through doping of ceria. In particular, the replacement of some of the Ce ions in its CaF_2-type structure introduces a lattice strain that weakens Ce-O bonds, decreases the oxygen vacancy formation energy and modifies oxygen ion diffusion [59]. Several isovalent and aliovalent elements have been used, though

zirconium-doped ceria materials represent the optimum solution in terms of facile solid solution formation in a wide range of compositions, high redox capacity and thermal stability. Essentially, the introduction of the smaller and non-reducible Zr^{4+} cation into CeO_2 causes a shrinkage of the FCC cell and renders unfavorable the zirconium eightfold fluorite-type coordination. The induced lattice strain can be minimized with more facile oxygen vacancy formation, allowing Zr to adopt a sevenfold coordination [17]. Moreover, the presence of ZrO_2 has been shown to modify the oxygen sub-lattice in CeO_2-ZrO_2 by introducing structural defects and increasing lattice oxygen mobility and reducibility, even at moderate temperatures [60,61].

One of the major challenges in the use of CeO_2 in TWCs is that it should withstand the elevated temperatures (even higher than 1000 °C) to which the catalyst is sometimes exposed. At this elevated temperature, extensive sintering and, concomitantly, a rapid decrease in the surface area take place. This, in turn, inhibits OSC and reducibility; therefore, the development of more thermally stable CeO_2 formulations has attracted a lot of research interest. Furthermore, since pollutant emissions in engines equipped with catalytic converters mainly occur during warm-up, it was essential to improve the catalytic activity at temperatures lower than 300 °C, also taking into account the fact that OSC of ceria under real conditions is limited by the presence of water and carbon dioxide [62]. In addition, the reduction or, ideally, the elimination of noble metals (NMs) use in TWCs is among the most important challenges in the area of catalysis, given the scarcity and, in turn, high price associated with NMs. In this direction, the combination of CeO_2 with earth-abundant oxides under the guidance of the rational design and fine-tuning approach can lead to unique catalyst formulations with the desired cost and efficiency [63]. Moreover, the washcoat composition, the metal loading, the use of rare earth and alkali/alkaline promoters, and the size/shape engineering of catalyst counterparts are some of the most commonly considered strategies for the rational design of TWCs [64–69]. Collectively, the recent advances in the field of TWCs have been summarized in various review papers [70–72].

3.2. Catalytic Combustion/Oxidation Processes

The predominant reasons for the use of catalysts in combustion reactions are mainly linked with the removal and control of pollutants from exhaust flue gases, such as volatile organic compounds (VOCs), CO and soot [73]. In contrast to conventional combustion, catalytically assisted combustion can be defined as a complete oxidation reaction promoted at the surface of a catalyst and thus it is a flameless process. As is the case in any catalytically driven reaction, the selection of the catalytic material is important, with ceria-based materials, in particular, being one of the most promising and studied materials in combustion applications due to their unique features.

3.2.1. Soot Oxidation

Carbon particulates (commonly called soot) are one of the main pollutants emitted by diesel engines, along with CO, NO_x and unburned hydrocarbons, and their adverse effects on human health have showcased the need for strict regulatory measures regarding the allowable emissions. However, NO_x and soot emissions cannot be reduced solely through engine modifications; thus, in order to fulfill the legal emission limits, flue gas-after-treatment technologies have been introduced in recent years. The use of particulate filters and deNO_x catalysts is a promising approach, following the basic concept of TWCs for gasoline engines. In general, soot abatement in diesel exhaust conditions commonly consists of a two-step technology. The first step is the mechanical filtration of carbonaceous particles from the gas phase using a diesel particulate filter. The second step is the actual burning of soot particles inside the filter. This way, the undesired back pressure in the filter due to the accumulation of particulates is avoided [74,75]. Some of the drawbacks include complex filter regeneration and limited soot-catalyst contact efficiency, while the catalyst is additionally required to exert activity and stability over a wide temperature range.

In the early 1990s, ceria-based catalysts were developed for diesel engines [76], and since then, several ceria-based formulations have been investigated in the reaction of soot oxidation, as summarized in Refs. [77,78]. The redox and oxygen storage properties of ceria are the key characteristics that render CeO_2 a very active material in the reaction of soot combustion, as they promote the production of active oxygen species that are essential for the low-temperature oxidation and, in turn, decrease the energy needs for filter regeneration. A plethora of works have investigated these oxygen species with the aim of elucidating the underlying reaction mechanism. It is generally assumed that oxygen species in the form of superoxides (O^{2-}) originate from the interaction between the gaseous oxygen and surface oxygen vacancies of CeO_{2-x}, essentially enabling the carbon oxidation path. Ceria reduction (with the formation of oxygen vacancies) and CO_2 formation is promoted at the C-CeO_2 interface, where carbon acts as the reductant. In an oxygen-free atmosphere, ceria reduction cannot proceed further, owing to the limitation induced by the C-CeO_2 contact and by the number of available surface/lattice oxygen species. However, in the presence of gas-phase oxygen, reduced ceria reacts with O_2, yielding O_2^{2-} and O^{2-} species that migrate to the carbon surface and efficiently form CO_2, with significantly less energy demand. In this way, a modified interface in the vicinity between soot and the surface of ceria is established, and the reaction cycle can be repeated indefinitely [40]. Soot oxidation in diesel automotive catalysis is a rather challenging multiphase reaction that is governed by the contact between the carbon particulates and the catalyst [79].

Several classes of materials were investigated with the aim of enhancing active oxygen species formation (and thereby the OSC) and increasing the C-CeO_2 contact [80]. Bare ceria is not sufficiently active for low-temperature oxidation and is not adequately stable at elevated temperatures, an issue that has been addressed with different strategies, such as alkali promotion and doping of ceria with other rare earth, transition or noble metals, the manipulation of the crystal shape and size at the nanoscale and the synthesis of ordered frameworks with advanced morphologies for an improved accommodation of the carbon particulates in the catalytic composite [78,81–85]. For instance, CO and soot oxidation activity was found to be strongly affected by the morphology of ceria nanoparticles, which directly affects the formation of oxygen vacancies, as shown in Figure 7 [85,86]. Similarly, Aneggi et al. [81] have indicated the surface-dependency of soot oxidation with the nanoshaped materials, i.e., ceria nanocubes exposing (100) crystal planes and nanorods with (100), (110) and partly (111) crystal facets, affecting the soot oxidation activity in a positive manner as compared to polycrystalline ceria dominated by (111) planes.

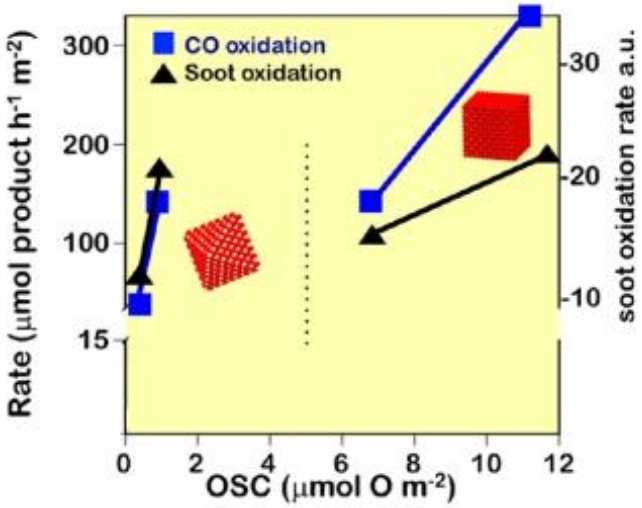

Figure 7. CO and C-soot oxidation rate versus OSC as measured in polyhedral and cubic shaped nanoparticles. Adapted from Refs. [85,86]. Copyright© 2017, American Chemical Society. Copyright© 2014, John Wiley and Sons.

In addition, ceria-based nanostructured catalysts doped with La and Nd were hydrothermally synthesized and investigated in soot combustion [87]. As depicted in Figure 8, the temperature required for the oxidation of soot is connected to particle size reduction. The equimolar Ce-La sample exhibited the optimum soot oxidation performance in loose contact by decreasing the temperature required for soot oxidation by ~80 °C due to its high intrinsic activity, optimal structure and high abundance in capping oxygen species and surface acid sites [87].

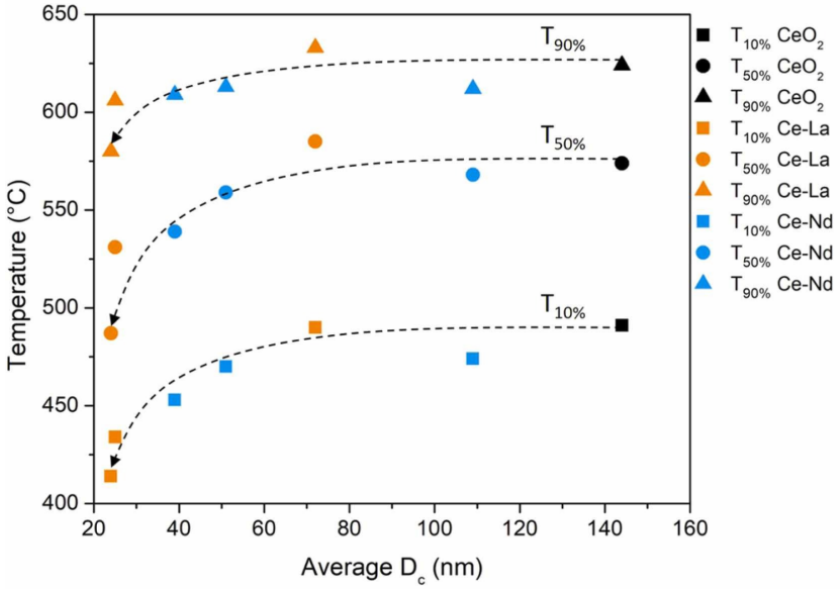

Figure 8. Variation of the catalytic performances as a function of the average crystallite size of the samples during soot oxidation in loose contact (the average of the two different D_C values was used for La-doped ceria, Ce75Nd25 and Ce50Nd50; samples were named CeXReY, where Re is the doping rare earth (La or Nd) while X and Y are the atomic percentages of Ce and of the doping element, respectively). Reproduced with permission from Ref. [87]. Copyright© 2022, Elsevier.

3.2.2. VOCs Combustion

Volatile organic compounds (VOCs) are organic compounds with boiling points in the range of 50–260 °C and are widely considered important atmospheric pollutants. Sources of atmospheric VOCs are either indoor activities, i.e., from household products such as office supplies, insulating materials, cleaning products and pressed woods or outdoor activities, most industrial processes and transport applications. The mitigation of VOC emissions has received particular attention over the past decades, considering their involvement in photochemical smog, depletion of atmospheric ozone and production of tropospheric ozone [88]. In the scope of VOC emissions mitigation, the following three main techniques have been applied: physical adsorption, thermal incineration and catalytic combustion. However, the latter is one of the most effective and economically feasible VOCs abatement strategies.

Although noble metal (NMs) catalysts, such as Pd and Pt, are among the most active materials for VOCs abatement, their high cost and sensitivity to poisoning hinder their widespread application. On the other hand, transition metal oxides (TMOs) exhibit adequate activity and chemical stability toward VOCs oxidation. More importantly, mixed metal oxides, such as CuO/CeO_2 or Co_3O_4/CeO_2, demonstrate superior reactivity as compared to single counterparts. The latter is mainly ascribed to the peculiar synergistic interactions between metal oxides, which are accounted for the increased metal dispersion and improved reducibility, both considered crucial parameters for VOCs oxidation following a Mars–van Krevelen mechanism [89–93]. In this regard, several strategies involving, among others, aliovalent doping and surface/structural promotion have been adopted to

improve the OSC and, in turn, VOCs oxidation [89–93]. Importantly, close relationships between the reducibility and lattice oxygen abundance with VOCs oxidation performance have been disclosed, revealing the pivotal role of these parameters as activity descriptors (Figure 9).

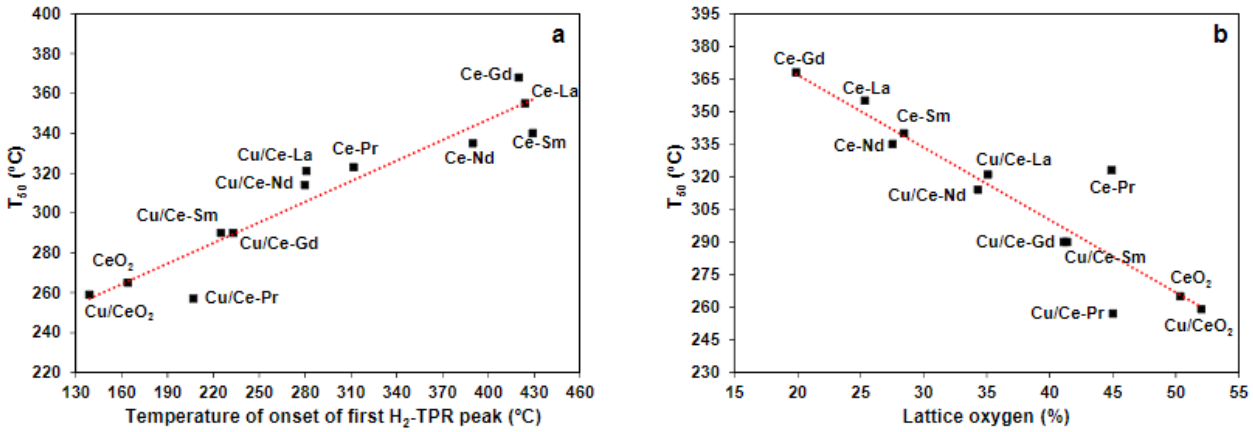

Figure 9. Correlation between the half-conversion temperature and (**a**) onset reduction temperature and (**b**) the lattice oxygen capacity for various ceria-based catalysts in ethyl acetate oxidation; Catalysts designation: $Ce_{0.5}Gd_{0.5}O_{1.75}$ (Ce-Gd), $Ce_{0.5}La_{0.5}O_{1.75}$ (Ce-La), $Ce_{0.5}Pr_{0.5}O_{1.75}$ (Ce-Pr), $Ce_{0.5}Nd_{0.5}O_{1.75}$ (Ce-Nd) and $Ce_{0.5}Sm_{0.5}O_{1.75}$ (Ce-Sm). Reproduced from Ref. [90]. Copyright© 2016, MDPI.

3.2.3. CO Oxidation

Carbon monoxide is mainly produced by automobile exhausts and incomplete combustion processes of fuels and solid wastes and has become one of the major air pollutants, along with its detrimental effects on human and animal health. A small exposure to carbon monoxide can be fatal, owing to its high affinity towards the replacement of oxygen and binding into hemoglobin in blood cells. The catalytic oxidation of CO to CO_2 is an effective and simple technology for mitigating the CO content in the air and has attracted great attention due to the low associated energy consumption and its thermodynamic favorability at low temperatures, generally lower than 300 °C [94]. The reaction of CO oxidation reaction is one of the most extensively studied reactions in the field of heterogeneous catalysis and is often considered a probe reaction for other oxidation processes due to its well-established reaction mechanism and overall underlying characteristics.

Typical catalytically active noble metals, such as Ag, Au, Pd and Pt, have been regarded as effective catalysts for low-temperature CO oxidation as well. However, among the recently developed catalysts, ceria-based catalysts are one of the most active non-noble metal catalysts due to their superior oxygen mobility and oxygen vacancy concentration. The superior oxygen mobility by the high redox capability of ceria is largely beneficial for the catalytic activity in CO oxidation using an active metal. Metal ions can provide abundant CO chemisorption sites, and CeO_2 provides the necessary oxygen vacancies in the metal-ceria interface, where adsorbed CO can be oxidized by the activated oxygen species [95]. Besides, the unique redox pair Ce^{4+}/Ce^{3+} induces strong interaction with the active phase, leading to a synergistic effect that improves the reducibility of the metallic phase as well [17].

In view of the above, the combination of ceria with earth-abundant metals can lead to cost-effective ceria-based mixed oxides with enhanced reducibility and catalytic activity, arising mainly from metal-ceria interactions. However, the surface/structural features of both the metal entity and ceria carrier (e.g., size and shape of each phase) can notably affect the interfacial phenomena, which then can be reflected in the catalytic performance [30,45,96–98]. The latter triggers unique opportunities for the rational design of highly active metal oxides by following a general optimization approach involving the

modulation of various interrelated factors, such as the size and morphology of parent oxides [29,96,98,99]. In addition, surface promotion (mainly by an alkali or alkaline earth metal) can be employed as an additional tool to fine-tune the local surface chemistry of mixed oxides [29,100,101].

The effect of ceria's structure and shape functionalization on the CO oxidation performance was clearly documented by two pioneering studies, which revealed the significance of morphology-dependent catalysis [102,103]. In particular, Zhou et al. [102] demonstrated the high CO oxidation reactivity of single-crystalline ceria nanorods in comparison to their counterparts of irregular morphology, while in the work by Aneggi et al. [103], a correlation between the exposed crystal planes and the specific reaction rate in polycrystalline ceria samples was disclosed. In light of the above aspects, highly active NMs-free composites have been recently developed, with similar or even superior reactivity to that of typical noble metal oxidation catalysts [29,99]. For instance, the combination of copper oxide with CeO_2 of rod-like morphology (CuO_x/CeO_2-NR) has been led to extremely active catalysts, offering complete elimination of CO at ca. 150 °C [104]. By means of various in situ and ex situ characterization tools, a close correlation between the catalytic activity and key activity descriptors, i.e., i) oxygen storage capacity and ii) abundance in oxygen vacancies, was disclosed (Figure 10).

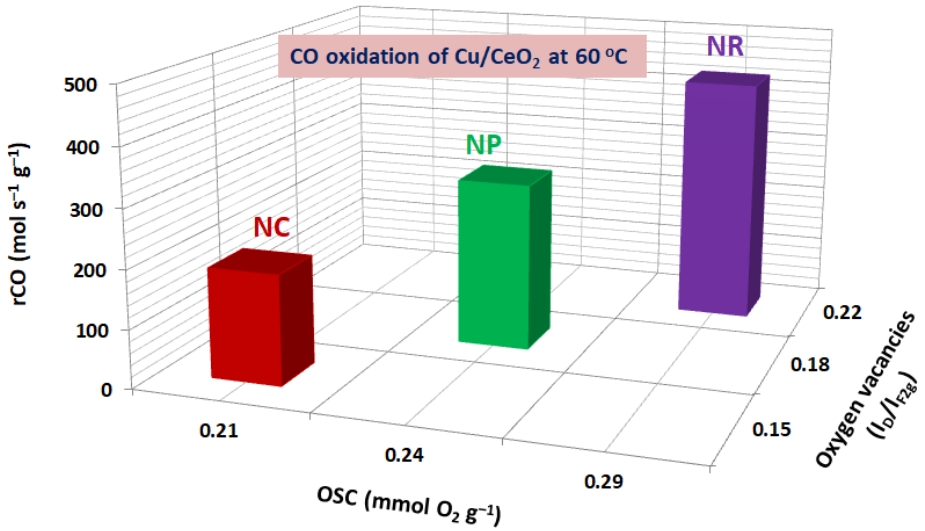

Figure 10. Relationship between the CO oxidation performance (r_{CO}, nmol g^{-1} s^{-1}) of Cu/CeO_2 samples and the oxygen storage capacity (OSC, mmol O_2 g^{-1}) as well as the abundance in oxygen vacancies (in terms of I_D/I_{F2g} ratio) of ceria nanorods (NR), nanopolyhedra (NP) and nanocubes (NC). Adapted from Ref. [99]. Copyright© 2021, MDPI.

Besides the key role of ceria morphology, numerous other synthesis/promotional parameters can be adjusted to further enhance the catalytic performance. In this regard, we recently revealed the key role of the synthesis procedure [105] and metal oxide composition [106] on the CO oxidation performance of CeO_2-based mixed oxides. Interestingly, independent of the fine-tuning approach followed, a perfect relationship between the catalytic activity and OSC was disclosed (Figure 11). These findings may be generalized and pave the way for the rational design of highly active and cost-efficient composites for various combustion and oxidation processes, given the prominence of the role of oxygen species mobility in any reaction involving the activation of gas-phase O_2.

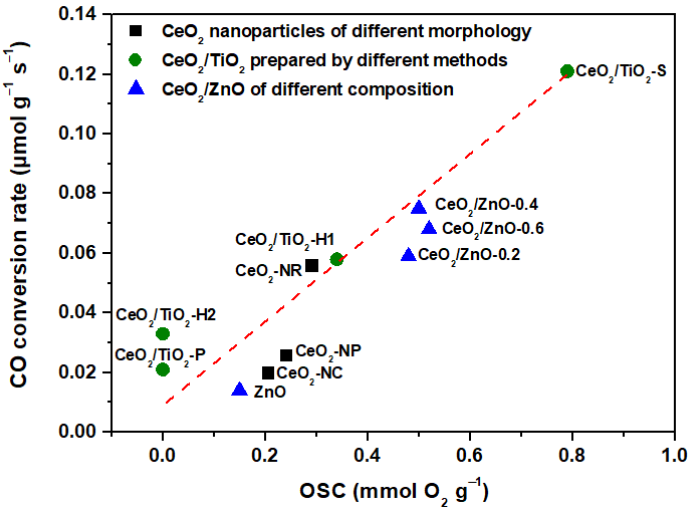

Figure 11. Relationship between the CO conversion rate at 200 °C with OSC of CeO_2-based oxides. Symbols inside the figure refer to: nanopolyhedra (NP), nanocubes (NC), nanorods (NR), precipitation (P), hydrothermal method in one (H1) and two (H2) steps and Stöber method (S). Created by the authors combining data from Refs. [105,106]. Copyright© 2020, MDPI.

3.2.4. Water Gas-Shift (WGS) and Preferential Oxidation of CO (CO-PROX)

Industrial processes such as Fischer–Tropsch (F-T) or methanol synthesis require well-defined mixtures of $H_2/CO/CO_2$ ratios for their optimum operation. For this reason, after being produced, usually, by reforming or gasification reactions, the molar ratio H_2/CO in the generated syngas mixture should be adjusted to the desired value to fit the selected downstream process. Moreover, the CO content in hydrogen streams must be sometimes kept at very low values, even below 10 ppm, in order to be used for ammonia synthesis, hydrogenation reactions or as possible fuel feedstock in proton exchange membrane fuel cells (PEMFCs) to avoid the poisoning of the employed catalysts. The most promising process to achieve both of these requirements is a combination of the forward water gas shift reaction (WGS) (Equation (9)) and the preferential oxidation of residual CO (CO-PROX) in the presence of excess H_2 using O_2 or air as the oxidant [107]. Moreover, since the operating temperature of low- and high-temperature PEMFCs is 80–250 °C, this is the optimum temperature window for the intermediate CO-PROX step, as well.

$$CO + H_2O \leftrightarrow CO_2 + H_2, \quad \Delta H_{298K} = -41.1 \text{ kJ/mol} \tag{9}$$

The WGS reaction is a mildly exothermic reaction that usually takes place in the following two consecutive stages: a high-temperature step, operating between 300 and 450 °C and a low-temperature stage between 200 and 300 °C. The former is commonly catalyzed by a Fe_2O_3-Cr_2O_3 catalyst, while the latter usually involves a Cu/ZnO catalytic system to reach equilibrium conversions. Moreover, CO oxidation in the final PROX step requires the development of highly selective catalysts, able to promote the removal of CO without consuming H_2 [40]. Various studies have shown that CeO_2-based catalysts supporting 3D transition metals such as Ni, Cu and Fe are highly active materials for the WGS and CO-PROX reactions, thanks to their increased redox and oxygen mobility properties, which can be further improved by doping of appropriate materials such as La, Pr or Zr in the ceria lattice [16].

Two reaction mechanisms have been proposed for CeO_2-based catalysts under WGS or CO PROX conditions, the formate and redox route. In the former mechanism, the reaction involves the formation of OH groups on Ce ions, which then react with adsorbed CO to form formate species and product generation is eventually realized by the decomposition of formates. As for the active metal phase, its role lies in the affinity for the adsorption of CO and the promotion of the cleavage of the C-H bond in the formate entities. Concerning

the redox route, reactive oxygen atoms are transferred from ceria to the metal nanoparticles, thus generating surface oxygen vacancies. Active oxygen then reacts with metal-bound adsorbed CO producing CO_2, while H_2O or O_2 produces hydrogen by restoring the surface oxide anions [108,109]. Irrespective of the dominant reaction pathway, the key role of redox properties and metal-support interactions has been well documented [110–113]. Hence, particular efforts have been lately devoted to the rational design of CeO_2-based oxides for WGS by fine-tuning the local surface structure and metal-ceria interactions by means of the aforementioned optimization strategies. In this perspective, the key role of ceria morphology on redox properties and metal-support interactions was disclosed over various CeO_2-based transition metals [114–116]. For instance, the addition of CuO over ceria carriers of different morphology (nanorods (NR), nanocubes (NC), nanopolyhedra (NP)) affects the reducibility to a different extent, following the order NR > NP > NC [114]. This, in turn, results in the formation of Cu^+ species through the redox equilibrium $Cu^{2+} + Ce^{3+} \leftrightarrow Cu^+ + Ce^{4+}$, which are considered highly active for CO adsorption and consequent activation. Hence, the superior WGS activity and stability of CuO_x/CeO_2 nanorods have been accordingly attributed to their abundance in oxygen vacancies and highly active monovalent copper species. Elsewhere, copper–ceria nanoparticles of different morphology (octahedral or spheres) exhibited the highest copper dispersion and the strongest copper–ceria interaction, resulting in the optimum CO conversion performance [115,116].

Thus, considering the above aspects, it can be certainly stated that CeO_2-based mixed oxides could serve as a highly versatile materials platform in numerous energy and environmental applications, replacing or at least reducing the use of rare and expensive NMs. However, a rational design approach is required in order to fine-tune the intrinsic and interfacial features and, in turn, the catalytic properties.

4. Structure/Surface Engineering of CeO_2 Nanoparticles

4.1. Fine-Tuning of Metal Oxides

In this section, the underlying mechanism of key engineering parameters, such as size, shape and electronic state, is shortly discussed to gain insight into their particular effect on the intrinsic characteristics and interfacial interactions. As previously mentioned, the adjustment of these specific parameters can notably modify the local surface chemistry and metal-support interactions with great implications in the catalytic performance [30,45,52,117–122].

In particular, the synergy between the different counterparts of mixed metal oxides (MMOs) can give rise to specific features (e.g., enhanced reducibility, oxygen vacancy formation, abundance in structural defects, etc.), as various interrelated phenomena are at work as follows: (i) electronic perturbations arising from metal-support interactions, (ii) improved reducibility and oxygen exchange kinetics through oxygen vacancy formation, (iii) formation of interfacial sites of high intrinsic activity. For instance, the size and shape engineering of the catalysts' counterparts at the nanoscale can affect various physicochemical properties of the mixed metal oxides, such as the surface area, the coordination environment, the redox properties or the formation of structural defects and oxygen vacancies. In a similar manner, aliovalent doping with surface or structural promoters can alter the electronic environment or the composition of the catalyst leading to different redox and structural features. These fine-tuning engineering strategies are separately discussed below.

However, it ought to be mentioned that there is an interrelationship among the aforementioned factors governing catalytic activity and for this reason, each parameter should be studied in relation to the others in order for concrete and reliable conclusions to be drawn. In this regard, the reader refers to some comprehensive reviews focusing on the general framework for catalyst optimization through size, shape, electronic engineering, employment of specific pretreatment protocols and the use of surface/structural promoters on ceria-based catalysts [29,99,117,120,121,123].

4.2. Size Effects

The modification of particle size can affect the surface area, the electronic/coordination environment and the formation of structural defects. By decreasing the Mos particle size down to the nanometer scale, a distinct effect in activity is observed, which is derived from the so-called "size effects". This size-reactivity dependency is the outcome of different contributions, including quantum size or confinement effects, interparticle interactions, electronic effects and the presence of atoms of low coordination number on the surface [29,30,96,124–126]. By reducing the particle size to a few nanometers, the surface-to-volume ratio is significantly increased, leading to abundant surface sites. More importantly, the interfacial electronic and geometric interactions are strongly affected by particle size modifications [96,125]. For instance, Pt/CeO_2 catalysts, including Pt nanoparticles of ca. 4.0 nm, exhibited the optimum WGS activity (Figure 12), as compared to Pt single atoms and Pt sub-nanoclusters (ca. 0.8 nm) [26].

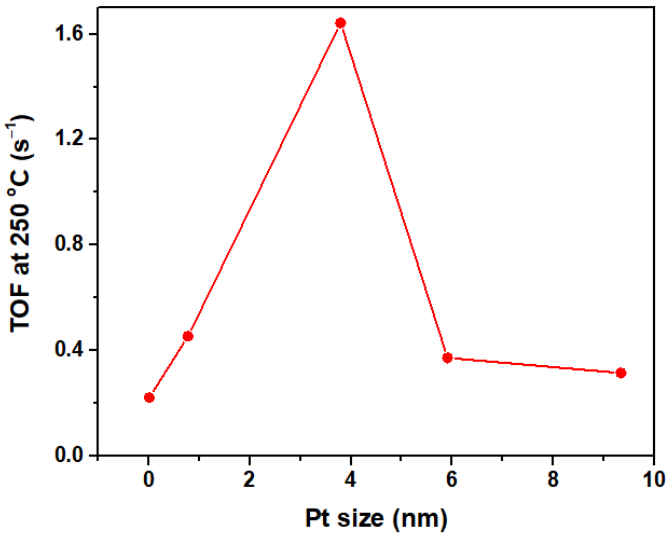

Figure 12. Turnover frequency at 250 °C of the Pt/CeO_2 samples with different Pt particle sizes. Adapted from Ref. [26]. Copyright© 2021, Elsevier.

The strong size dependence behavior of $Ru_n/CeO_2(111)$ (n = 1, 2, 4, 7) catalysts was recently shown through density functional theory (DFT) calculations in the dry reforming of methane [127]. DFT studies revealed that the CH_4 and CO_2 activation processes are size-dependent, with Ru coverages of around 0.1–0.2 monolayer (Ru_2 and Ru_4 models) exhibiting the best performance. The Ru_2 and Ru_4 models facilitated the activation of CO_2 due to their weak Pauli repulsion and strong CO adsorption ability [127].

Interestingly, particle size-induced modifications greatly affect the surface structure and, in turn, the local surface reactivity [128]. For instance, taking into consideration the particle shape modeling for a truncated cuboctahedron, the (111) and (100) facets, corner and edge sites are significantly changed for sizes below ca. 3 nm [128]. In particular, the close-packed (111) planes account for almost 80% of the surface atoms for particle sizes larger than 10 nm (Figure 13), with direct implications on the local geometry and reactivity [128]. Elsewhere, the importance of support size in the nanoscale was highlighted during the preferential oxidation of CO (CO-PROX) over copper–ceria catalysts [129,130]. The optimal catalytic performance was linked to highly dispersed copper sites interacting strongly with ceria nanoparticles of specific size.

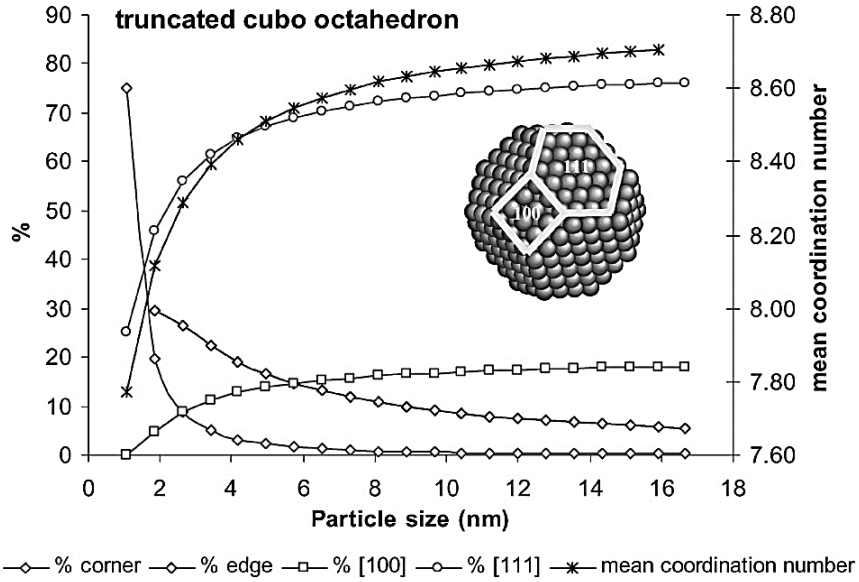

Figure 13. The distribution of the different types of sites and mean coordination number of surface atoms for truncated cuboctahedral particles. Reproduced with permission from Ref. [128]. Copyright© 2010, Taylor and Francis.

4.3. Shape Effects

Nanoscale engineering of the geometric (i.e., size and shape) and crystallographic (i.e., exposed facets) properties of individual particles is extremely important in the scope of modifying the surface chemistry characteristics of metal oxide catalysts in a controlled manner. In particular, the precise control of the particle morphology enables the selective exposure of specific crystallographic planes, which is associated with important implications in the reactant's adsorption/activation affinity. Moreover, the control of support morphology can notably influence the anchoring of active metal sites and, thus, the extent of metal-support interactions, offering an additional modulating tool [25,31,99,131–136]. This desirable surface coordination of catalytically active atoms or domains substantially alters the catalytic activity, selectivity and stability and is known as morphology dependence. To this end, the development of advanced synthesis and characterization techniques as well as the successful combination of theoretical simulations with experimental studies, have led to a rapid increase in rationally designed heterogeneous catalysts attaining the desired surface and morphological characteristics [57,137,138].

Thermodynamically, the most stable crystallographic orientations of ceria are the planes indexed as (100), (110) and (111) since the (211) surface, although reported as a relatively stable surface, undergoes facile reconstruction into stepped (111) (Figure 14). Surfaces with higher indices are inherently less stable and are more prone to reconstruction; therefore, the majority of works have focused on the three low-index surfaces [85]. In particular, the (111) surface is terminated by threefold-coordinated O atoms and sevenfold coordinated Ce atoms, (110) is terminated by a CeO_2 plane with threefold O and sixfold Ce atoms and (100) terminates by twofold-coordinated oxygen atoms [139]. In large, experimental and theoretical studies have shown that the (100) and (110) planes are more reactive than the (111) plane and that surfaces dominated by (100) and (110) planes enhance lattice oxygen migration from bulk to surface, an effect generally restricted in the case of (111)-dominated surfaces [140]. This general finding provides insights into enhancing the OSC of ceria-based materials by fine-tuning the shape of CeO_2 nanoparticles in order to selectively expose more reactive (110) and (100) facets.

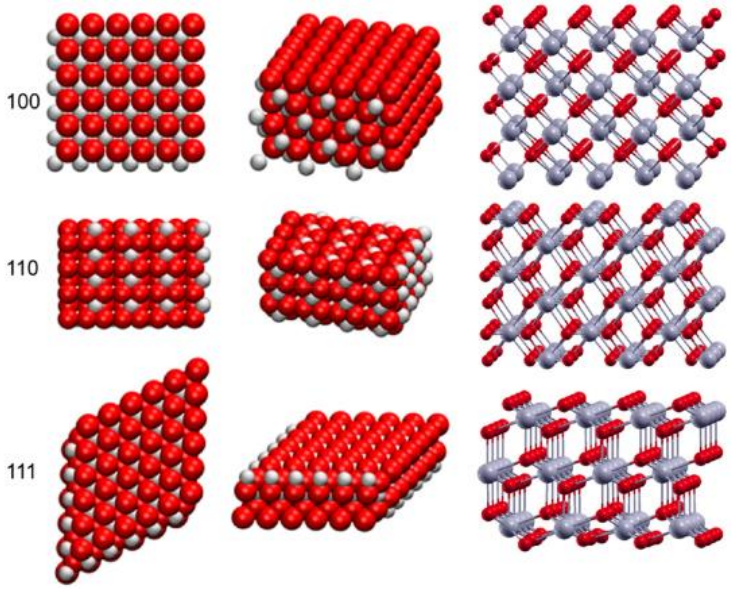

Figure 14. Top, side and perspective view of CeO_2 (100), (110) and (111) surfaces. Gray and red spheres represent Ce and O ions, respectively. Reproduced with permission from Ref. [85]. Copyright© 2017, American Chemical Society.

It is known that crystal morphology equilibrium depends on both kinetic and thermodynamic processes that are established during the process of particle growth, since the most stable surfaces will be formed thermodynamically, resulting more often than not in a specific shape. So, the synthesis of particles with different crystal planes associated with higher surface energy takes place via the kinetic control of nucleation and crystal growth rate in different directions. This can be controlled by several parameters such as pressure, temperature, pH, solvent and characteristics of precursors [141]. Indeed, the major advanced synthetic routes include hydrothermal and/or solvothermal synthesis, aqueous-phase precipitation and the electrochemical reduction of cerium salts. However, the alkali-assisted hydrothermal process appears to be the most effective and widely employed, driven by several advantages such as the short reaction time, simple precursor requirements, homogeneous morphology and development of nanoparticles with a variety of well-defined shapes, such as wires, polyhedra, rods, spheres and cubes. Typically, salts of either Ce^{3+} or Ce^{4+} are employed as parent materials since the former is critical in the anisotropic growth of ceria nanocrystals and the latter favors the formation of spherical particles [22,99,142–144].

Ergo, nanostructured catalytic materials preferentially exposing specific crystal planes possess unique features related to size as well as shape effects [85,125,140,143,145–147]. In particular, ceria shape effects on the catalytic activity constitute an extensively investigated topic in heterogeneous catalysis, including our research efforts in the field [29,35,85,98,99,104,114,132,143,145,146,148–152]. Surface reconstruction through nanofaceting of specific crystal planes can affect ceria's intrinsic properties and, consequently, its catalytic activity and stability [153].

Most prominently, the facet-dependent catalytic activity of ceria nanocatalysts has been demonstrated in the probe reaction of CO oxidation [104,154] and the WGS reaction [155–157]. Generally, particles of nanorod morphology, exposing (110) and (100) facets, demonstrate the highest activity, followed by nanocubes exposing (100) facets and, lastly, octahedral ((111) and (001) facets)), with the turnover frequency values following the order; (110) > (100) > (111). The outstanding performance of nanorods stems largely from the increased exposure of the more reactive (110) and (100) facets, which also possess higher amounts of oxygen vacancies. This is ascribed to the finding that the energy formation of oxygen vacancies in CeO_2 nanoparticles is indeed facet-dependent and decreases in the following order: rods ~ cubes > polyhedra [143,158].

In this regard, ceria nanoparticles of well-defined morphology (i.e., rods, polyhedra, cubes) were successfully synthesized through the hydrothermal method by our research group, with the rod-shaped catalysts exhibiting high reducibility and oxygen kinetics [99,104,132,148,150,152]. Moreover, the length of ceria nanorods was found to increase with the increasing temperature of hydrothermal treatment, also affecting the concentration of oxygen vacancies [159]. In addition, a dependency was found between the exposed facets and the metal-support interaction during various reactions over CeO_2-based transition metals, such as CO_2 methanation [160–162] and dry reforming of methane [163,164]. For instance, nickel crystallites of ~1 nm dispersed on ceria nanorods mainly exposing (111) crystal planes exhibited remarkable activity and stability for DRM as compared to nanocubes and nanospheres, a behavior that was ascribed to the high dispersion of Ni, the improved reducibility and CO_2 binding strength [164].

Interestingly, similar morphology-dependent effects can be obtained by adjusting not only the shape of the support but also of metal phase. In this regard, a DFT study was performed in order to gain insight into the influence of various Cu surfaces (Cu(211), Cu(100), Cu(111)) on the WGS activity and mechanism, with the coordination number (CN) of the Cu active site being in the range of 7–9 [165]. The Cu(211) surface showed the highest stability and superior WGS performance with the d-band center values following the following sequence: Cu(211) > Cu(100) > Cu(111), showing a decrease in the d-band center values with increasing coordination number [165]. The increase in the d-band centers results in an increase in the adsorption strength of CO and H_2O adsorbates, corroborating the d-band center theory [165].

Lastly, considering the paramount importance of MSIs in metal/ceria catalysts, the surface terminations of ceria nanoparticles are crucial in the stabilization of the nanoparticles of the active metallic phase. Moreover, the size, morphology and electronic environment of metal nanoparticles can be markedly affected in a ceria facet-dependent manner. Typically, rod-like ceria nanoparticles tend to stabilize metal atoms and clusters, whereas CeO_2 nanocubes favor the formation of larger metal crystallites. Besides, on top of the effect of metal loading and the preferential location of metal nanoparticles over different ceria crystal planes, the electronic state of the deposited metal nanoparticles is also facet-dependent, as it strongly depends on the reducibility and oxygen vacancy abundance of ceria. This results in highly reduced particles anchored over CeO_2(100) compared to the slightly oxidized metal nanoparticles in the vicinity of CeO_2(111) [85,143].

4.4. Surface and Structural Promotion

As described above, the local surface chemistry of metal oxides can be finely tuned through size and shape engineering. However, doping via the addition of low amounts of a specific metal phase can serve as an additional modulating strategy. In specific, the catalytic performance of metal oxides can be altered through the use of promoters, which can be divided into the following two main categories: electronic and structural. Electronic promoters, referring mostly to alkali metals, induce changes in the work function of the catalytic surface, thus modifying its chemisorptive properties. Structural promoters include mainly aliovalent doping of the catalytic support for the enhancement of its structural properties, providing, in turn, indirect implications on the surface chemistry of active metal sites.

In view of the above discussion, we have shown that the deN_2O performance of CuO/CeO_2 mixed oxides can be optimized through the co-adjustment of textural/structural properties (though co-precipitation method) and alkali promotion (Cs addition), as depicted in Figure 15, demonstrating the effectiveness of the proposed fine-tuning approaches [166].

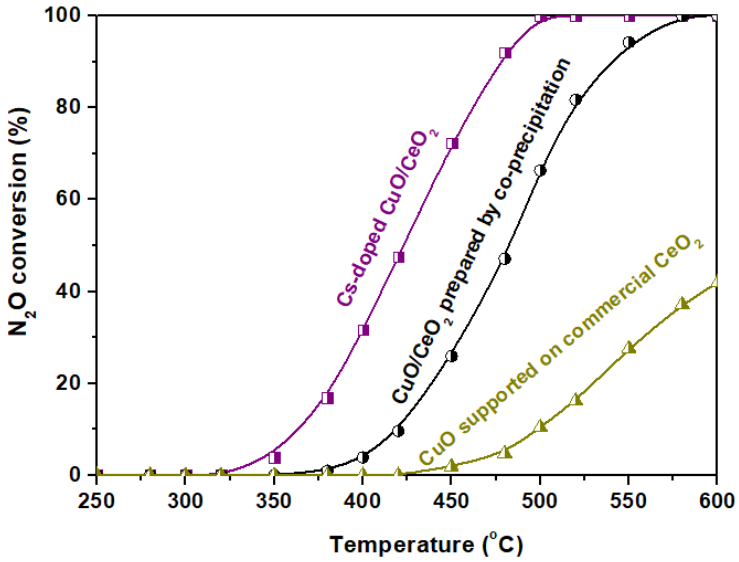

Figure 15. Optimization of deN_2O performance of CuO/CeO_2 mixed oxides by co-adjusting synthesis parameters (co-precipitation method) and electronic state (alkali addition). For comparison, the corresponding performance of CuO supported on commercial ceria is included. Reaction conditions: 0.1% N_2O balanced with He; WHSV = 90,000 mL g^{-1} h^{-1}. Adapted from Ref. [166]. Copyright© 2018, Royal Society of Chemistry.

Elsewhere, the effect of the n_{NaOH}/n_{Ce} ratio was studied over ceria catalysts prepared with liquid nitrogen (LN-CeO_2) [167]. As shown in Figure 16, a linear correlation was found between the sodium content and the oxygen vacancy concentration in LN-CeO_2 samples [167].

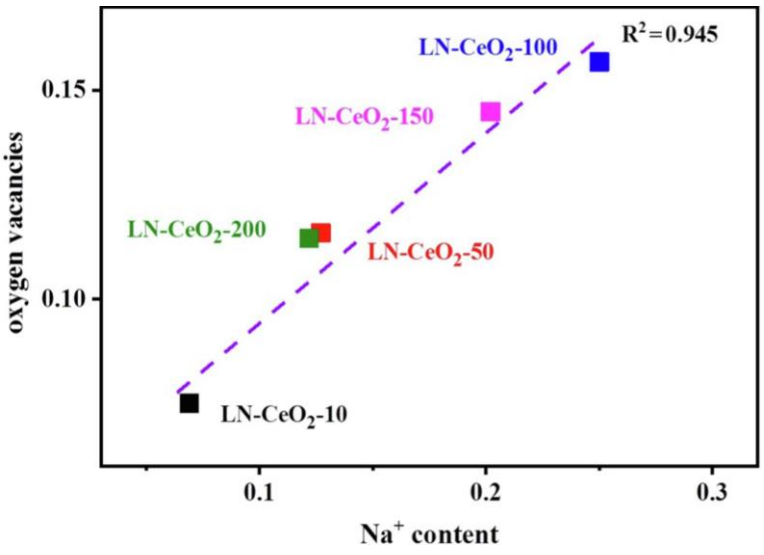

Figure 16. Relationship between oxygen vacancies concentration and Na content in ceria catalysts prepared with liquid nitrogen (LN-CeO_2). Reproduced with permission from Ref. [167]. Copyright © 2022, Elsevier.

Moreover, methane activation was examined through density functional theory by doping ceria (111) with alkaline earth metals [168]. In specific, a linear relationship was observed between the active oxygen vacancies' formation energy and the dissociated species' adsorption energy (Figure 17), revealing that the dissociative adsorption of methane is promoted by the favorable oxygen vacancy formation [168].

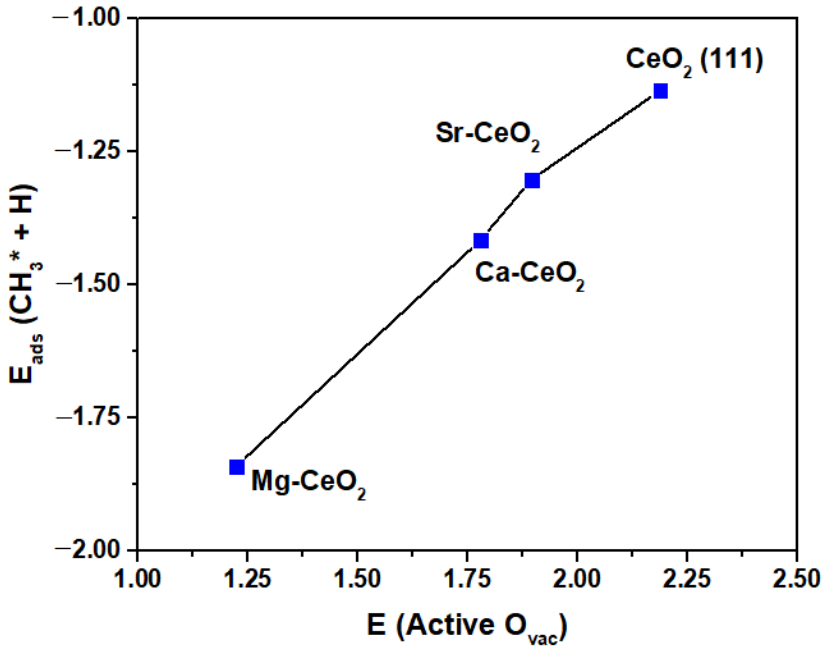

Figure 17. The correlation between the adsorption energy of the dissociation products and the formation energy of the active oxygen vacancy on the bare and doped (111) surfaces of CeO_2, where CH_3* is the surface-adsorbed CH_3 species). Adapted from Ref. [168]. Copyright© 2016, Royal Society of Chemistry.

In addition, the oxidation of CO was studied over ceria doped with 20 at.% transition metals (TM = Cu, Co, Mn, Fe, Ni, Zr, Zn) prepared through microwave-assisted sol-gel synthesis [169]. The adsorption strength of CO was found to follow the following trend: Cu > Co > Mn > Zn > CeO_2 on the basis of DFT calculations, while the same order was revealed for the descriptor α that illustrates the lattice oxygen participation in CO oxidation (Figure 18), with the Cu-doped sample exhibiting abundance in labile lattice oxygen [169]. In a similar manner, Ga-doped nickel-ceria catalysts exhibited high activity and stability in the DRM reaction, as gallium addition offered an ample amount of oxygen species in the catalytic surface that enable the suppression of carbon deposition and preserve the catalytic activity [170].

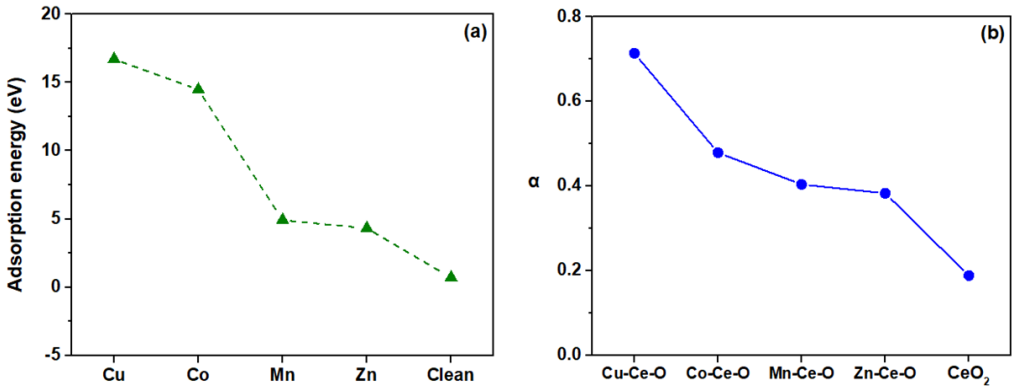

Figure 18. (**a**) Adsorption energy of CO as a function of TM (the clean surface of undoped ceria is also given), (**b**) Ratio (α) of the amount of $C^{16}O$ (mmol g^{-1}) consumed to the ^{18}O (μmol g^{-1}) exchanged after 20 min in CO oxidation on the same doped-ceria catalysts. Adapted from Ref. [169]. Copyright© 2021, American Chemical Society. Notice to readers: Further permissions related to the material excerpt should be directed to the ACS.

In light of the above aspects, it can be inferred that highly efficient catalysts can be obtained by co-adjusting the structural and surface characteristics of ceria-based binary oxides. The latter can be accomplished through the use of appropriate synthesis and doping routes toward modulating the intrinsic characteristics of the individual counterparts and metal-oxide interactions. Similar conclusions can be drawn for numerous other binary oxides and metal-supported catalysts, providing design principles for the development of cost-efficient catalyst formulations for various energy and environmental applications, as exemplified below by the reaction of CO_2 hydrogenation.

5. Implications in CO_2 Hydrogenation Reactions

In this section, the role of adjusting key activity descriptors of ceria-based materials is exemplified by their application in ambient-pressure CO_2 hydrogenation towards CO and CH_4, a very important reaction within the general scheme of carbon capture and utilization (CCU) [171–173]. Among the different supports that have already been presented for this reaction, ceria and CeO_2-based mixed oxides have been extensively studied over the past years, exploiting the intriguing and unique catalytically relevant properties of ceria-based systems and especially metal/ceria composites, in line with the aforementioned discussion. Indeed, the combination of an active metal phase with ceria as the supporting oxide has been demonstrated to be one of the most effective catalytic strategies for low-temperature reduction of CO_2 via H_2 [20,21]. Since the main scope of the present work revolves around CO_2 hydrogenation at atmospheric pressure for the production of CH_4 and CO, the recent progress in ceria-based heterogeneous catalysts for the formation of other CO_2 hydrogenation products (e.g., methanol) is not discussed here, as a comprehensive summary can be found in relevant literature reviews. Besides, the analysis of the specific characteristics and activity-property correlations of CeO_2-based materials for CO and CH_4 generation from CO_2 and H_2 presented next are largely valid for the thermocatalytic CO_2 hydrogenation reaction towards other products as well.

5.1. CeO_2-Based Catalysts for the rWGS Reaction

The conversion of carbon dioxide via the reverse water–gas shift reaction (rWGS, Equation (10)) produces a gas mixture consisting primarily of CO and H_2, most often referred to as syngas. The importance of this reaction lies in the fact that CO is a highly reactive C-containing molecule (especially compared to CO_2, see Figure 19) that can be employed in a plethora of downstream processes for the production of carbonaceous added-value fuels and chemicals, depending on the H_2/CO ratio [173,174]. Indeed, as shown in Figure 20, CO is an extremely versatile organic building block compound, and its employment (along with hydrogen) as chemical and fuel feedstock highlights the significance of the rWGS reaction within the context of valorizing CO_2 emissions in a CCU scheme [175]. From a thermodynamical standpoint, the rWGS reaction is an equilibrium reaction favored at higher temperatures (usually above 500 °C) due to its mild endothermicity, as well as at high H_2/CO_2 ratios (practically higher than the stoichiometric value of 1) in order to provide enough chemical energy to counterbalance the chemical inertness of the CO_2 molecule [176,177].

$$CO_2 + H_2 \leftrightarrow CO + H_2O, \quad \Delta H_{298K} = +41.1 \text{ kJ/mol} \tag{10}$$

Although the forward WGS reaction is a widely established and essentially fully optimized process for the adjustment of the H_2/CO ratio in many industrial processes, the same does not apply as of yet to the reverse reaction. Therefore, deep knowledge of the rWGS reaction mechanistics is required in order to provide insights into the rational design of effective and robust heterogeneous catalytic systems. In this way, given its potentially important role outside the lab-scale environment, the design and scaling up of efficiently integrated and intensified rWGS-based processes is expected to be of paramount importance in the near future [174].

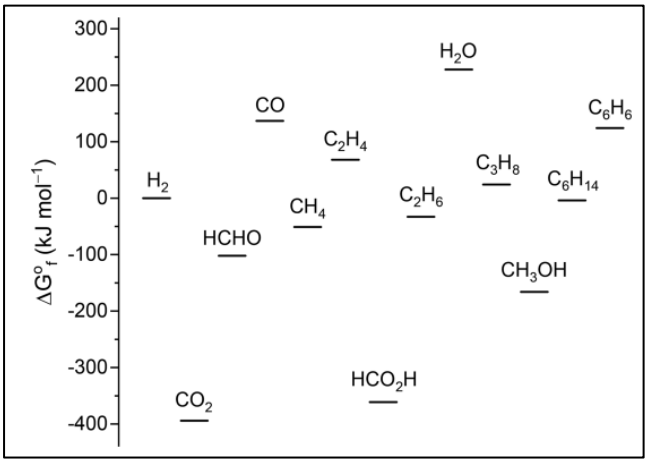

Figure 19. Values of standard Gibbs free formation energy for some carbon compounds at different C oxidation states. Reproduced with permission from Ref. [174]. Copyright© 2020, American Chemical Society.

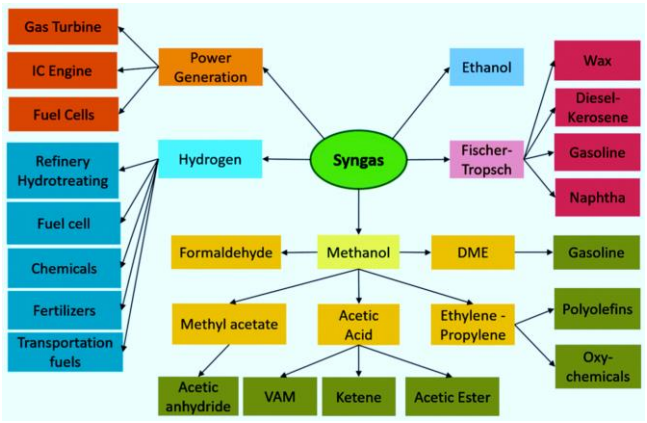

Figure 20. The potential routes for syngas exploitation. Reproduced with permission from Ref. [178]. Copyright© 2020, MDPI.

So far, various catalytic systems for the rWGS reaction based on both noble metals and transition metals on different oxide supports have been studied in the literature, although the observed reaction mechanism is largely catalyst-dependent, albeit two main routes are reported, namely, the dissociative or associative routes (Figure 21). Specifically, the one route (i.e., Path A) refers, on the one hand, to the activation of gas-phase CO_2, followed by the direct cleavage of the C-O bond in reactive *CO_2 species, which eventually generates *CO and *O. On the other side, gaseous H_2 is dissociated on the metal center producing active H adatoms that migrate through a spillover mechanism in the vicinity of the *CO entities, eventually generating loosely bound carbonyl species that are desorbed from the catalytic surface as gaseous carbon monoxide. This route is also commonly referred to as the redox mechanism/pathway. Alternatively, the production of CO from CO_2 and H_2 can occur associatively through the intermediate formation of formate species (i.e., Path B). Through this mechanism, gaseous CO_2 is firstly hydrogenated to formate entities that enable the cleavage of the C-O bond, while H_2 activation proceeds in the same manner as in the case of the dissociative mechanism. In practice, the associatively catalyzed rWGS reaction requires the presence of a material containing two functional groups that collectively enable the activation of gas-phase H_2 as well as the scission of the carbon-oxygen bond [174,177].

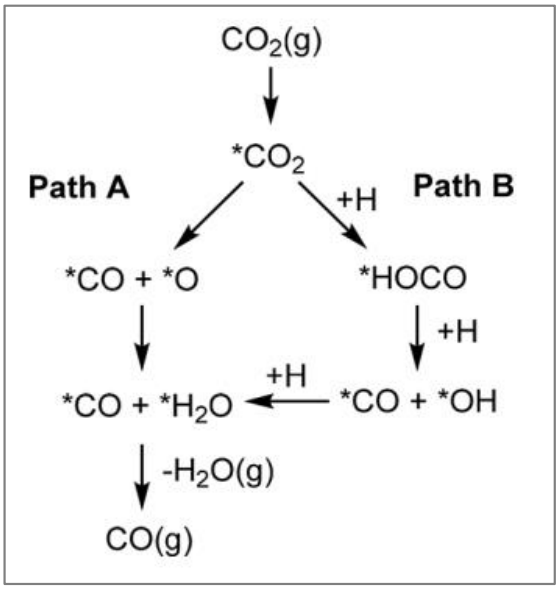

Figure 21. The main proposed pathways for the rWGS reaction. Reproduced with permission from Ref. [174]. Copyright© 2020, American Chemical Society.

Practically, the activity of a catalyst in the rWGS reaction is an unavoidably multivariable phenomenon, accounting for contributions from the hydrogenation ability of the employed active metal(s) phase, the reducibility (equivalently, the oxygen vacancy concentration) of the metal oxide support(s), the extent of metal-support interactions, the dispersion of the metallic phase, etc. In any case, however, a rather dominant feature is the adsorption/desorption affinity of the metal/support interface towards CO-like entities, *CO. Indeed, weak *CO binding generally results in facile desorption of carbonyl moieties and thus augmented gas-phase CO generation. On the other hand, stronger *CO binding in the catalytic surface is conducive to complete hydrogenation towards gaseous CH_4, effectively reducing CO selectivity [174,177]. Recently, a categorization of various rWGS catalysts based on their CO adsorption affinity was reviewed by Bahmanpour et al. [179].

From the above discussion, it is evident that ceria-based catalysts are excellent candidate materials for the rWGS reaction since they are associated with a multitude of properties that can enhance CO generation [123]. More specifically, the redox properties of cerium oxide have been shown to be indeed very advantageous for attaining high rWGS performance for many ceria-based catalysts, especially at temperatures higher than 500 °C. In this regard, the reaction over a ceria-based catalyst generally proceeds through a redox process that includes two steps, i.e., the reduction of CeO_2 by H_2 and the formation of a surface oxygen vacancy and the regeneration of the vacancy via its oxidation by CO_2 (Equations (5) and (3)) at over 300 °C [34,180]. In particular, concerning the behavior of ceria under a CO_2/H_2 mixture, the oxidation of CeO_{2-x} by CO_2 (or, equivalently, the reduction of CO_2 by CeO_{2-x}) is thermodynamically feasible even without external heat provision or under low CO_2 partial pressure [181,182]. Although there are some studies reporting on adequate rWGS performance of bare CeO_2 [183–185], its role as supporting material in a metal/ceria combination is far more prominent, as indicated by the high number of literary works examining these catalytic materials for the specific reaction. In general, the majority of works concerning the rWGS performance of ceria-based catalysts explore the addition of either Pt, Ru and Pd noble metals or late *3d*-transition metals, i.e., Ni, Cu, Co and Fe as the active phase [20,21].

Furthermore, CeO_2 holds a key role in rWGS systems via tuning effects, one aspect of which is the metal-induced adjustment of the redox capabilities of ceria via the formation of oxygen vacancies, a critical parameter for the activation of gas-phase CO_2. In the presence of metal phase sites, this process may be greatly facilitated due to their increased H_2

dissociation ability, which leads to active hydrogen adatoms that can migrate to ceria sites via the so-called spillover effect and lead to more oxygen vacancies, i.e., higher reduction degree. The above has been demonstrated in a variety of experimental works, such as [186–188]. In addition to hydrogen spillover, the incorporated metal has been shown to improve CO_2 adsorption and lower the energy barrier for CO generation via formate species [187,189]. Moreover, the higher metal dispersion induced by ceria is particularly relevant in determining the product distribution under CO_2 hydrogenation mixtures, as it has been demonstrated that large metal particles tend to favor CH_4 production, whereas highly dispersed metallic nanoparticles are selective towards CO [190,191]. Furthermore, CeO_2 can be an effective promoting material for other oxide-based rWGS catalysts, such as In_2O_3 or Ga_2O_3 [192,193], by increasing the availability of surface intermediate species such as bicarbonates. The supporting effect of CeO_2 in the rWGS reaction is even more pronounced when considering the peculiar SMSI phenomena in ceria-based systems, as stated above. Via metal-support interactions, cerium oxide is able to largely modify the electronic properties of the supported metallic phase and also affect the adsorption capacity and binding strength of the main intermediate species [194]. Elsewhere, Goguet et al. [195] have demonstrated that the rWGS reaction over Pt/CeO_2 proceeds mainly via the formation of surface carbonyls from carbonate species and the rapid reoxidation of ceria from CO_2, boosted by the high oxygen vacancy concentration of CeO_2 (Figure 22).

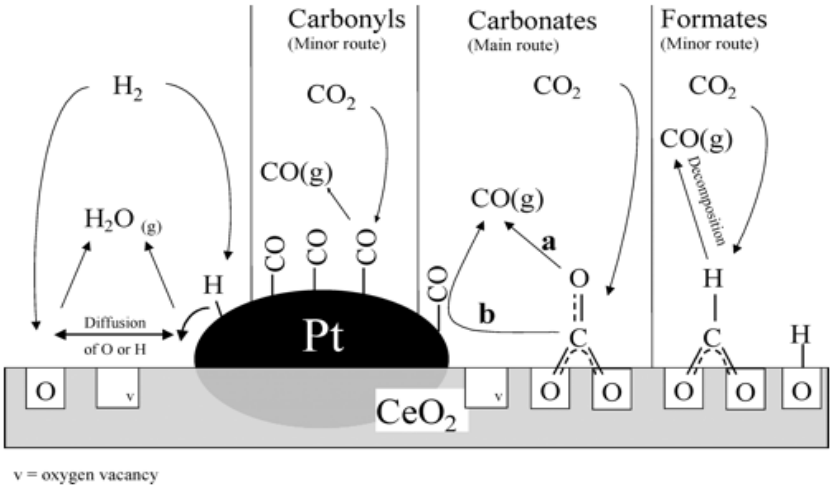

Figure 22. The proposed rWGS reaction mechanism over Pt/CeO_2. Reproduced with permission from Ref. [195]. Copyright© 2004, American Chemical Society.

As in the case of the WGS reaction, the density of oxygen vacancies for various ceria-based systems has been shown to be a strong descriptor for high rWGS catalytic performance. Specifically, an inverse CeO_2/CuO_x catalyst enhanced the formation of both mono- and di-valent copper ions, which were postulated to enhance the catalytic performance due to their ability to form surface oxygen vacancies [196]. Elsewhere [197], the high activity of a Cu/CeO_2 hollow sphere catalyst was attributed to the high oxygen vacancy density, whereas inferior performance was attained by other Cu/CeO_2 catalysts characterized by a lower density of vacancies (Figure 23), a finding also demonstrated in a study examining $Cu/CeO_{2-\delta}$, showing that Cu^0 and oxygen vacancies were the active sites [198]. Moreover, in the work by Li et al. [199], it was demonstrated by means of NAP-XPS that metallic copper and partially reduced CeO_2 associated with increased oxygen vacancies are the active sites for the CO_2-to-CO transformation over Cu/CeO_{2-x}, suggesting strong interaction between Cu and partially reduced ceria entities.

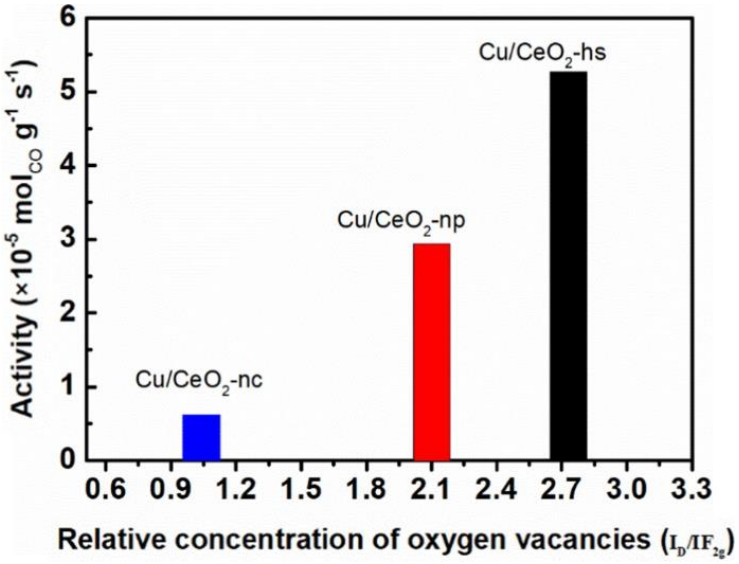

Figure 23. Effect of oxygen vacancies in the rWGS activity over Cu/CeO_2 nanoparticles. Reproduced with permission from Ref. [197]. Copyright© 2020, Elsevier.

Moreover, the redox properties and, in turn, the rWGS performance of CeO_2-based catalysts can be significantly enhanced by means of morphology/facet fine-tuning of ceria nanoparticles. Such CeO_2 nanoparticles have been studied in a variety of works, providing insights regarding the investigation of the facet dependency of the rWGS catalytic performance of ceria. It has been demonstrated that nanopolyhedral CeO_2 particles exhibit the lowest catalytic activity, whereas either nanorods [200] or nanocubes [183] or even both [184] were shown to be the most active, in general agreement with theoretical results demonstrating a lower formation energy barrier for oxygen vacancies for (100) and (110) surfaces. In a similar manner, we recently showed the increased rWGS activity of copper catalysts supported on ceria nanorods (NR) compared to the nanocubes (NC), mostly ascribed to the increased low-temperature reducibility of the Cu/CeO_2-NR sample (Figure 24) [150]. Moreover, as depicted in Figure 24c, the Cu/CeO_2-NR sample is highly active towards CO production even after 12 h at 450 °C under hydrogen excess conditions, implying the stability of Cu/CeO_2-NR samples. It should be noted, however, the ex-situ characterization of oxygen vacancies and the relatively few studies examining the morphology-dependency of the rWGS reaction over ceria-based materials have not yet elucidated the complete role of the different ceria facets in the rWGS performance of metal/nanoceria catalyst.

Moreover, besides modulating the local surface structure of ceria-based catalysts through size and shape effects methodologies, the fine-tuning of electronic structure by the addition of an appropriate promoter is another approach for boosting the rWGS activity of CeO_2-based catalytic systems. In this regard, we recently reported on the beneficial effect of Cs addition into a series of copper–ceria catalysts towards enhanced CO selectivity [201]. The addition of cesium induced a stabilization of the partially reduced copper species as well as an increase in the catalyst basicity, largely suppressing methane generation (Figure 25). This finding is in agreement with another study regarding the structural promotion of a highly active CO_2 methanation Ni catalyst supported on CeO_2 nanorods with ZnO. Notably, ZnO addition completely shifted the reaction pathway towards CO formation, ascribed to the zinc-induced modifications in redox properties and CO desorption affinity [202]. Similarly, the suppression of CO_2 methanation on Ni/CeO_2 was achieved by doping with Na, K and Cs [203]. Although all promoted catalysts exhibited electronic, structural and textural property changes compared to bare Ni/CeO_2, doping with Cs showed the optimal catalytic activity, as seen by the improved CO selectivity and stability for long-term runs in cyclable temperature ranges. Elsewhere, it was found that over a K-promoted nickel-ceria catalyst, a K/Ni ratio of one was the optimum in terms of CO_2

conversion and CO_2 methanation suppression, as well as enhanced CO selectivity [204]. The formation of CO instead of CH_4 on the catalyst surface was favored due to the electronic interactions of K-Ni and K-Ni/CeO_2. Interestingly, a linear correlation between Na content and oxygen vacancies was disclosed in Na-doped ceria catalysts, which was, in turn, responsible for the increased intrinsic rWGS activity on the highly-loaded Na-CeO_2 [167]. Moreover, the promotion of Fe/CeO_2-Al_2O_3 catalysts with either Cu, Mo or Ni showed that the highest CO yield was attained over the copper catalyst [205]. The authors ascribed this result to the strong interaction between Fe and Cu, which in turn modified the electronic density of Fe and facilitated the activation of CO_2 on the catalytic surface, as revealed by XPS. Nonetheless, it should be stated that the alkali promotion effect in CeO_2-based catalysts for the rWGS has not been extensively studied. Moreover, the promoting effect of P species was demonstrated in a novel approach regarding a Ni_2P/CeO_2 catalyst prepared using the stepwise saturated volume impregnation method [206]. Indeed, compared to conventional Ni/CeO_2, the employment of the nickel phosphide phase resulted in higher CO yield values, even under a high space velocity of 300 $L \cdot g^{-1} \cdot h^{-1}$. This was ascribed to the moderate CO_2 adsorption affinity and the simultaneously high H_2 adsorption ability of Ni_2P/CeO_2, which collectively prevented the deep hydrogenation of CO-like species to CH_4.

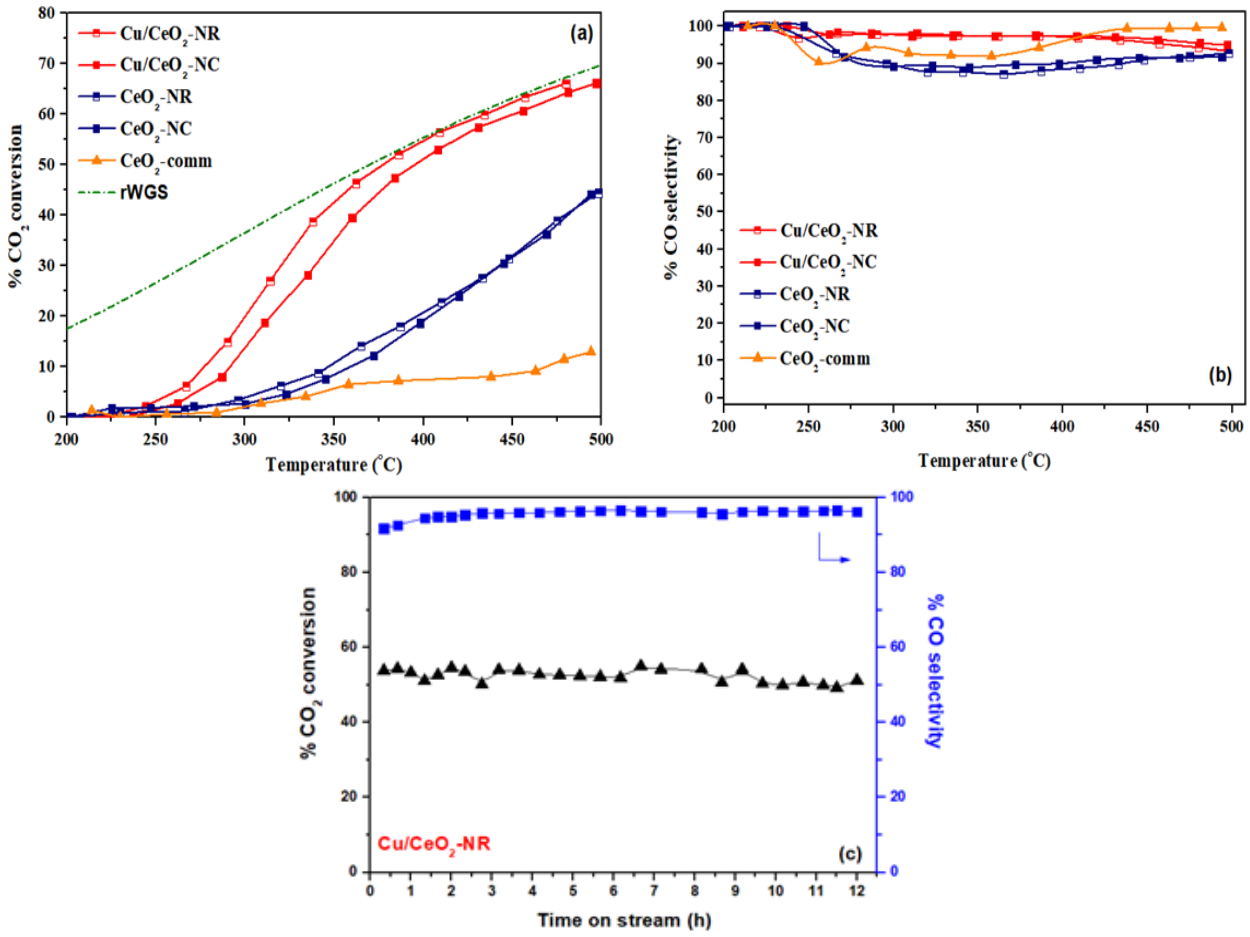

Figure 24. Values of CO_2 conversion (**a**) and CO selectivity (**b**) as a function of temperature and time on stream (**c**) for Cu/CeO_2 catalysts with variable ceria nanomorphology (NR: nanorods, NC: nanocubes). Adapted from Ref. [150]. Copyright© 2019, MDPI.

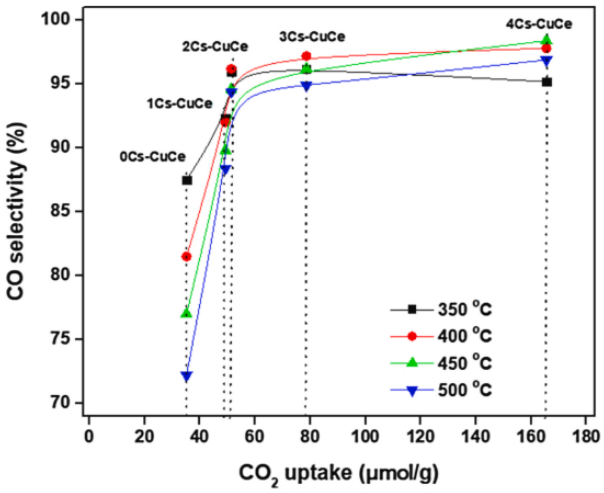

Figure 25. Correlation between CO selectivity, Cs content and total basicity of the samples in various Cs-doped Cu/CeO_2 catalysts. Reproduced with permission from Ref. [201]. Copyright© 2021, Elsevier.

In all, a summary of the most active rWGS ceria-based catalysts and the key adjusted parameter inducing high CO production is given in Table 1. It must be stated that only the state-of-the-art ceria-based catalytic systems (involving both noble and non-noble metals as active phases) have been included in this table for the sake of gaining insight into both the current advances in the field as well as into the effectiveness of the fine-tuning approaches described herein. It is evident that highly efficient rWGS catalysts, in terms of low-temperature CO_2 conversion and CO selectivity, can be obtained by combining ceria with various transition metals and concurrently adjusting their physicochemical properties by the routes highlighted above. Most importantly, from a practical perspective, NMs-free catalysts formulations with similar or even superior rWGS performance to that of NMs-based catalysts can be obtained by modulating the structural and surface characteristics. For instance, Cs-doped Cu/Ceria-nanorods exhibit superior CO yield values compared to Pt/CeO_2 under similar reaction conditions of T = 400 °C and H_2:CO_2 = 1, demonstrating the effectiveness of the rational design and optimization routes.

Table 1. State-of-the-art CeO_2-based catalysts for the rWGS reaction at 1 bar.

Sample	H_2:CO_2	T (°C)	X_{CO2} (%)	S_{CO} (%)	Adjusted Parameter	Ref.
			Noble metal-based			
RuNi/CeZr	4	350	53	93	Active metal phase	[207]
$Ru_{45}Fe_{55}/Sm\text{-}CeO_2$	1	500	23	100	Metal phase composition	[208]
$In_2O_3\text{-}CeO_2$	1	500	20	100	In/Ce ratio	[192]
$Pt/CeO_2\text{-}TiO_2$	1	500	25	99	Ce/Ti ratio	[209]
Pt/CeO_2	1	400	16	100	Calcination temperature	[187]
Pt/CeO_2-nanorods	3	400	40	94	Pt addition method	[210]
Pd/CeO_2	5	500	51	87	Active metal phase	[211]
			Transition metal-based			
CeO_2	3	550	51	-	Calcination temperature	[185]
Cu/CeO_2	3	300	18	100	Catalyst support	[188]
$Fe_{15.3}Cu_{9.4}/CeAl$	4	500	46	99	Metal promoter	[205]
$Cu/m\text{-}CeO_{2-\delta}$	4	400	43	100	Cu loading	[198]
$Cu\text{-}CeO_2$	4	340	16	100	Active metal phase	[212]
Cu/CeO_2-nanorods	4	400	38	97	CeO_2 morphology	[150]
$Cs\text{-}CuO/CeO_2$	1	450	25	97	Cs loading	[201]
$CuCeO_x$	4	400	33	100	Ce/Cu ratio	[186]
$Co\text{-}CeO_2$	1	550	29	98	Ni loading	[213]
NiFe/CeAl	4	500	60	98	Metal promoter	[214]

5.2. CeO_2-Based Catalysts for the Sabatier Reaction

The methanation of CO_2 via H_2, also called the Sabatier reaction (Equation (11)), was discovered by the French chemists Paul Sabatier and Jean-Baptiste Senderens at the start of the 20th century and was applied industrially mainly to remove traces of CO_x from the H_2-rich stream in ammonia plants. Later, the reaction was further investigated for the production of synthetic natural gas (SNG) in the 1970s oil crisis [215–217]. In the last decades, however, CO_2 methanation has again been in the spotlight, this time being the core reaction in the so-called power-to-gas scheme (alternatively termed as power-to-methane), which involves the mass production of hydrogen via RES-powered water electrolysis and the large-scale capture of CO_2 from the flue gases of hard-to-abate sectors such as cement industries or power plants (Figure 26). This route can effectively offer a simultaneous solution to excess renewable energy curtailment, valorization of CO_2 emissions, and natural gas grid stability at times when large decarbonization is practically impossible and the energy crisis has caused natural gas prices to skyrocket worldwide [172,218–221]. In addition, the reaction is also appealing for long-term outer space missions, as evidenced by the recent efforts from NASA considering the Sabatier reaction for Mars exploration, where CO_2 is abundant [222].

$$CO_2 + 4H_2 \leftrightarrow CH_4 + 2H_2O,\ \Delta H_{298K} = -164.8\ kJ/mol \quad (11)$$

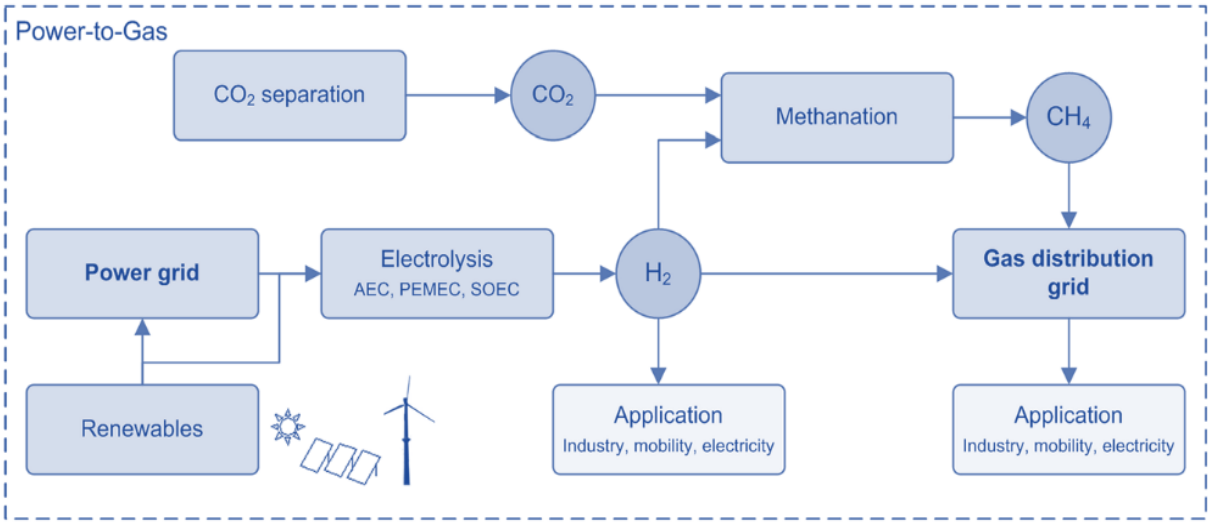

Figure 26. The power-to-gas concept. Reproduced with permission from Ref. [223]. Copyright© 2016, John Wiley and Sons.

As can be seen from Equation (11), CO_2 methanation is a highly exothermic and mole-reducing reaction; thus, it is expected thermodynamically to be favored at lower reaction temperatures and high pressure, respectively. Moreover, the presence of over-stoichiometric hydrogen in the reactor inlet (i.e., at an inlet molar ratio of H_2:CO_2 larger than 4) enhances CH_4 yield [174,224]. Indeed, it is largely reported that the operating range for industrial CO_2 methanation is mainly around 300–500 °C and 10–30 bar. However, in addition to CO_2 methanation, the rWGS reaction almost always takes place to a certain extent under a CO_x/H_2 feed, mainly due to the formation of hotspots (>500 °C) in the reactor induced by the reaction's exothermicity, leading to operation under a temperature range where CO formation is not negligible thermodynamically [172,223,225,226].

On the micro-scale, although the mechanism of the reaction of CO_2 methanation has not been unambiguously elucidated, two main pathways have been generally proposed, namely, the CO route and the formate route (Table 2). The former is associated with the initial conversion of CO_2 to intermediate carbonyl-like species (denoted as either *CO or CO-

s) via the direct dissociation of gaseous CO_2 to *CO and *O, which are fully hydrogenated towards *CH_4 that is eventually desorbed from the surface forming gas-phase methane. As for the second route, formate species (*HCOO) instead of *CO is the main intermediate observed during the reaction, followed by a reaction with chemisorbed hydrogen adatoms. With regards to the role of metal-ceria catalysts in the mechanism of hydrogen activation, it is considered that gas-phase H_2 is activated via dissociation on metal particles that are increasingly active towards hydrogen activation in the vicinity of ceria surfaces. The adsorbed hydrogen adatoms rapidly migrate to the ceria support via spillover phenomena and are able to react with low-energy and abundant C-containing intermediates onto CeO_{2-x} and result in gaseous methane molecules [227]. In general, numerous factors have been shown to affect the reaction pathway, most prominently the active metal phase nature, support topology, metal-support interphase and reaction conditions [228,229].

Table 2. Proposed elementary reaction steps for the reaction of CO_2 methanation, where "s" denotes an adsorption site onto the catalytic surface. Adapted from Ref. [228]. Copyright© 2021, Elsevier.

CO Formation Pathway	Formate Formation Pathway
(1a) H_2,g + 2s = 2H-s	(2a) H_2,g + 2s = 2H-s
(1b) CO_2,g + 2s = CO-s +O-s	(2b) CO_2,g + s = CO_2-s
(1c) CO-s = CO,g + s	(2c) CO_2-s + H-s = HCOO-s + s
(1d) CO-s + s = C-s + O-s	(2d) HCOO-s + H-s = HCO-s + OH-s
(1e) C-s + 4H-s = CH_4-s + 4s	(2e) HCO-s + H-s = CH-s + OH-s
(1f) CH_4-s = CH_4,g + 4s	(2f) CH-s + 3H-s = CH_4,g + 4s
(1g) O-s + 2H-s = H_2O-s + 2s	(2g) OH-s + H-s = H_2O,g + 2s
(1h) H_2O-s = H_2O,g + s	

As is the case for the rWGS reaction, the predominant catalyst category for CO_2 methanation also involves the participation of an active metallic phase supported on a metal oxide. In line with the above, the role of the metal phase is mainly the rapid activation of gaseous H_2, which subsequently migrates to the support, onto which the activation of gas-phase CO_2 towards reactive C-containing intermediate species takes place. In this regard, the most active metal phases reported in the literature are Ru, Rh, Ni and Co, while the most active supporting oxides are Al_2O_3, ZrO_2 and CeO_2, with bimetallic or mixed oxide catalysts, are also reported to be active in several cases [230–232]. However, Ni-based catalysts essentially dominate the relevant literary works, based on the combination of the high activity of Ni towards H_2 activation and its cost-effectiveness compared to the noble metals Ru and Rh [233].

The employment of ceria-based materials for the reaction of CO_2 methanation has been reported from as early as 1997 when for the first time, the high activity of noble metal catalysts supported on CeO_2 was demonstrated, as compared to other oxides [234]. The results had been ascribed to the increased oxygen vacancy concentration on CeO_{2-x} and their filling by the produced H_2O, explaining the transient nature of the catalytic performance. Ever since this publication, a multitude of ceria-based catalysts has been studied and found to attain higher activity in terms of both CO_2 conversion and methane selectivity compared to other oxides. In essence, transition metal sites are practically indispensable in the case of CH_4 formation via CO_2 hydrogenation since the reaction requires four times more hydrogen than the rWGS reaction, and at the same time ceria alone is not capable of substantially activating gaseous hydrogen via its dissociation, as is the well-established case over transition metals [32,235]. Despite the different results in the literature, the general consensus of the role of ceria in CO_2 methanation is to provide the catalytic system with high concentrations of oxygen vacancies and Ce^{3+} ions that are highly effective for the activation of CO_2 via a redox reaction, as well as an intrinsically active interphase near the metal active sites.

In all, the effect of the CeO_2 support (and the associated SMSI) over metal/ceria systems leads to enhanced metal dispersion, which augments the abovementioned hydrogen dissociation, enabling the complete hydrogenation of CO_2-derived intermediates and leading to enhanced CH_4 production. To this end, the majority of studies have focused on the structure-sensitivity nature of ceria-based catalysts using predominantly Ni or Ru as active metallic phases. This is largely due to SMSI phenomena occurring in Ni-CeO_2 and Ru-CeO_2 systems that result in remarkable methanation performance, especially at temperatures lower than 350 °C, evidenced by both theoretical and experimental works [20,236–239]. The interaction between Ni, Ru and CeO_2 can be enhanced by appropriately modifying the metal particle size and the oxygen vacancy density (or, equivalently, the reducibility).

Indicatively, over a series of CeO_2-supported Ru catalysts, the optimum performance was established by the catalyst with intermediate Ru particle sizes between 1 and 2 nm, owing to the compromise between the sufficiently low particle size to boost SMSI and the presence of sufficiently large Ru crystallites necessary for H_2 dissociation and spillover (Figure 27) [240]. Besides, by means of detailed in situ X-ray photoelectron spectroscopy and operando infrared spectroscopy characterizations, the key role of metal-support interactions leading to enhanced intrinsic CO_2 methanation activity was also reported in a comparative study of Co/CeO_2 and Co/SiO_2 [241]. Indeed, it was demonstrated that Co/CeO_2 was associated with a significantly higher concentration and reactivity of formates and carbonyls in the periphery of the active cobalt-ceria interphase. In the work by Ye et al. [242] comparing the CO_2 methanation performance of Ni/CeO_2 catalysts prepared by conventional impregnation and sol-gel method, the latter was characterized by the optimum nickel-ceria interactions, owing to the presence of nickel particles embedded into the CeO_2 structure and the resulting Ni-Ce-O solid solution that were crucial for the stabilization of metallic Ni nanoparticles and improved thermal stability. In a similar manner, the use of an optimal chelating ligand-to-cations ratio of 0.1 over Ni catalysts supported on Sm-doped CeO_2 can modulate metal-support interactions and, in turn, CO_2 methanation performance [243]. Elsewhere, in a study of Ni/CeO_2 catalysts with variable nickel-ceria interactions induced via different preparation protocols, the interface between NiO and CeO_2 was considered responsible for CO_2 activation, whereas metallic Ni promoted the dissociation of gaseous hydrogen [244]. Similarly, the heating method during the synthesis of Ni/CeO_2 induced changes in the SMSI phenomena, evidenced by the variabilities in Ni dispersion [245]. A structure-sensitive effect was reported since the catalyst prepared by microwave heating exhibited the strongest SMSI and, in turn, the highest turnover frequency. Intriguingly, however, in a series of Ni- and Ru-based catalysts prepared by wet impregnation [237], Ni/CeO_2 possessed the smallest and Ru/CeO_2 the largest metal particle size. Nonetheless, similar catalytic activity was attained, indicating the complex role of the support in affecting the intrinsic activity of the metal phase and, in turn, the turnover frequency. In a novel approach, the effect of support particle size was explored in a series of Ni/CeO_2-nanocubes catalysts with variable CeO_2 crystallite size and similarly sized nickel particles by changing NaOH concentration (i.e., 6, 9 and 12 M) during the synthesis of ceria nanocubes [246]. It was inferred that CO_2 methanation activity increased with decreasing ceria size (or equivalently, with decreasing NaOH concentration), attributable to the enhanced nickel-ceria interaction, leading to increased ceria reducibility and surface basicity and lower values for the apparent activation energy (Figure 28).

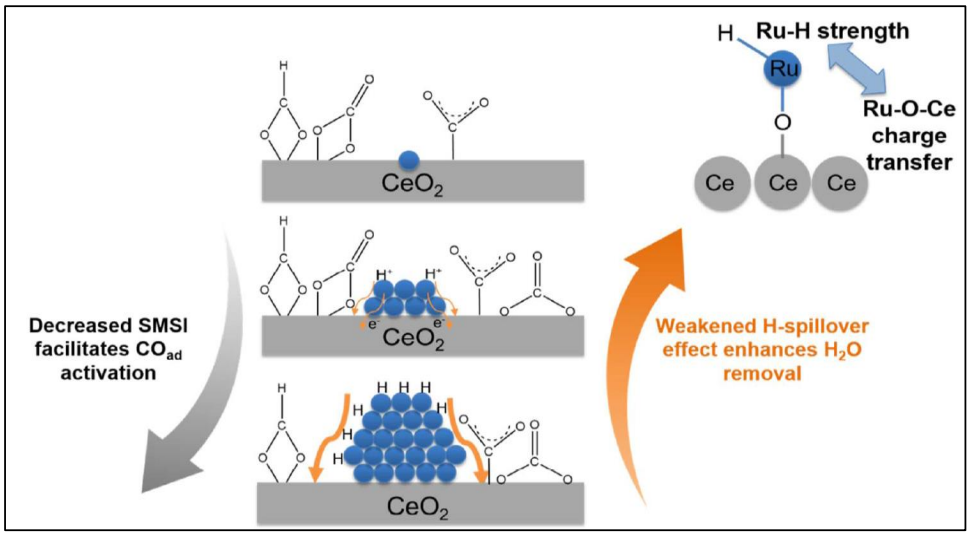

Figure 27. Schematic depiction of the competitive effects of SMSI and hydrogen spillover leading to competing activation and surface CO dehydration for CeO_2-supported Ru single atoms (up), nanoclusters (middle) and large nanoparticles (bottom). Reproduced with permission from Ref. [240]. Copyright© 2018, American Chemical Society.

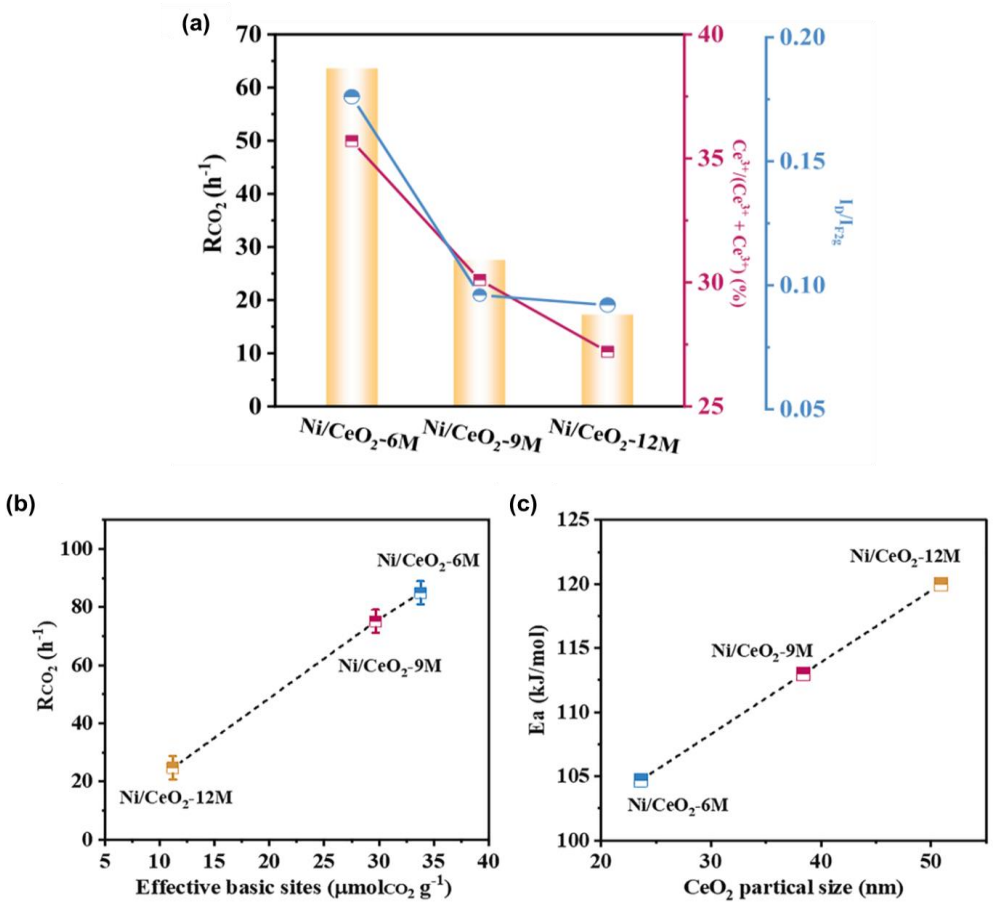

Figure 28. Correlation of turnover frequency with NaOH concentration and ceria reducibility (**a**), reaction rate at 548 K versus effective (sum of weak and medium) basic sites (**b**) and apparent activation energy values (**c**) as a function of CeO_2 nanocubes size. Reproduced with permission from Ref. [246]. Copyright© 2023, Elsevier.

In another study, the effect of oxygen vacancies was decoupled from the Ni size effect by the synthesis of Ni/CeO_2 samples with similar oxygen vacancy concentrations [247]. It was disclosed that the turnover frequency decreased with increasing Ni nanoparticle size in the range between 8 and 21 nm, highlighting the equally crucial role of geometric effects in the catalytic activity. In this regard, we recently showed that the variation of Ni loading (and, equivalently, the nickel particle size) in a series of highly active Ni/CeO_2-nanorods notably affects the catalytic performance (Figure 29) [248]. Noteworthy, Ni/CeO_2 samples with a Ni particle size of ca. 20 nm demonstrated a superior methane yield (~92% at 275 °C), one of the highest values reported so far. Interestingly, the oxygen vacancy concentration was in general agreement with the catalytic activity, highlighting the crucial role of ceria reducibility towards high methane yield values induced by the synergy of nickel-ceria species in the metal-support interphase. Even more importantly, the crucial role of under-coordinated nickel sites (i.e., corners/steps) located on larger Ni particles were revealed through a structure-sensitivity analysis. In other words, a compromise between the nickel-ceria perimeter and the competitive presence of large nickel particles is required for optimum performance.

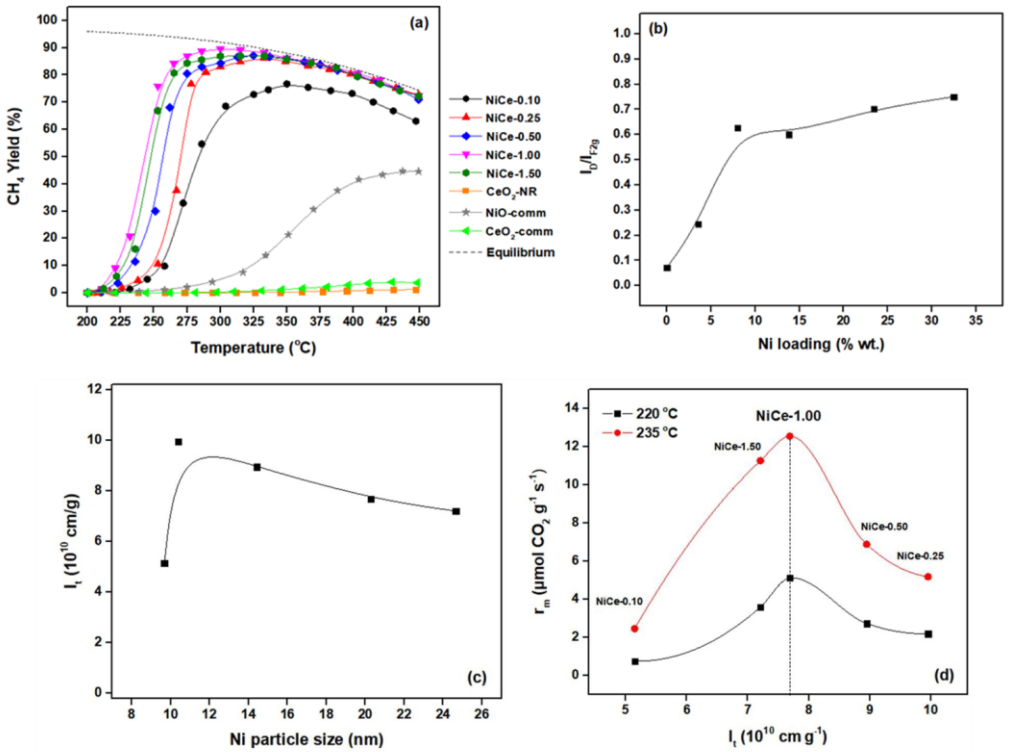

Figure 29. Methane yield (**a**), oxygen vacancy concentration (**b**), Ni particle size effect on the total nickel-ceria perimeter (**c**,**d**) relationship between the mass-normalized reaction rate and Ni-CeO_2 perimeter. Reproduced with permission from Ref. [248]. Copyright© 2021, Elsevier.

As is now evident, the effect of oxygen vacancies is rather prominent in the case of CeO_2-based CO_2 methanation catalysts, as variabilities in their population can exert significant changes in the catalytic activity [120,234]. Indicatively, the role of oxygen vacancies in CO_2 methanation was thoroughly explored by operando spectroscopy and steady-state isotope transient kinetic analysis (SSITKA) over Ru/CeO_2 and Ru/α-Al_2O_3 [249]. Markedly, CO_2 methanation proceeds via the formate route over Ru/CeO_2 (containing a large number of vacancies), and the rate-determining step is the formate dissociation to methanol, catalyzed by oxygen vacancies (Figure 30). On the contrary, the reaction pathway is completely shifted towards the CO route over the Ru surface in Ru/α-Al_2O_3 (i.e., in the absence of oxygen vacancies), showcasing the active site-dependent reaction mechanism. Moreover,

activity evaluation and the oscillating reaction over Ru/CeO_2 further corroborate that the oxygen vacancies offer a much lower activation temperature compared with the one in the case of Ru/α-Al_2O_3. Moreover, the complex roles and interplay of Ni and CeO_x species in terms of oxygen exchange kinetics were in situ explored by NAP-XPS [250]. It was disclosed that substantial oxygen exchange occurs between gas-phase species and ceria under CO_2 hydrogenation conditions. Specifically, the authors revealed that oxygen transfer progresses through a combination of two mechanisms, namely, simple hetero-exchange between one O atom from a gaseous molecule one O atom from ceria and multiple hetero-exchange between an oxygen-containing gas-phase molecule and at least two oxygen atoms of the support. Both these phenomena were accentuated by the presence of the oxygen vacancies since kinetic analysis revealed that oxygen exchange rate is fast compared to the CO_2 hydrogenation rate. In a similar manner, the catalytic activity and product selectivity were found to be ascribable to the interfacial oxygen vacancies and the structure of Ni species, respectively, in a series of Ni/CeO_2 catalysts with variable Ni particle sizes [251]. In particular, the increase in Ni loading led to a higher population of surface oxygen vacancies in the nickel-ceria interface, which resulted in higher CO_2 activation. Meanwhile, the increased Ni particle size along with more reduced nickel entities, was deemed beneficial for the increased CO binding capacity, eventually attaining higher CH_4 yield values. Elsewhere, improved CO_2 methanation performance over Ni/CeO_2 was observed precisely due to the formation of the so-called Ni-V_{ox}-Ce interfacial sites [252,253].

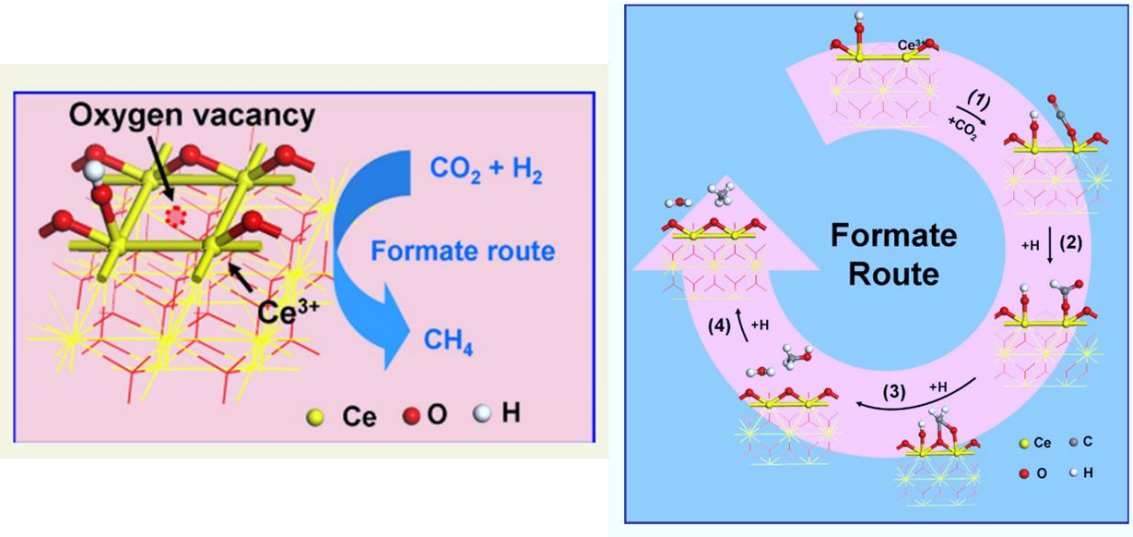

Figure 30. Schematic illustration of the formate route catalyzed by oxygen vacancies for the reaction of CO_2 methanation over Ru/CeO_2. Reproduced with permission from Ref. [249]. Copyright© 2016, American Chemical Society.

The effect of the synthesis method is another prominent way of manipulating the concentration of oxygen vacancies and the reducibility of ceria. In this regard, a series of nickel-ceria catalysts were hydrothermally prepared by varying the ethylene glycol/water ratio [238]. The variability in the solvent composition during the synthesis procedure induced changes in the oxygen vacancy concentration and in turn in the population of reducible surface sites below 450 °C, the abundance of which correlated with the catalytic activity. The effect of the synthesis method on the ceria reducibility was also demonstrated in a nickel catalyst supported on ceria-zirconia, whereby the catalyst prepared by impregnation possessed the most enhanced redox properties and increased CO_2 methanation activity [254]. In another study, the preparation of Ni/CeO_2 catalysts derived from a Ce-MOF precursor either by impregnation or by the one-pot method was explored, revealing the vital role of oxygen vacancy concentration towards optimal catalytic performance [255].

In a similar manner compared to the production of CO from CO_2 hydrogenation, the performance of ceria-based CO_2 methanation catalysts has been shown to also exhibit a degree of facet-dependency, according to the order for oxygen vacancy formation. In general, nanorod ceria particles are more active in terms of CH_4 yield, followed by nanocubes and nano-octahedra, evidenced by the observed changes in the reaction mechanism [256–260]. The relative abundance of interfacial sites is another crucial parameter that has been demonstrated to partly determine the catalytic performance, being strongly affected by the exposed crystal planes. Indeed, the following order for interfacial site concentration has been reported; Ru/CeO_2-nanorods > Ru/CeO_2-nanocubes > Ru/CeO_2-nano-octahedra, in agreement with the CH_4 selectivity values [261]. Elsewhere, the facet dependency of ceria-based catalysts was examined in terms of the effect of CeO_2 morphology in the distribution of frustrated Lewis pair (FLP) structures [262]. By means of systematical ex-situ and in-situ surface analysis in combination with DFT calculations, it was demonstrated that Ni/CeO_2-nanorods possessed the highest potential for FLP construction, which in turn resulted in the optimum CO_2 conversion to CH_4 via the cooperation of O_V and OH species, along with the co-promotion of the emerged CO* route and formate pathway. Notably, in all the above studies, the catalyst possessing the most defective structure was the most active, although this catalyst was not always a nanorod sample, a finding deriving from the inherent variability of the defective structure of ceria nanorods, as the synthesis method affects the growth direction, exposed facets and the abundance of defects [263]. In this regard, the morphology effect of CeO_2 nanoparticles was examined in Ni-based catalysts prepared hydrothermally [264], whereby the catalyst supported on ceria nanopolyhedra attained the highest CO_2 methanation activity, owing to the relatively high surface area and low-temperature reducibility. At the same time, although the strongest SMSI were reported for the nanorod catalyst, this exerted a detrimental effect regarding the catalytic activity. In a similar manner, Ni/CeO_2 nanoparticles with exposed (111) crystal planes exhibited superior CO_2 methanation performance compared to other distinct morphologies (rod, cubic, octahedron), ascribed mainly to their excellent reduction ability [160]. It is also worth noticing that exceptional thermal stability and sintering resistance was disclosed for all Ni-based catalysts, independent of nanoceria morphology.

Another topic that requires attention on the basis of ceria-catalyzed CO_2 methanation is the employment of promoting substances. Aliovalent doping can alter the selectivity and product distribution as well as the catalytic stability in CO_2 methanation. For instance, our research group has recently shown [202] that the addition of Zn into Ni/CeO_2 led to a complete change in the reaction pathway, with $Ni/ZnO\text{-}CeO_2$ being very selective towards CO, in complete contrast to the high CO_2-to-CH_4 activity of Ni/CeO_2. This finding was attributed to the zinc-induced changes in the nickel-ceria catalyst, namely, a decrease in the BET surface area, surface basicity, low-temperature reducibility and CO desorption affinity, collectively disfavoring the complete hydrogenation of CO-like species towards CH_4 (Figure 31). Elsewhere, Mn or In were used as dopants in Ni/CeO_2, revealing that methane was the main product in the Mn-doped catalyst and CO in the In-doped one, with Mn or In doping increasing the catalyst's surface area and pore volume while generating more surface oxygen vacancies [265]. In effect, the reducibility of Ni species was modified, with Mn species facilitating the reduction of nickel, as opposed to the indium-containing catalyst. Furthermore, adding cobalt in Ni/CeO_2 catalysts significantly enhanced CO_2 conversion and methane selectivity, with the $CoNi/CeO_2$ catalyst exhibiting the highest amount of medium basic sites and the optimum performance in both plasma and non-plasma reactions [266]. In this regard, europium ions (Eu^{3+}) were introduced into a nickel-ceria catalyst with the scope of the enhancement of metal-support interactions. Indeed, Eu doping led to higher Ni dispersion, thus creating more interfacial sites and significantly enhancing the low-temperature activity [267].

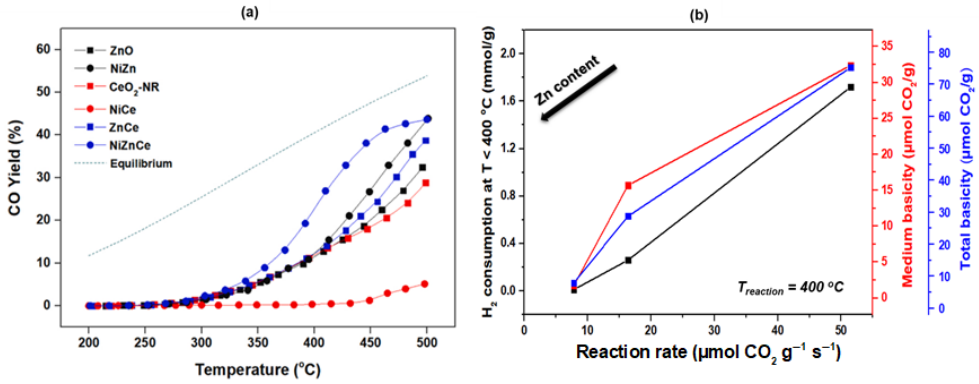

Figure 31. Temperature-dependent CO yield values (**a**) and correlation of reaction rate with reducibility and basicity (**b**) for Ni/CeO_2-NR, Ni/ZnO and Ni/ZnO-CeO_2-NR catalysts, where NR: nanorods. Adapted from Ref. [202]. Copyright© 2022, Elsevier.

Elsewhere, the low-temperature CO_2 methanation over Ni/CeO_2 was enhanced through a novel approach involving the regulation of the rate-determining step through the increase in surface oxygen vacancies and medium-strength surface basic sites on the support [268]. This was achieved by doping ceria with La species, resulting in the formation of a La-Ce-O solid solution with a thin layer of $La_2O_2CO_3$ on the surface, thereby facilitating the adsorption and direct dissociation of CO_2 (Figure 32). Similar results were attained over vacancy-engineered Ni/CeO_2 catalysts doped with yttria, whereby the introduction of Y_2O_3 to CeO_2 enhances surface oxygen vacancies generation under reaction conditions [269]. The authors also conducted a spectrokinetic analysis, further revealing the promoting role of these sites towards the direct dissociation of carbon dioxide, which is kinetically a more favorable step compared to the associative route. In another work, Sn was used as a dopant in the synthesis of typical CO_2 methanation nickel-ceria catalysts in order to examine the importance of interface microstructure on CO_2 hydrogenation reactivity [270]. The strong interaction between Sn cations and Ni species in Ni/$Ce_{0.9}Sn_{0.1}O_x$ resulted in the formation of a complex Ni-O-Sn-O-Ce interface, which was distinctly different from the Ni-O-Ce interface in Ni/CeO_2. CO_2 chemisorption, as well as HCO_3* generation, was decreased due to the enrichment of surface acidic Sn cations on Ni/$Ce_{0.9}Sn_{0.1}O_x$, thus inhibiting the formate path for CH_4. Conversely, the presence of interface Sn cations favored carbonates generation, thus promoting CO yield.

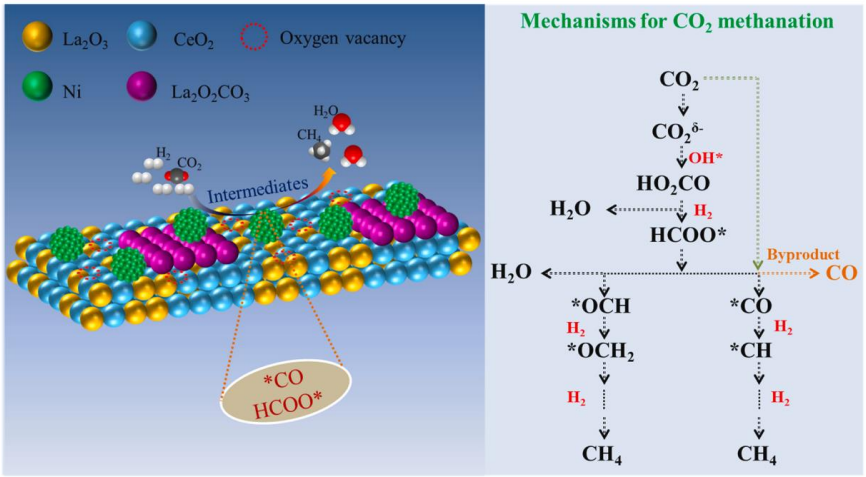

Figure 32. The main CO_2 methanation route over Ni/CeO_2-La-600, where CeO_2-La-600 denotes La species introduced into CeO_2 support and calcined at 600 °C. Reproduced with permission from Ref. [268]. Copyright© 2022, Elsevier.

Collectively, a summary of the state-of-the-art ceria-based catalysts employed for stoichiometric CO_2 methanation is shown in Table 3, where a remark regarding the adjusted parameter for enhancing the catalytic activity in each study is shown. In essence, the catalysts are representatively categorized as those containing Ru (noble metal) and Ni (non-noble metal) since they are by far the most dominant and active catalysts in the literature.

Table 3. State-of-the-art CeO_2-based catalysts for stoichiometric CO_2 methanation at 1 bar.

Sample	T (°C)	X_{CO2} (%)	S_{CH4} (%)	Adjusted Parameter	Ref.
			Ru-based		
$Ru/CeO_2/Al_2O_3$	300	83	100	CeO_2 content	[271]
Ru/CeO_2	300	83	99	Support nature	[235]
$Ru\text{-}Ni/Ce_{0.9}Zr_{0.1}O_2$	230	98	100	Ru loading	[272]
Ru/CeO_2	350	78	99	Support nature	[237]
Ru/CeO_2	300	82	98	Ru particle size	[240]
			Ni-based		
Ni/CeO_2-nanorods	300	91	100	Ni loading/support morphology	[248]
Ni/CeO_2	300	90	100	Support nature	[273]
Ni/CeO_2	300	86	99	Ni addition method	[274]
$Ni\text{-}CeO_2/MCM\text{-}41$	380	86	100	CeO_2 content	[275]
$Ni/La\text{-}CeO_2$	300	88	99	Support calcination temperature	[268]
Ni-Ce/rGO	350	85	99	Mixed support nature	[276]
Ni/CeO_2	340	91	100	CeO_2 synthesis method	[277]

By comparing the state-of-the-art catalysts for ambient-pressure CO_2 methanation under a stoichiometric reactant ratio, it could be inferred that highly active non-noble metal catalysts can be obtained by adjusting the aforementioned activity descriptors by means of appropriate synthesis and modification routes. For instance, by concomitantly modulating the Ni particle size and ceria support morphology [248], extremely active composites can be obtained with similar or even superior reactivity to state-of-the-art Ru-based catalysts.

6. Conclusions and Perspectives

The role of cerium oxide in the field of environmentally related heterogeneous catalysis has, by all means, become prominent over the last decades, evidenced by the voluminous amount of scientific literature with regard to the applications of ceria-based catalytic composites in several reactions. In this regard, CeO_2-based materials constitute, by now, the state-of-the-art catalysts for three-way converters as well as soot combustion and CO oxidation. The improved catalytic performance of these materials stems from the multitude of intriguing properties of CeO_2, most prominently its augmented redox capabilities arising from the rapid interchangeability between Ce^{3+} and Ce^{4+} with the concurrent facile formation of oxygen vacancies, as well as the metal-support interactions that generate intrinsically active interphases in the metal-ceria nexus that can effectively activate the gaseous reactant molecules. Moreover, the facile and tunable surface chemistry and local structure of CeO_2 nanoparticles can potentially lead to finely tuned catalytic materials that are associated with augmented characteristics depending on the target application.

Specifically, and as has been reviewed in the present work, several methodologies have been applied so far toward enhancing the catalytic performance of CeO_2-supported catalysts. These fine-tuning strategies essentially exploit the already mentioned properties of the oxide of cerium and its combination with one or more metallic active phases and can be contextualized as part of an overall structure/surface functionalization. In other words, size and shape engineering in conjunction with promotion/doping can exert profound changes in the redox properties and metal-ceria interactions and can collectively be regarded as an excellent and rather facile adjustment tool for the synthesis of CeO_2-based materials with increased performance and characteristics pertaining to the selected catalytic application.

Advancing from the above, the extent to which ceria may constitute an important component in the general field of heterogeneous catalysis is still an open question and can be very well exemplified by its role in the thermocatalytic CO_2 hydrogenation towards CO or CH_4 production. Indeed, even though the reverse water–gas shift reaction and CO_2 methanation have been known and studied for decades, they have attracted great interest, particularly in the last years, within the context of CO_2 emissions mitigation and excess renewable energy curtailment. As is the case with the majority of chemical reactions, however, the phasing away of noble metal-based catalysts is one of the Holy Grails of the field of heterogeneous catalysis, despite their increased performance and stability compared to less costly or non-critical materials. In this regard and precisely due to its peculiar properties, ceria-based oxides have emerged as promising candidate compounds for the complete substitution of noble metals in highly efficient CO_2 hydrogenation catalysts, evidenced by the similar or superior performance of "fine-tuned" transition metal-based catalysts supported on ceria, most prominently Ni/CeO_2 for CO_2 methanation and Cu/CeO_2 for rWGS reaction. Equally importantly, the conclusions that can be drawn from the detailed study of ceria-supported catalysts for CO_2 hydrogenation via the identification of the key activity descriptors and fine-tuning strategies can be transferred to other important reactions governed by similar underlying phenomena (e.g., reactions progressing via a Mars–van Krevelen mechanism), indicatively dry methane reforming, Fischer–Tropsch synthesis or ethanol steam reforming.

Nonetheless, although a great deal of activity descriptors have been identified and studied regarding ceria-based catalysts for numerous environmentally relevant chemical reactions probed herein by CO_2 hydrogenation, the extent to which these properties actually contribute to the reaction mechanism is still a rather nascent field compared to other well-established and commercial catalysts. With this in mind and considering the rapid development of advanced characterization technologies, in-situ/operando techniques need to be employed in order to monitor in real-time the dynamic evolution of the structure of active sites (e.g., dynamic OSC measurements, CO adsorption/desorption affinity or metal-ceria solid solution formation) under actual reaction conditions, to identify the rate-determining step and to elucidate possible structure–sensitivity relationships. In this regard, even more dedicated functionalization synthesis protocols can be applied, with the scope of fully identifying the nature and local geometry of the metal-ceria active sites with the highest intrinsic activity and facilitating their stabilization towards maximizing the production of either CO or CH_4.

Lastly, in spite of the plethora of published scientific works for ceria-catalyzed CO_2 hydrogenation, there is always room for further analysis. In this regard, it should be mentioned that the majority of studies examining size effects focus on the variations of metal particle size in more or less similarly sized ceria crystallites. Although this is an important parameter by itself and can lead to important conclusions regarding the effect of metal loading and/or particle size in the metal-ceria interphase and taking into consideration the tunable nature of ceria nanoparticles, the fabrication of metal/ceria catalysts with specific metal loading supported on variable CeO_2 sizes would provide valuable insights towards structure-sensitivity relationships that are decoupled from size effects on the metallic phase side, arising from different degree of MSIs induced by the local geometry of CeO_2 crystallites. Moreover, the synthesis of bi- or tri-metallic formulations based on the aforementioned fine-tuning strategies can greatly alter the reaction pathway and completely shift the products of the CO_2 hydrogenation reaction to either CO or CH_4. Lastly, the modification of metal dispersion using advanced synthesis methods, dispersing agents, and special pretreatment protocols can exert a profound influence on local surface chemistry and metal-support interactions with direct implications on activity/selectivity. As a general conclusion remark, it could be stated that mechanistic understanding at an atomic level under reaction conditions in conjunction with the offered fine-tuning strategies can provide cost-efficient and highly active earth-abundant metal oxide systems, not only for CO_2 hydrogenation process but for various energy and environmental applications.

Author Contributions: Conceptualization, G.V. and M.K.; methodology, G.V. and M.K.; validation, G.V., M.K. and G.E.M.; formal analysis, G.V. and M.L.; investigation, G.V. and M.L.; resources, G.E.M.; data curation, G.V. and M.L.; writing—original draft preparation, G.V. and M.L.; writing—review and editing, M.K.; supervision, M.K. and G.E.M.; project administration, G.E.M. and M.K.; funding acquisition, G.E.M. All authors have read and agreed to the published version of the manuscript.

Funding: This research has been co-financed by the European Union NextGenerationEU under the call RESEARCH-CREATE-INNOVATE 16971 Recovery and Resilience Facility (project code: TAEDK-06169).

Data Availability Statement: Not applicable.

Conflicts of Interest: The authors declare no conflict of interest.

References

1. Cormack, A.N.; Lamphier, S.; Wang, B.; Gubb, T.; Reed, K. Simulations of ceria nanoparticles. *Proc. R. Soc. A* **2015**, *471*, 20150218. [CrossRef]
2. Scirè, S.; Palmisano, L. 1—Cerium and cerium oxide: A brief introduction. In *Cerium Oxide (CeO_2): Synthesis, Properties and Applications*; Elsevier Inc.: Amsterdam, The Netherlands, 2020; pp. 1–12. [CrossRef]
3. Hedrick, J.B.; Sinha, S.P. Cerium-based polishing compounds: Discovery to manufacture. *J. Alloy. Compd.* **1994**, *207–208*, 377–382. [CrossRef]
4. Kilbourn, B.T. Cerium and Cerium Compounds. In *Kirk-Othmer Encyclopedia of Chemical Technology*; John Wiley & Sons, Inc.: Hoboken, NJ, USA, 2011. [CrossRef]
5. Finny, A.S.; Othman, A.; Andreescu, S. 7—Cerium oxide nanoparticles for chemical and biological sensors: Properties, sensing designs, and applications. In *Cerium Oxide (CeO_2): Synthesis, Properties and Applications*; Elsevier Inc.: Amsterdam, The Netherlands, 2020; pp. 259–277. [CrossRef]
6. Shcherbakov, A.B.; Zholobak, N.M.; Ivanov, V.K. 8—Biological, biomedical and pharmaceutical applications of cerium oxide. In *Cerium Oxide (CeO_2): Synthesis, Properties and Applications*; Elsevier Inc.: Amsterdam, The Netherlands, 2020; pp. 279–358. [CrossRef]
7. Yang, J.; Ji, B.; Si, J.; Zhang, Q.; Yin, Q.; Xie, J.; Tian, C. Synthesis and properties of ceria based electrolyte for IT-SOFCs. *Int. J. Hydrog. Energy* **2016**, *41*, 15979–15984. [CrossRef]
8. Prashanth Kumar, V.; Reddy, Y.S.; Kistaiah, P.; Prasad, G.; Vishnuvardhan Reddy, C. Thermal and electrical properties of rare-earth co-doped ceria ceramics. *Mater. Chem. Phys.* **2008**, *112*, 711–718. [CrossRef]
9. Singh, K.R.B.; Nayak, V.; Sarkar, T.; Singh, R.P. Cerium oxide nanoparticles: Properties, biosynthesis and biomedical application. *RSC Adv.* **2020**, *10*, 27194–27214. [CrossRef]
10. Budavari, S. *The Merck Index: An Encyclopedia of Chemicals, Drugs, and Biologicals*, 13th ed.; O'Neil, M.J., Ed.; Merck & Company, Incorporated: Rahway, NJ, USA, 2001; ISBN 9780911910131.
11. Krishnamurthy, N.; Gupta, C.K. *Extractive Metallurgy of Rare Earths*, 2nd ed; CRC Press: Boca Raton, FL, USA, 2016; ISBN 9781466576346.
12. Chakhmouradian, A.R.; Wall, F. Rare Earth Elements: Minerals, Mines, Magnets (and More). *Elements* **2012**, *8*, 333–340. [CrossRef]
13. Reinhardt, K.; Winkler, H. Cerium Mischmetal, Cerium Alloys, and Cerium Compounds. In *Ullmann's Encyclopedia of Industrial Chemistry*; Wiley-VCH Verlag GmbH & Co. KGaA: Weinheim, Germany, 2000. [CrossRef]
14. Mullins, D.R. The surface chemistry of cerium oxide. *Surf. Sci. Rep.* **2015**, *70*, 42–85. [CrossRef]
15. Razmgar, K.; Altarawneh, M.; Oluwoye, I.; Senanayake, G. Ceria-Based Catalysts for Selective Hydrogenation Reactions: A Critical Review. *Catal. Surv. Asia* **2021**, *25*, 27–47. [CrossRef]
16. Aneggi, E.; De Leitenburg, C.; Boaro, M.; Fornasiero, P.; Trovarelli, A. 3—Catalytic applications of cerium dioxide. In *Cerium Oxide (CeO_2): Synthesis, Properties and Applications*; Elsevier Inc.: Amsterdam, The Netherlands, 2020; pp. 45–108. [CrossRef]
17. Trovarelli, A. *Catalysis by Ceria and Related Materials*, 2nd ed; Trovarelli, A., Fornasiero, P., Eds.; World Scientific: Singapore, 2013; ISBN 978-1-84816-963-0.
18. Melchionna, M.; Fornasiero, P. The role of ceria-based nanostructured materials in energy applications. *Mater. Today* **2014**, *17*, 349–357. [CrossRef]
19. Huang, X.; Zhang, K.; Peng, B.; Wang, G.; Muhler, M.; Wang, F. Ceria-Based Materials for Thermocatalytic and Photocatalytic Organic Synthesis. *ACS Catal.* **2021**, *11*, 9618–9678. [CrossRef]
20. Chang, K.; Zhang, H.; Cheng, M.; Lu, Q. Application of Ceria in CO_2 Conversion Catalysis. *ACS Catal.* **2020**, *10*, 613–631. [CrossRef]
21. Wang, F.; Wei, M.; Evans, D.G.; Duan, X. CeO_2-based heterogeneous catalysts toward catalytic conversion of CO_2. *J. Mater. Chem. A* **2016**, *4*, 5773–5783. [CrossRef]
22. Xu, Y.; Mofarah, S.S.; Mehmood, R.; Cazorla, C.; Koshy, P.; Sorrell, C.C. Design strategies for ceria nanomaterials: Untangling key mechanistic concepts. *Mater. Horiz.* **2021**, *8*, 102–123. [CrossRef]

23. Capdevila-Cortada, M.; Vilé, G.; Teschner, D.; Pérez-Ramírez, J.; López, N. Reactivity descriptors for ceria in catalysis. *Appl. Catal. B Environ.* **2016**, *197*, 299–312. [CrossRef]
24. Grasselli, R.K. Fundamental Principles of Selective Heterogeneous Oxidation Catalysis. *ChemInform* **2003**, *34*, 79–88. [CrossRef]
25. Zhao, P.; Qin, F.; Huang, Z.; Sun, C.; Shen, W.; Xu, H. Morphology-dependent oxygen vacancies and synergistic effects of Ni/CeO_2 catalysts for N_2O decomposition. *Catal. Sci. Technol.* **2018**, *8*, 276–288. [CrossRef]
26. Yuan, K.; Guo, Y.; Lin, Q.-L.; Huang, L.; Ren, J.-T.; Liu, H.-C.; Yan, C.-H.; Zhang, Y.-W. Size effect-tuned water gas shift reaction activity and pathway on ceria supported platinum catalysts. *J. Catal.* **2021**, *394*, 121–130. [CrossRef]
27. Ullah, N.; Tang, R.; Li, Z. Nanostructured Ceria-zirconia Supported Ni Catalysts for High Performance CO_2 Methanation: Phase and morphology effect on activity. *J. Taiwan Inst. Chem. Eng.* **2022**, *134*, 104317. [CrossRef]
28. Rajkumar, T.; Sápi, A.; Ábel, M.; Kiss, J.; Szenti, I.; Baán, K.; Gómez-Pérez, J.F.; Kukovecz, Á.; Kónya, Z. Surface Engineering of CeO_2 Catalysts: Differences Between Solid Solution Based and Interfacially Designed $Ce_{1-x}M_xO_2$ and MO/CeO_2 (M = Zn, Mn) in CO_2 Hydrogenation Reaction. *Catal. Lett.* **2021**, *151*, 3477–3491. [CrossRef]
29. Konsolakis, M.; Lykaki, M. Recent advances on the rational design of non-precious metal oxide catalysts exemplified by CuO_x/CeO_2 binary system: Implications of size, shape and electronic effects on intrinsic reactivity and metal-support interactions. *Catalysts* **2020**, *10*, 160. [CrossRef]
30. Konsolakis, M. The role of Copper–Ceria interactions in catalysis science: Recent theoretical and experimental advances. *Appl. Catal. B Environ.* **2016**, *198*, 49–66. [CrossRef]
31. Du, X.; Zhang, D.; Shi, L.; Gao, R.; Zhang, J. Morphology dependence of catalytic properties of Ni/CeO_2 nanostructures for carbon dioxide reforming of methane. *J. Phys. Chem. C* **2012**, *116*, 10009–10016. [CrossRef]
32. Schweke, D.; Shelly, L.; Ben David, R.; Danon, A.; Kostirya, N.; Hayun, S. Comprehensive Study of the Ceria-H_2 System: Effect of the Reaction Conditions on the Reduction Extent and Intermediates. *J. Phys. Chem. C* **2020**, *124*, 6180–6187. [CrossRef]
33. Bumajdad, A.; Eastoe, J.; Mathew, A. Cerium oxide nanoparticles prepared in self-assembled systems. *Adv. Colloid Interface Sci.* **2009**, *147–148*, 56–66. [CrossRef]
34. Ma, Y.; Gao, W.; Zhang, Z.; Zhang, S.; Tian, Z.; Liu, Y.; Ho, J.C.; Qu, Y. Regulating the surface of nanoceria and its applications in heterogeneous catalysis. *Surf. Sci. Rep.* **2018**, *73*, 1–36. [CrossRef]
35. Wu, K.; Sun, L.-D.; Yan, C.-H. Recent Progress in Well-Controlled Synthesis of Ceria-Based Nanocatalysts towards Enhanced Catalytic Performance. *Adv. Energy Mater.* **2016**, *6*, 1600501. [CrossRef]
36. Li, J.; Zhang, Z.; Tian, Z.; Zhou, X.; Zheng, Z.; Ma, Y.; Qu, Y. Low pressure induced porous nanorods of ceria with high reducibility and large oxygen storage capacity: Synthesis and catalytic applications. *J. Mater. Chem. A* **2014**, *2*, 16459–16466. [CrossRef]
37. Li, P.; Chen, X.; Li, Y.; Schwank, J.W. A review on oxygen storage capacity of CeO_2-based materials: Influence factors, measurement techniques, and applications in reactions related to catalytic automotive emissions control. *Catal. Today* **2019**, *327*, 90–115. [CrossRef]
38. Boaro, M.; Giordano, F.; Recchia, S.; Santo, V.D.; Giona, M.; Trovarelli, A. On the mechanism of fast oxygen storage and release in ceria-zirconia model catalysts. *Appl. Catal. B Environ.* **2004**, *52*, 225–237. [CrossRef]
39. Duprez, D.; Descorme, C.; Birchem, T.; Rohart, E. Oxygen storage and mobility on model three-way catalysts. *Top. Catal.* **2001**, *16*, 49–56. [CrossRef]
40. Montini, T.; Melchionna, M.; Monai, M.; Fornasiero, P. Fundamentals and Catalytic Applications of CeO_2-Based Materials. *Chem. Rev.* **2016**, *116*, 5987–6041. [CrossRef]
41. Tauster, S.J.; Fung, S.C.; Garten, R.L. Strong metal-support interactions. Group 8 noble metals supported on titanium dioxide. *J. Am. Chem. Soc.* **1978**, *100*, 170–175. [CrossRef]
42. Bernal, S.; Calvino, J.J.; Cauqui, M.A.; Gatica, J.M.; Larese, C.; Pérez Omil, J.A.; Pintado, J.M. Some recent results on metal/support interaction effects in NM/CeO_2 (NM: Noble metal) catalysts. *Catal. Today* **1999**, *50*, 175–206. [CrossRef]
43. Parastaev, A.; Muravev, V.; Huertas Osta, E.; Van Hoof, A.J.F.; Kimpel, T.F.; Kosinov, N.; Hensen, E.J.M. Boosting CO_2 hydrogenation via size-dependent metal–support interactions in cobalt/ceria-based catalysts. *Nat. Catal.* **2020**, *3*, 526–533. [CrossRef]
44. Pacchioni, G. Electronic interactions and charge transfers of metal atoms and clusters on oxide surfaces. *Phys. Chem. Chem. Phys.* **2013**, *15*, 1737. [CrossRef]
45. Hermes, E.D.; Jenness, G.R.; Schmidt, J.R. Decoupling the electronic, geometric and interfacial contributions to support effects in heterogeneous catalysis. *Mol. Simul.* **2015**, *41*, 123–133. [CrossRef]
46. Campbell, C.T. Electronic perturbations. *Nat. Chem.* **2012**, *4*, 597–598. [CrossRef]
47. Zhou, Y.; Nakashima, M.; White, J.M. Interaction of platinum with ceria and silica. *J. Phys. Chem.* **1988**, *92*, 812–818. [CrossRef]
48. Akalay, I.; Guilleux, M.-F.; Tempère, J.-F.; Delafosse, D. Effects of the oxidation state of cerium on the reactivity and sulphur resistance of Ni^0/zeolite, Ni^0/silica and Ni^0/CeO_2 catalysts in butane hydrogenolysis. *J. Chem. Soc. Faraday Trans. 1 Phys. Chem. Condens. Phases* **1987**, *83*, 1137. [CrossRef]
49. Senanayake, S.D.; Rodriguez, J.A.; Stacchiola, D. Electronic metal-support interactions and the production of hydrogen through the water-gas shift reaction and ethanol steam reforming: Fundamental studies with well-defined model catalysts. *Top. Catal.* **2013**, *56*, 1488–1498. [CrossRef]
50. James, T.E.; Hemmingson, S.L.; Ito, T.; Campbell, C.T. Energetics of Cu Adsorption and Adhesion onto Reduced CeO_2(111) Surfaces by Calorimetry. *J. Phys. Chem. C* **2015**, *119*, 17209–17217. [CrossRef]

51. Zhou, J.; Gao, Z.; Xiang, G.; Zhai, T.; Liu, Z.; Zhao, W.; Liang, X.; Wang, L. Interfacial compatibility critically controls Ru/TiO_2 metal-support interaction modes in CO_2 hydrogenation. *Nat. Commun.* **2022**, *13*, 327. [CrossRef] [PubMed]
52. Van Deelen, T.W.; Hernández Mejía, C.; De Jong, K.P. Control of metal-support interactions in heterogeneous catalysts to enhance activity and selectivity. *Nat. Catal.* **2019**, *2*, 955–970. [CrossRef]
53. Sun, X.-C.; Yuan, K.; Hua, W.-D.; Gao, Z.-R.; Zhang, Q.; Yuan, C.-Y.; Liu, H.-C.; Zhang, Y.-W. Weakening the Metal–Support Interactions of M/CeO_2 (M = Co, Fe, Ni) Using a NH_3-Treated CeO_2 Support for an Enhanced Water–Gas Shift Reaction. *ACS Catal.* **2022**, *12*, 11942–11954. [CrossRef]
54. Twigg, M.V. Catalytic control of emissions from cars. *Catal. Today* **2011**, *163*, 33–41. [CrossRef]
55. Heck, R.M.; Farrauto, R.J. Automobile exhaust catalysts. *Appl. Catal. A Gen.* **2001**, *221*, 443–457. [CrossRef]
56. Mock, S.A.; Sharp, S.E.; Stoner, T.R.; Radetic, M.J.; Zell, E.T.; Wang, R. CeO_2 nanorods-supported transition metal catalysts for CO oxidation. *J. Colloid Interface Sci.* **2016**, *466*, 261–267. [CrossRef]
57. Rodriguez, J.A.; Grinter, D.C.; Liu, Z.; Palomino, R.M.; Senanayake, S.D. Ceria-based model catalysts: Fundamental studies on the importance of the metal-ceria interface in CO oxidation, the water-gas shift, CO_2 hydrogenation, and methane and alcohol reforming. *Chem. Soc. Rev.* **2017**, *46*, 1824–1841. [CrossRef]
58. Guo, Y.; Liu, Z.; Zhang, F.; Wang, D.-J.; Yuan, K.; Huang, L.; Liu, H.-C.; Senanayake, S.D.; Rodriguez, J.A.; Yan, C.-H.; et al. Modulation of the Effective Metal-Support Interactions for the Selectivity of Ceria Supported Noble Metal Nanoclusters in Atmospheric CO_2 Hydrogenation. *ChemCatChem* **2021**, *13*, 874–881. [CrossRef]
59. Reddy, B.M.; Thrimurthulu, G.; Katta, L. Design of Efficient $Ce_xM_{1-x}O_{2-\delta}$ (M = Zr, Hf, Tb and Pr) Nanosized Model Solid Solutions for CO Oxidation. *Catal. Lett.* **2011**, *141*, 572–581. [CrossRef]
60. Balducci, G.; Islam, M.S.; Kašpar, J.; Fornasiero, P.; Graziani, M. Bulk Reduction and Oxygen Migration in the Ceria-Based Oxides. *Chem. Mater.* **2000**, *12*, 677–681. [CrossRef]
61. Balducci, G.; Kašpar, J.; Fornasiero, P.; Graziani, M.; Islam, M.S. Surface and Reduction Energetics of the CeO_2-ZrO_2 Catalysts. *J. Phys. Chem. B* **1998**, *102*, 557–561. [CrossRef]
62. Möller, R.; Votsmeier, M.; Onder, C.; Guzzella, L.; Gieshoff, J. Is oxygen storage in three-way catalysts an equilibrium controlled process? *Appl. Catal. B Environ.* **2009**, *91*, 30–38. [CrossRef]
63. Yentekakis, I.V.; Konsolakis, M. Three Way Catalysis. In *Perovskites and Related Mixed Oxides: Concepts and Applications*; Granger, P., Parvulescu, V.I., Kallaguine, S., Prellier, W., Eds.; Wiley-VCH Verlag GmbH & Co. KGaA: Weinheim, Germany, 2015. [CrossRef]
64. Di Sarli, V.; Landi, G.; Lisi, L.; Saliva, A.; Di Benedetto, A. Catalytic diesel particulate filters with highly dispersed ceria: Effect of the soot-catalyst contact on the regeneration performance. *Appl. Catal. B Environ.* **2016**, *197*, 116–124. [CrossRef]
65. Lv, C.; Chen, H.; Hu, M.; Ai, T.; Fu, H. Nano-oxides washcoat for enhanced catalytic oxidation activity toward the perovskite-based monolithic catalyst. *Environ. Sci. Pollut. Res.* **2021**, *28*, 37142–37157. [CrossRef]
66. Matsouka, V.; Konsolakis, M.; Yentekakis, I.V.; Papavasiliou, A.; Tsetsekou, A.; Boukos, N. Thermal aging behavior of Pt-only TWC converters under simulated exhaust conditions: Effect of rare earths (CeO_2, La_2O_3) and alkali (Na) modifiers. *Top. Catal.* **2011**, *54*, 1124. [CrossRef]
67. Papavasiliou, A.; Tsetsekou, A.; Matsouka, V.; Konsolakis, M.; Yentekakis, I.V. An investigation of the role of Zr and La dopants into $Ce_{1-x-y}Zr_xLa_yO_\delta$ enriched γ-Al_2O_3 TWC washcoats. *Appl. Catal. A Gen.* **2010**, *382*, 73–84. [CrossRef]
68. Papavasiliou, A.; Tsetsekou, A.; Matsouka, V.; Konsolakis, M.; Yentekakis, I.V.; Boukos, N. Synergistic structural and surface promotion of monometallic (Pt) TWCs: Effectiveness and thermal aging tolerance. *Appl. Catal. B Environ.* **2011**, *106*, 228–241. [CrossRef]
69. Pérez, V.R.; Bueno-López, A. Catalytic regeneration of Diesel Particulate Filters: Comparison of Pt and CePr active phases. *Chem. Eng. J.* **2015**, *279*, 79–85. [CrossRef]
70. Kritsanaviparkporn, E.; Baena-Moreno, F.M.; Reina, T.R. Catalytic Converters for Vehicle Exhaust: Fundamental Aspects and Technology Overview for Newcomers to the Field. *Chem. (Easton).* **2021**, *3*, 630–646. [CrossRef]
71. Patel, K.D.; Subedar, D.; Patel, F. Design and development of automotive catalytic converter using non-noble catalyst for the reduction of exhaust emission: A review. *Mater. Today Proc.* **2022**, *57*, 2465–2472. [CrossRef]
72. Rood, S.; Eslava, S.; Manigrasso, A.; Bannister, C. Recent advances in gasoline three-way catalyst formulation: A review. *Proc. Inst. Mech. Eng. Part D: J. Automob. Eng.* **2020**, *234*, 936–949. [CrossRef]
73. Kozuch, S.; Martin, J.M.L. "Turning over" definitions in catalytic cycles. *ACS Catal.* **2012**, *2*, 2787–2794. [CrossRef]
74. Ciambelli, P.; Palma, V.; Russo, P.; Vaccaro, S. Performances of a catalytic foam trap for soot abatement. *Catal. Today* **2002**, *75*, 471–478. [CrossRef]
75. Shelef, M.; McCabe, R.W. Twenty-five years after introduction of automotive catalysts: What next? *Catal. Today* **2000**, *62*, 35–50. [CrossRef]
76. Van Doorn, J.; Varloud, J.; Mériaudeau, P.; Perrichon, V.; Chevrier, M.; Gauthier, C. Effect of support material on the catalytic combustion of diesel soot particulates. *Appl. Catal. B Environ.* **1992**, *1*, 117–127. [CrossRef]
77. Bueno-López, A. Diesel soot combustion ceria catalysts. *Appl. Catal. B Environ.* **2014**, *146*, 1–11. [CrossRef]
78. Liu, S.; Wu, X.; Weng, D.; Ran, R. Ceria-based catalysts for soot oxidation: A review. *J. Rare Earths* **2015**, *33*, 567–590. [CrossRef]
79. Neeft, J.P.A.; Makkee, M.; Moulijn, J.A. Catalysts for the oxidation of soot from diesel exhaust gases. I. An exploratory study. *Appl. Catal. B Environ.* **1996**, *8*, 57–78. [CrossRef]

80. Aneggi, E.; De Leitenburg, C.; Trovarelli, A. Ceria-based formulations for catalysts for diesel soot combustion. In *Catalysis by Ceria and Related Materials*, 2nd ed.; Trovarelli, A., Fornasiero, P., Eds.; World Scientific: Singapore, 2013; pp. 565–621. [CrossRef]
81. Aneggi, E.; Wiater, D.; De Leitenburg, C.; Llorca, J.; Trovarelli, A. Shape-dependent activity of ceria in soot combustion. *ACS Catal.* **2014**, *4*, 172–181. [CrossRef]
82. Mishra, U.K.; Chandel, V.S.; Singh, O.P. A review on cerium oxide–based catalysts for the removal of contaminants. *Emergent Mater.* **2022**, *5*, 1443–1476. [CrossRef]
83. Mukherjee, D.; Reddy, B.M. Noble metal-free CeO_2-based mixed oxides for CO and soot oxidation. *Catal. Today* **2018**, *309*, 227–235. [CrossRef]
84. Salaev, M.A.; Salaeva, A.A.; Kharlamova, T.S.; Mamontov, G.V. Pt–CeO_2-based composites in environmental catalysis: A review. *Appl. Catal. B Environ.* **2021**, *295*, 120286. [CrossRef]
85. Trovarelli, A.; Llorca, J. Ceria Catalysts at Nanoscale: How Do Crystal Shapes Shape Catalysis? *ACS Catal.* **2017**, *7*, 4716–4735. [CrossRef]
86. Vilé, G.; Colussi, S.; Krumeich, F.; Trovarelli, A.; Pérez-Ramírez, J. Opposite face sensitivity of CeO_2 in hydrogenation and oxidation catalysis. *Angew. Chem. Int. Ed.* **2014**, *53*, 12069–12072. [CrossRef]
87. Sartoretti, E.; Novara, C.; Chiodoni, A.; Giorgis, F.; Piumetti, M.; Bensaid, S.; Russo, N.; Fino, D. Nanostructured ceria-based catalysts doped with La and Nd: How acid-base sites and redox properties determine the oxidation mechanisms. *Catal. Today* **2022**, *390–391*, 117–134. [CrossRef]
88. Li, W.B.; Wang, J.X.; Gong, H. Catalytic combustion of VOCs on non-noble metal catalysts. *Catal. Today* **2009**, *148*, 81–87. [CrossRef]
89. Carabineiro, S.A.C.; Chen, X.; Konsolakis, M.; Psarras, A.C.; Tavares, P.B.; Órfão, J.J.M.; Pereira, M.F.R.; Figueiredo, J.L. Catalytic oxidation of toluene on Ce-Co and La-Co mixed oxides synthesized by exotemplating and evaporation methods. *Catal. Today* **2015**, *244*, 161–171. [CrossRef]
90. Carabineiro, S.A.C.; Konsolakis, M.; Marnellos, G.E.-N.; Asad, M.F.; Soares, O.S.G.P.; Tavares, P.B.; Pereira, M.F.R.; Órfão, J.J.M.; Figueiredo, J.L. Ethyl acetate abatement on copper catalysts supported on ceria doped with rare earth oxides. *Molecules* **2016**, *21*, 644. [CrossRef]
91. Konsolakis, M.; Carabineiro, S.A.C.; Marnellos, G.E.; Asad, M.F.; Soares, O.S.G.P.; Pereira, M.F.R.; Órfão, J.J.M.; Figueiredo, J.L. Volatile organic compounds abatement over copper-based catalysts: Effect of support. *Inorg. Chim. Acta* **2017**, *455*, 473–482. [CrossRef]
92. Konsolakis, M.; Carabineiro, S.A.C.; Tavares, P.B.; Figueiredo, J.L. Redox properties and VOC oxidation activity of Cu catalysts supported on $Ce_{1-x}Sm_xO_\delta$ mixed oxides. *J. Hazard. Mater.* **2013**, *261*, 512–521. [CrossRef] [PubMed]
93. Konsolakis, M.; Ioakeimidis, Z. Surface/structure functionalization of copper-based catalysts by metal-support and/or metal-metal interactions. *Appl. Surf. Sci.* **2014**, *320*, 244–255. [CrossRef]
94. Soliman, N.K. Factors affecting CO oxidation reaction over nanosized materials: A review. *J. Mater. Res. Technol.* **2019**, *8*, 2395–2407. [CrossRef]
95. Shan, Y.; Liu, Y.; Li, Y.; Yang, W. A review on application of cerium-based oxides in gaseous pollutant purification. *Sep. Purif. Technol.* **2020**, *250*, 117181. [CrossRef]
96. Cargnello, M.; Doan-Nguyen, V.V.T.; Gordon, T.R.; Diaz, R.E.; Stach, E.A.; Gorte, R.J.; Fornasiero, P.; Murray, C.B. Control of metal nanocrystal size reveals metal-support interface role for ceria catalysts. *Science* **2013**, *341*, 771–773. [CrossRef]
97. Mistry, H.; Behafarid, F.; Reske, R.; Varela, A.S.; Strasser, P.; Roldan Cuenya, B. Tuning Catalytic Selectivity at the Mesoscale via Interparticle Interactions. *ACS Catal.* **2016**, *6*, 1075–1080. [CrossRef]
98. Zhou, Y.; Li, Y.; Shen, W. Shape Engineering of Oxide Nanoparticles for Heterogeneous Catalysis. *Chem. Asian J.* **2016**, *11*, 1470–1488. [CrossRef]
99. Konsolakis, M.; Lykaki, M. Facet-Dependent Reactivity of Ceria Nanoparticles Exemplified by CeO_2-Based Transition Metal Catalysts: A Critical Review. *Catalysts* **2021**, *11*, 452. [CrossRef]
100. Waikar, J.; More, P. Low temperature oxidation of CO using alkali- and alkaline-earth metal-modified ceria-supported metal catalysts: A review. *Bull. Mater. Sci.* **2021**, *44*, 263. [CrossRef]
101. Cam, T.S.; Omarov, S.O.; Chebanenko, M.I.; Izotova, S.G.; Popkov, V.I. Recent progress in the synthesis of CeO_2-based nanocatalysts towards efficient oxidation of CO. *J. Sci. Adv. Mater. Devices* **2022**, *7*, 100399. [CrossRef]
102. Zhou, K.; Wang, X.; Sun, X.; Peng, Q.; Li, Y. Enhanced catalytic activity of ceria nanorods from well-defined reactive crystal planes. *J. Catal.* **2005**, *229*, 206–212. [CrossRef]
103. Aneggi, E.; Llorca, J.; Boaro, M.; Trovarelli, A. Surface-structure sensitivity of CO oxidation over polycrystalline ceria powders. *J. Catal.* **2005**, *234*, 88–95. [CrossRef]
104. Lykaki, M.; Pachatouridou, E.; Carabineiro, S.A.C.; Iliopoulou, E.; Andriopoulou, C.; Kallithrakas-Kontos, N.; Boghosian, S.; Konsolakis, M. Ceria nanoparticles shape effects on the structural defects and surface chemistry: Implications in CO oxidation by Cu/CeO_2 catalysts. *Appl. Catal. B Environ.* **2018**, *230*, 18–28. [CrossRef]
105. Stefa, S.; Lykaki, M.; Fragkoulis, D.; Binas, V.; Pandis, P.K.; Stathopoulos, V.N.; Konsolakis, M. Effect of the preparation method on the physicochemical properties and the CO oxidation performance of nanostructured CeO_2/TiO_2 oxides. *Processes* **2020**, *8*, 847. [CrossRef]

106. Stefa, S.; Lykaki, M.; Binas, V.; Pandis, P.K.; Stathopoulos, V.N.; Konsolakis, M. Hydrothermal Synthesis of ZnO-Doped Ceria Nanorods: Effect of ZnO Content on the Redox Properties and the CO Oxidation Performance. *Appl. Sci.* **2020**, *10*, 7605. [CrossRef]
107. Trimm, D.L. Minimisation of carbon monoxide in a hydrogen stream for fuel cell application. *Appl. Catal. A Gen.* **2005**, *296*, 1–11. [CrossRef]
108. Wootsch, A.; Descorme, C.; Duprez, D. Preferential oxidation of carbon monoxide in the presence of hydrogen (PROX) over ceria-zirconia and alumina-supported Pt catalysts. *J. Catal.* **2004**, *225*, 259–266. [CrossRef]
109. Li, Y.; Fu, Q.; Flytzani-Stephanopoulos, M. Low-temperature water-gas shift reaction over Cu- and Ni-loaded cerium oxide catalysts. *Appl. Catal. B Environ.* **2000**, *27*, 179–191. [CrossRef]
110. Yu, W.-Z.; Wu, M.-Y.; Wang, W.-W.; Jia, C.-J. In Situ Generation of the Surface Oxygen Vacancies in a Copper–Ceria Catalyst for the Water–Gas Shift Reaction. *Langmuir* **2021**, *37*, 10499–10509. [CrossRef]
111. Shi, J.; Li, H.; Genest, A.; Zhao, W.; Qi, P.; Wang, T.; Rupprechter, G. High-performance water gas shift induced by asymmetric oxygen vacancies: Gold clusters supported by ceria-praseodymia mixed oxides. *Appl. Catal. B Environ.* **2022**, *301*, 120789. [CrossRef]
112. Rodriguez, J.A.; Graciani, J.; Evans, J.; Park, J.B.; Yang, F.; Stacchiola, D.; Senanayake, S.D.; Ma, S.; Pérez, M.; Liu, P.; et al. Water-Gas Shift Reaction on a Highly Active Inverse CeO_x/Cu(111) Catalyst: Unique Role of Ceria Nanoparticles. *Angew. Chem. Int. Ed.* **2009**, *48*, 8047–8050. [CrossRef] [PubMed]
113. Mudiyanselage, K.; Senanayake, S.D.; Feria, L.; Kundu, S.; Baber, A.E.; Graciani, J.; Vidal, A.B.; Agnoli, S.; Evans, J.; Chang, R.; et al. Importance of the Metal–Oxide Interface in Catalysis: In Situ Studies of the Water–Gas Shift Reaction by Ambient-Pressure X-ray Photoelectron Spectroscopy. *Angew. Chem. Int. Ed.* **2013**, *52*, 5101–5105. [CrossRef] [PubMed]
114. Lykaki, M.; Stefa, S.; Carabineiro, S.A.C.; Soria, M.A.; Madeira, L.M.; Konsolakis, M. Shape Effects of Ceria Nanoparticles on the Water—Gas Shift Performance of CuO_x/CeO_2 Catalysts. *Catalysts* **2021**, *11*, 753. [CrossRef]
115. Ren, Z.; Peng, F.; Li, J.; Liang, X.; Chen, B. Morphology-Dependent Properties of Cu/CeO_2 Catalysts for the Water-Gas Shift Reaction. *Catalysts* **2017**, *7*, 48. [CrossRef]
116. Yao, S.Y.; Xu, W.Q.; Johnston-Peck, A.C.; Zhao, F.Z.; Liu, Z.Y.; Luo, S.; Senanayake, S.D.; Martínez-Arias, A.; Liu, W.J.; Rodriguez, J.A. Morphological effects of the nanostructured ceria support on the activity and stability of CuO/CeO_2 catalysts for the water-gas shift reaction. *Phys. Chem. Chem. Phys.* **2014**, *16*, 17183–17195. [CrossRef]
117. Mitchell, S.; Qin, R.; Zheng, N.; Pérez-Ramírez, J. Nanoscale engineering of catalytic materials for sustainable technologies. *Nat. Nanotechnol.* **2021**, *16*, 129–139. [CrossRef]
118. P Puigdollers, A.R.; Schlexer, P.; Tosoni, S.; Pacchioni, G. Increasing oxide reducibility: The role of metal/oxide interfaces in the formation of oxygen vacancies. *ACS Catal.* **2017**, *7*, 6493–6513. [CrossRef]
119. Chung, C.-H.; Tu, F.-Y.; Chiu, T.-A.; Wu, T.-T.; Yu, W.-Y. Critical roles of surface oxygen vacancy in heterogeneous catalysis over ceria-based materials: A selected review. *Chem. Lett.* **2021**, *50*, 856–865. [CrossRef]
120. Hussain, I.; Tanimu, G.; Ahmed, S.; Aniz, C.U.; Alasiri, H.; Alhooshani, K. A review of the indispensable role of oxygen vacancies for enhanced CO_2 methanation activity over CeO_2-based catalysts: Uncovering, influencing, and tuning strategies. *Int. J. Hydrog. Energy* **2022**, *in press*. [CrossRef]
121. Lou, Y.; Xu, J.; Zhang, Y.; Pan, C.; Dong, Y.; Zhu, Y. Metal-support interaction for heterogeneous catalysis: From nanoparticles to single atoms. *Mater. Today Nano* **2020**, *12*, 100093. [CrossRef]
122. Torres-Sempere, G.; Pastor-Perez, L.; Odriozola, J.A.; Yu, J.; Duran-Olivencia, F.J.; Bobadilla, L.F.; Reina, T.R. Recent advances on gas-phase CO_2 conversion: Catalysis design and chemical processes to close the carbon cycle. *Curr. Opin. Green Sustain. Chem.* **2022**, *36*, 100647. [CrossRef]
123. Ebrahimi, P.; Kumar, A.; Khraisheh, M. A Review of CeO_2 Supported Catalysts for CO_2 Reduction to CO through the Reverse Water Gas Shift Reaction. *Catalysts* **2022**, *12*, 1101. [CrossRef]
124. Yang, F.; Deng, D.; Pan, X.; Fu, Q.; Bao, X. Understanding nano effects in catalysis. *Natl. Sci. Rev.* **2015**, *2*, 183–201. [CrossRef]
125. Cao, S.; Tao, F.; Tang, Y.; Li, Y.; Yu, J. Size- and shape-dependent catalytic performances of oxidation and reduction reactions on nanocatalysts. *Chem. Soc. Rev.* **2016**, *45*, 4747–4765. [CrossRef]
126. Roldan Cuenya, B. Synthesis and catalytic properties of metal nanoparticles: Size, shape, support, composition, and oxidation state effects. *Thin Solid Film.* **2010**, *518*, 3127–3150. [CrossRef]
127. Qu, P.-F.; Wang, G.-C. Theoretical insight into the strong size-dependence of dry reforming of methane over Ru/CeO_2. *J. CO2 Util.* **2022**, *65*, 102221. [CrossRef]
128. Uzio, D.; Berhault, G. Factors governing the catalytic reactivity of metallic nanoparticles. *Catal. Rev.* **2010**, *52*, 106–131. [CrossRef]
129. Di Benedetto, A.; Landi, G.; Lisi, L. Improved CO-PROX performance of CuO/CeO_2 catalysts by using nanometric ceria as support. *Catalysts* **2018**, *8*, 209. [CrossRef]
130. Gong, L.; Jie, W.; Liu, Y.; Lin, X.; Deng, W.; Qiu, M.; Hu, X.; Liu, Q. Enhanced Activity for CO Preferential Oxidation over CuO Catalysts Supported on Nanosized CeO_2 with High Surface Area and Defects. *Catalysts* **2021**, *11*, 884. [CrossRef]
131. Yang, W.; Wang, X.; Song, S.; Zhang, H. Syntheses and Applications of Noble-Metal-free CeO_2-Based Mixed-Oxide Nanocatalysts. *Chem* **2019**, *5*, 1743–1774. [CrossRef]
132. Lykaki, M.; Papista, E.; Kaklidis, N.; Carabineiro, S.A.C.; Konsolakis, M. Ceria nanoparticles' morphological effects on the N_2O decomposition performance of Co_3O_4/CeO_2 mixed oxides. *Catalysts* **2019**, *9*, 233. [CrossRef]

133. Wan, J.; Lin, J.; Guo, X.; Wang, T.; Zhou, R. Morphology effect on the structure-activity relationship of Rh/CeO_2-ZrO_2 catalysts. *Chem. Eng. J.* **2019**, *368*, 719–729. [CrossRef]
134. Dou, B.; Yang, D.; Kang, T.; Xu, Y.; Hao, Q.; Bin, F.; Xu, X. Morphology effects of CeO_2-ZrO_2 on the catalytic performance of CuO/CeO_2-ZrO_2 for toluene oxidation. *Carbon Resour. Convers.* **2021**, *4*, 55–60. [CrossRef]
135. Sudduth, B.; Yun, D.; Sun, J.; Wang, Y. Facet-Dependent Selectivity of CeO_2 nanoparticles in 2-Propanol Conversion. *J. Catal.* **2021**, *404*, 96–108. [CrossRef]
136. Zhang, X.; You, R.; Li, D.; Cao, T.; Huang, W. Reaction Sensitivity of Ceria Morphology Effect on Ni/CeO_2 Catalysis in Propane Oxidation Reactions. *ACS Appl. Mater. Interfaces* **2017**, *9*, 35897–35907. [CrossRef]
137. Feng, K.; Wang, Y.; Guo, M.; Zhang, J.; Li, Z.; Deng, T.; Zhang, Z.; Yan, B. In-situ/operando techniques to identify active sites for thermochemical conversion of CO_2 over heterogeneous catalysts. *J. Energy Chem.* **2021**, *62*, 153–171. [CrossRef]
138. Garcia, X.; Soler, L.; Divins, N.J.; Vendrell, X.; Serrano, I.; Lucentini, I.; Prat, J.; Solano, E.; Tallarida, M.; Escudero, C.; et al. Ceria-based catalysts studied by near ambient pressure x-ray photoelectron spectroscopy: A review. *Catalysts* **2020**, *10*, 286. [CrossRef]
139. Ganduglia-Pirovano, M.V.; Hofmann, A.; Sauer, J. Oxygen vacancies in transition metal and rare earth oxides: Current state of understanding and remaining challenges. *Surf. Sci. Rep.* **2007**, *62*, 219–270. [CrossRef]
140. Li, Y.; Shen, W. Morphology-dependent nanocatalysts: Rod-shaped oxides. *Chem. Soc. Rev.* **2014**, *43*, 1543–1574. [CrossRef]
141. Burda, C.; Chen, X.; Narayanan, R.; El-Sayed, M.A. Chemistry and Properties of Nanocrystals of Different Shapes. *Chem. Rev.* **2005**, *105*, 1025–1102. [CrossRef]
142. Qiao, Z.-A.; Wu, Z.; Dai, S. Shape-controlled ceria-based nanostructures for catalysis applications. *ChemSusChem* **2013**, *6*, 1821–1833. [CrossRef]
143. Huang, W.; Gao, Y. Morphology-dependent surface chemistry and catalysis of CeO_2 nanocrystals. *Catal. Sci. Technol.* **2014**, *4*, 3772–3784. [CrossRef]
144. Sun, C.; Li, H.; Chen, L. Nanostructured ceria-based materials: Synthesis, properties, and applications. *Energy Environ. Sci.* **2012**, *5*, 8475–8505. [CrossRef]
145. Zhou, Y.; Chen, A.; Ning, J.; Shen, W. Electronic and geometric structure of the copper-ceria interface on Cu/CeO_2 catalysts. *Chin. J. Catal.* **2020**, *41*, 928–937. [CrossRef]
146. Wen, Y.; Huang, Q.; Zhang, Z.; Huang, W. Morphology-Dependent Catalysis of CeO_2-Based Nanocrystal Model Catalysts. *Chin. J. Chem.* **2022**, *40*, 1856–1866. [CrossRef]
147. Li, Y.; Liu, Q.; Shen, W. Morphology-dependent nanocatalysis: Metal particles. *Dalton Trans.* **2011**, *40*, 5811–5826. [CrossRef]
148. Varvoutis, G.; Lykaki, M.; Stefa, S.; Papista, E.; Carabineiro, S.A.C.; Marnellos, G.E.; Konsolakis, M. Remarkable efficiency of Ni supported on hydrothermally synthesized CeO_2 nanorods for low-temperature CO_2 hydrogenation to methane. *Catal. Commun.* **2020**, *142*, 106036. [CrossRef]
149. Ta, N.; Liu, J.; Shen, W. Tuning the shape of ceria nanomaterials for catalytic applications. *Chin. J. Catal.* **2013**, *34*, 838–850. [CrossRef]
150. Konsolakis, M.; Lykaki, M.; Stefa, S.; Carabineiro, S.A.C.; Varvoutis, G.; Papista, E.; Marnellos, G.E. CO_2 Hydrogenation over Nanoceria-Supported Transition Metal Catalysts: Role of Ceria Morphology (Nanorods versus Nanocubes) and Active Phase Nature (Co versus Cu). *Nanomaterials* **2019**, *9*, 1739. [CrossRef]
151. Datta, S.; Torrente-Murciano, L. Nanostructured faceted ceria as oxidation catalyst. *Curr. Opin. Chem. Eng.* **2018**, *20*, 99–106. [CrossRef]
152. Lykaki, M.; Stefa, S.; Carabineiro, S.A.C.; Pandis, P.K.; Stathopoulos, V.N.; Konsolakis, M. Facet-Dependent Reactivity of Fe_2O_3/CeO_2 Nanocomposites: Effect of Ceria Morphology on CO Oxidation. *Catalysts* **2019**, *9*, 371. [CrossRef]
153. Zhang, Y.; Zhao, S.; Feng, J.; Song, S.; Shi, W.; Wang, D.; Zhang, H. Unraveling the physical chemistry and materials science of CeO_2-based nanostructures. *Chem* **2021**, *7*, 2022–2059. [CrossRef]
154. Hu, Z.; Liu, X.; Meng, D.; Guo, Y.; Guo, Y.; Lu, G. Effect of Ceria Crystal Plane on the Physicochemical and Catalytic Properties of Pd/Ceria for CO and Propane Oxidation. *ACS Catal.* **2016**, *6*, 2265–2279. [CrossRef]
155. Agarwal, S.; Lefferts, L.; Mojet, B.L.; Ligthart, D.A.J.M.; Hensen, E.J.M.; Mitchell, D.R.G.; Erasmus, W.J.; Anderson, B.G.; Olivier, E.J.; Neethling, J.H.; et al. Exposed surfaces on shape-controlled ceria nanoparticles revealed through AC-TEM and water-gas shift reactivity. *ChemSusChem* **2013**, *6*, 1898–1906. [CrossRef]
156. Han, W.-Q.; Wen, W.; Hanson, J.C.; Teng, X.; Marinkovic, N.; Rodriguez, J.A. One-Dimensional Ceria as Catalyst for the Low-Temperature Water−Gas Shift Reaction. *J. Phys. Chem. C* **2009**, *113*, 21949–21955. [CrossRef]
157. Yi, N.; Si, R.; Saltsburg, H.; Flytzani-Stephanopoulos, M. Active gold species on cerium oxide nanoshapes for methanol steam reforming and the water gas shift reactions. *Energy Environ. Sci.* **2010**, *3*, 831–837. [CrossRef]
158. Mai, H.-X.; Sun, L.-D.; Zhang, Y.-W.; Si, R.; Feng, W.; Zhang, H.-P.; Liu, H.-C.; Yan, C.-H. Shape-selective synthesis and oxygen storage behavior of ceria nanopolyhedra, nanorods, and nanocubes. *J. Phys. Chem. B* **2005**, *109*, 24380–24385. [CrossRef]
159. Zhang, J.; Xia, X.; Mao, X.; Li, J.; Chen, C.; Liu, F.; Lan, Y.-P. Length effect of ceria nanorod on its oxygen vacancy formation and photocatalytic property. *J. Mater. Sci. Mater. Electron.* **2022**, *33*, 4628–4642. [CrossRef]
160. Bian, Y.; Xu, C.; Wen, X.; Xu, L.; Cui, Y.; Wang, S.; Wu, C.; Qiu, J.; Cheng, G.; Chen, M. CO_2 methanation over the Ni-based catalysts supported on nano-CeO_2 with varied morphologies. *Fuel* **2023**, *331*, 125755. [CrossRef]

161. Hu, F.; Ye, R.; Jin, C.; Liu, D.; Chen, X.; Li, C.; Lim, K.H.; Song, G.; Wang, T.; Feng, G.; et al. Ni nanoparticles enclosed in highly mesoporous nanofibers with oxygen vacancies for efficient CO_2 methanation. *Appl. Catal. B Environ.* **2022**, *317*, 121715. [CrossRef]
162. Pu, T.; Chen, J.; Tu, W.; Xu, J.; Han, Y.-F.; Wachs, I.E.; Zhu, M. Dependency of CO_2 methanation on the strong metal-support interaction for supported Ni/CeO_2 catalysts. *J. Catal.* **2022**, *413*, 821–828. [CrossRef]
163. Shen, D.; Li, Z.; Shan, J.; Yu, G.; Wang, X.; Zhang, Y.; Liu, C.; Lyu, S.; Li, J.; Li, L. Synergistic Pt-CeO_2 interface boosting low temperature dry reforming of methane. *Appl. Catal. B Environ.* **2022**, *318*, 121809. [CrossRef]
164. Lorber, K.; Zavašnik, J.; Arčon, I.; Huš, M.; Teržan, J.; Likozar, B.; Djinović, P. CO_2 Activation over Nanoshaped CeO_2 Decorated with Nickel for Low-Temperature Methane Dry Reforming. *ACS Appl. Mater. Interfaces* **2022**, *14*, 31862–31878. [CrossRef]
165. Li, Z.; Li, N.; Wang, N.; Zhou, B.; Yin, P.; Song, B.; Yu, J.; Yang, Y. Mechanism Investigations on Water Gas Shift Reaction over Cu(111), Cu(100), and Cu(211) Surfaces. *ACS Omega* **2022**, *7*, 3514–3521. [CrossRef]
166. Lykaki, M.; Papista, E.; Carabineiro, S.A.C.; Tavares, P.B.; Konsolakis, M. Optimization of N_2O decomposition activity of CuO-CeO_2 mixed oxides by means of synthesis procedure and alkali (Cs) promotion. *Catal. Sci. Technol.* **2018**, *8*, 2312–2322. [CrossRef]
167. Lu, B.; Zhang, T.; Zhang, L.; Xu, Y.; Zhang, Z.; Wu, F.; Li, X.; Luo, C. Promotion effects of oxygen vacancies on activity of Na-doped CeO_2 catalysts for reverse water gas shift reaction. *Appl. Surf. Sci.* **2022**, *587*, 152881. [CrossRef]
168. Carey, J.J.; Nolan, M. Cation doping size effect for methane activation on alkaline earth metal doping of the CeO_2 (111) surface. *Catal. Sci. Technol.* **2016**, *6*, 3544–3558. [CrossRef]
169. Polychronopoulou, K.; Alkhoori, A.A.; Efstathiou, A.M.; Jaoude, M.A.; Damaskinos, C.M.; Baker, M.A.; Almutawa, A.; Anjum, D.H.; Vasiliades, M.A.; Belabbes, A.; et al. Design Aspects of Doped CeO_2 for Low-Temperature Catalytic CO Oxidation: Transient Kinetics and DFT Approach. *ACS Appl. Mater. Interfaces* **2021**, *13*, 22391–22415. [CrossRef]
170. Bai, Y.; Sun, K.; Wu, J.; Zhang, M.; Zhao, S.; Kim, Y.D.; Liu, Y.; Gao, J.; Liu, Z.; Peng, Z. The Ga-promoted Ni/CeO_2 catalysts for dry reforming of methane with high stability induced by the enhanced CO_2 activation. *Mol. Catal.* **2022**, *530*, 112577. [CrossRef]
171. Rafiee, A.; Rajab Khalilpour, K.; Milani, D.; Panahi, M. Trends in CO_2 conversion and utilization: A review from process systems perspective. *J. Environ. Chem. Eng.* **2018**, *6*, 5771–5794. [CrossRef]
172. Hidalgo, D.; Martín-Marroquín, J.M. Power-to-methane, coupling CO_2 capture with fuel production: An overview. *Renew. Sustain. Energy Rev.* **2020**, *132*, 110057. [CrossRef]
173. González-Castaño, M.; Dorneanu, B.; Arellano-García, H. The reverse water gas shift reaction: A process systems engineering perspective. *React. Chem. Eng.* **2021**, 954–976. [CrossRef]
174. De, S.; Dokania, A.; Ramirez, A.; Gascon, J. Advances in the Design of Heterogeneous Catalysts and Thermocatalytic Processes for CO_2 Utilization. *ACS Catal.* **2020**, *10*, 14147–14185. [CrossRef]
175. Portillo, E.; Gandara-Loe, J.; Reina, T.R.; Pastor-Pérez, L. Is the RWGS a viable route for CO_2 conversion to added value products? A techno-economic study to understand the optimal RWGS conditions. *Sci. Total Environ.* **2022**, *857*, 159394. [CrossRef] [PubMed]
176. Zhang, D.; Du, X.; Shi, L.; Gao, R. Shape-controlled synthesis and catalytic application of ceria nanomaterials. *Dalton Trans.* **2012**, *41*, 14455–14475. [CrossRef] [PubMed]
177. Su, X.; Yang, X.; Zhao, B.; Huang, Y. Designing of highly selective and high-temperature endurable RWGS heterogeneous catalysts: Recent advances and the future directions. *J. Energy Chem.* **2017**, *26*, 854–867. [CrossRef]
178. Chae, H.J.; Kim, J.-H.; Lee, S.C.; Kim, H.-S.; Jo, S.B.; Ryu, J.-H.; Kim, T.Y.; Lee, C.H.; Kim, S.J.; Kang, S.-H.; et al. Catalytic Technologies for CO Hydrogenation for the Production of Light Hydrocarbons and Middle Distillates. *Catalysts* **2020**, *10*, 99. [CrossRef]
179. Bahmanpour, A.M.; Signorile, M.; Kröcher, O. Recent progress in syngas production via catalytic CO_2 hydrogenation reaction. *Appl. Catal. B Environ.* **2021**, *295*, 120319. [CrossRef]
180. Yang, S.-C.; Su, W.-N.; Rick, J.; Lin, S.-D.; Liu, J.-Y.; Pan, C.-J.; Lee, J.-F.; Hwang, B.-J. Oxygen vacancy engineering of cerium oxides for carbon dioxide capture and reduction. *ChemSusChem* **2013**, *6*, 1326–1329. [CrossRef]
181. Staudt, T.; Lykhach, Y.; Tsud, N.; Skála, T.; Prince, K.C.; Matolín, V.; Libuda, J. Ceria reoxidation by CO_2: A model study. *J. Catal.* **2010**, *275*, 181–185. [CrossRef]
182. Ackermann, S.; Sauvin, L.; Castiglioni, R.; Rupp, J.L.M.; Scheffe, J.R.; Steinfeld, A. Kinetics of CO_2 Reduction over Nonstoichiometric Ceria. *J. Phys. Chem. C* **2015**, *119*, 16452–16461. [CrossRef]
183. Kovacevic, M.; Mojet, B.L.; Van Ommen, J.G.; Lefferts, L. Effects of Morphology of Cerium Oxide Catalysts for Reverse Water Gas Shift Reaction. *Catal. Lett.* **2016**, *146*, 770–777. [CrossRef]
184. Liu, Y.; Li, Z.; Xu, H.; Han, Y. Reverse water-gas shift reaction over ceria nanocube synthesized by hydrothermal method. *Catal. Commun.* **2016**, *76*, 1–6. [CrossRef]
185. Cao, F.; Xiao, Y.; Zhang, Z.; Li, J.; Xia, Z.; Hu, X.; Ma, Y.; Qu, Y. Influence of oxygen vacancies of CeO_2 on reverse water gas shift reaction. *J. Catal.* **2022**, *414*, 25–32. [CrossRef]
186. Zhou, G.; Dai, B.; Xie, H.; Zhang, G.; Xiong, K.; Zheng, X. CeCu composite catalyst for CO synthesis by reverse water-gas shift reaction: Effect of Ce/Cu mole ratio. *J. CO2 Util.* **2017**, *21*, 292–301. [CrossRef]
187. Chen, X.; Su, X.; Liang, B.; Yang, X.; Ren, X.; Duan, H.; Huang, Y.; Zhang, T. Identification of relevant active sites and a mechanism study for reverse water gas shift reaction over Pt/CeO_2 catalysts. *J. Energy Chem.* **2016**, *25*, 1051–1057. [CrossRef]

188. Yang, S.-C.; Pang, S.H.; Sulmonetti, T.P.; Su, W.-N.; Lee, J.-F.; Hwang, B.-J.; Jones, C.W. Synergy between Ceria Oxygen Vacancies and Cu Nanoparticles Facilitates the Catalytic Conversion of CO_2 to CO under Mild Conditions. *ACS Catal.* **2018**, *8*, 12056–12066. [CrossRef]
189. Guo, C.; Wei, S.; Zhou, S.; Zhang, T.; Wang, Z.; Ng, S.-P.; Lu, X.; Wu, C.-M.L.; Guo, W. Initial Reduction of CO_2 on Pd-, Ru-, and Cu-Doped CeO_2(111) Surfaces: Effects of Surface Modification on Catalytic Activity and Selectivity. *ACS Appl. Mater. Interfaces* **2017**, *9*, 26107–26117. [CrossRef]
190. Aitbekova, A.; Wu, L.; Wrasman, C.J.; Boubnov, A.; Hoffman, A.S.; Goodman, E.D.; Bare, S.R.; Cargnello, M. Low-Temperature Restructuring of CeO_2-Supported Ru Nanoparticles Determines Selectivity in CO_2 Catalytic Reduction. *J. Am. Chem. Soc.* **2018**, *140*, 13736–13745. [CrossRef]
191. Lu, B.; Kawamoto, K. Preparation of mesoporous CeO_2 and monodispersed NiO particles in CeO_2, and enhanced selectivity of NiO/CeO_2 for reverse water gas shift reaction. *Mater. Res. Bull.* **2014**, *53*, 70–78. [CrossRef]
192. Wang, W.; Zhang, Y.; Wang, Z.; Yan, J.; Ge, Q.; Liu, C. Reverse water gas shift over In_2O_3-CeO_2 catalysts. *Catal. Today* **2016**, *259*, 402–408. [CrossRef]
193. Zhao, B.; Pan, Y.; Liu, C. The promotion effect of CeO_2 on CO_2 adsorption and hydrogenation over Ga_2O_3. *Catal. Today* **2012**, *194*, 60–64. [CrossRef]
194. Li, S.; Xu, Y.; Chen, Y.; Li, W.; Lin, L.; Li, M.; Deng, Y.; Wang, X.; Ge, B.; Yang, C.; et al. Tuning the Selectivity of Catalytic Carbon Dioxide Hydrogenation over Iridium/Cerium Oxide Catalysts with a Strong Metal–Support Interaction. *Angew. Chem. Int. Ed.* **2017**, *56*, 10761–10765. [CrossRef] [PubMed]
195. Goguet, A.; Meunier, F.C.; Tibiletti, D.; Breen, J.P.; Burch, R. Spectrokinetic investigation of reverse water-gas-shift reaction intermediates over a Pt/CeO_2 catalyst. *J. Phys. Chem. B* **2004**, *108*, 20240–20246. [CrossRef]
196. Xie, Y.; Yin, Y.; Zeng, S.; Gao, M.; Su, H. Coexistence of Cu^+ and Cu^{2+} in star-shaped CeO_2/Cu_xO catalyst for preferential CO oxidation. *Catal. Commun.* **2017**, *99*, 110–114. [CrossRef]
197. Zhang, Y.; Liang, L.; Chen, Z.; Wen, J.; Zhong, W.; Zou, S.; Fu, M.; Chen, L.; Ye, D. Highly efficient Cu/CeO_2-hollow nanospheres catalyst for the reverse water-gas shift reaction: Investigation on the role of oxygen vacancies through in situ UV-Raman and DRIFTS. *Appl. Surf. Sci.* **2020**, *516*, 146035. [CrossRef]
198. Zhou, G.; Xie, F.; Deng, L.; Zhang, G.; Xie, H. Supported mesoporous Cu/$CeO_{2-\delta}$ catalyst for CO_2 reverse water–gas shift reaction to syngas. *Int. J. Hydrog. Energy* **2020**, *45*, 11380–11393. [CrossRef]
199. Li, M.; Pham, T.H.M.; Oveisi, E.; Ko, Y.; Luo, W.; Züttel, A. Revealing the Surface Chemistry for CO_2 Hydrogenation on Cu/CeO_{2-x} Using Near-Ambient-Pressure X-ray Photoelectron Spectroscopy. *ACS Appl. Energy Mater.* **2021**, *4*, 12326–12335. [CrossRef]
200. Lin, L.; Yao, S.; Liu, Z.; Zhang, F.; Li, N.; Vovchok, D.; Martínez-Arias, A.; Castañeda, R.; Lin, J.; Senanayake, S.D.; et al. In Situ Characterization of Cu/CeO_2 Nanocatalysts for CO_2 Hydrogenation: Morphological Effects of Nanostructured Ceria on the Catalytic Activity. *J. Phys. Chem. C* **2018**, *122*, 12934–12943. [CrossRef]
201. Varvoutis, G.; Lykaki, M.; Papista, E.; Carabineiro, S.A.C.; Psarras, A.C.; Marnellos, G.E.; Konsolakis, M. Effect of alkali (Cs) doping on the surface chemistry and CO_2 hydrogenation performance of CuO/CeO_2 catalysts. *J. CO2 Util.* **2021**, *44*, 101408. [CrossRef]
202. Varvoutis, G.; Karakoulia, S.A.; Lykaki, M.; Stefa, S.; Binas, V.; Marnellos, G.E.; Konsolakis, M. Support-induced modifications on the CO_2 hydrogenation performance of Ni/CeO_2: The effect of ZnO doping on CeO_2 nanorods. *J. CO2 Util.* **2022**, *61*, 102057. [CrossRef]
203. Gandara-Loe, J.; Zhang, Q.; Villora-Picó, J.J.; Sepúlveda-Escribano, A.; Pastor-Pérez, L.; Reina, T.R. Design of Full-Temperature-Range RWGS Catalysts: Impact of Alkali Promoters on Ni/CeO_2. *Energy Fuels* **2022**, *36*, 6362–6373. [CrossRef]
204. Gandara-Loe, J.; Portillo, E.; Odriozola, J.A.; Reina, T.R.; Pastor-Pérez, L. K-Promoted Ni-Based Catalysts for Gas-Phase CO_2 Conversion: Catalysts Design and Process Modelling Validation. *Front. Chem.* **2021**, *9*, 785571. [CrossRef]
205. Yang, L.; Pastor-Pérez, L.; Villora-Pico, J.J.; Gu, S.; Sepúlveda-Escribano, A.; Reina, T.R. CO_2 valorisation via reverse water-gas shift reaction using promoted Fe/CeO_2-Al_2O_3 catalysts: Showcasing the potential of advanced catalysts to explore new processes design. *Appl. Catal. A Gen.* **2020**, *593*, 117442. [CrossRef]
206. Cui, S.; Wang, X.; Wang, L.; Zheng, X. Enhanced selectivity of the CO_2 reverse water–gas reaction over a Ni_2P/CeO_2 catalyst. *Dalt. Trans.* **2021**, *50*, 5978–5987. [CrossRef]
207. Le Saché, E.; Pastor-Pérez, L.; Haycock, B.J.; Villora-Picó, J.J.; Sepúlveda-Escribano, A.; Reina, T.R. Switchable Catalysts for Chemical CO_2 Recycling: A Step Forward in the Methanation and Reverse Water–Gas Shift Reactions. *ACS Sustain. Chem. Eng.* **2020**, *8*, 4614–4622. [CrossRef]
208. Panaritis, C.; Edake, M.; Couillard, M.; Einakchi, R.; Baranova, E.A. Insight towards the role of ceria-based supports for reverse water gas shift reaction over RuFe nanoparticles. *J. CO2 Util.* **2018**, *26*, 350–358. [CrossRef]
209. Lee, S.M.; Eom, H.; Kim, S.S. A study on the effect of CeO_2 addition to a Pt/TiO_2 catalyst on the reverse water gas shift reaction. *Environ. Technol.* **2021**, *42*, 182–192. [CrossRef]
210. Zhao, Z.; Wang, M.; Ma, P.; Zheng, Y.; Chen, J.; Li, H.; Zhang, X.; Zheng, K.; Kuang, Q.; Xie, Z.-X. Atomically dispersed Pt/CeO_2 catalyst with superior CO selectivity in reverse water gas shift reaction. *Appl. Catal. B Environ.* **2021**, *291*, 120101. [CrossRef]
211. Martin, N.M.; Velin, P.; Skoglundh, M.; Bauer, M.; Carlsson, P.-A. Catalytic hydrogenation of CO_2 to methane over supported Pd, Rh and Ni catalysts. *Catal. Sci. Technol.* **2017**, *7*, 1086–1094. [CrossRef]

212. Dai, B.; Zhou, G.; Ge, S.; Xie, H.; Jiao, Z.; Zhang, G.; Xiong, K. CO_2 reverse water-gas shift reaction on mesoporous M-CeO_2 catalysts. *Can. J. Chem. Eng.* **2017**, *95*, 634–642. [CrossRef]
213. Wang, L.; Zhang, S.; Liu, Y. Reverse water gas shift reaction over Co-precipitated Ni-CeO_2 catalysts. *J. Rare Earths* **2008**, *26*, 66–70. [CrossRef]
214. Yang, L.; Pastor-Pérez, L.; Gu, S.; Sepúlveda-Escribano, A.; Reina, T.R. Highly efficient Ni/CeO_2-Al_2O_3 catalysts for CO_2 upgrading via reverse water-gas shift: Effect of selected transition metal promoters. *Appl. Catal. B Environ.* **2018**, *232*, 464–471. [CrossRef]
215. Huynh, H.L.; Yu, Z. CO_2 Methanation on Hydrotalcite-Derived Catalysts and Structured Reactors: A Review. *Energy Technol.* **2020**, *8*, 1901475. [CrossRef]
216. Kopyscinski, J.; Schildhauer, T.J.; Biollaz, S.M.A. Production of synthetic natural gas (SNG) from coal and dry biomass—A technology review from 1950 to 2009. *Fuel* **2010**, *89*, 1763–1783. [CrossRef]
217. Varvoutis, G.; Lampropoulos, A.; Mandela, E.; Konsolakis, M.; Marnellos, G.E. Recent Advances on CO_2 Mitigation Technologies: On the Role of Hydrogenation Route via Green H_2. *Energies* **2022**, *15*, 4790. [CrossRef]
218. Bargiacchi, E. 9—Power-to-Fuel existing plants and pilot projects. In *Power to Fuel*; Elsevier: Amsterdam, The Netherlands, 2021; pp. 211–237. [CrossRef]
219. Sterner, M.; Specht, M. Power-to-Gas and Power-to-X—The history and results of developing a new storage concept. *Energies* **2021**, *14*, 6594. [CrossRef]
220. Eveloy, V.; Gebreegziabher, T. A Review of Projected Power-to-Gas Deployment Scenarios. *Energies* **2018**, *11*, 1824. [CrossRef]
221. Mazza, A.; Bompard, E.; Chicco, G. Applications of power to gas technologies in emerging electrical systems. *Renew. Sustain. Energy Rev.* **2018**, *92*, 794–806. [CrossRef]
222. Vogt, C.; Monai, M.; Kramer, G.J.; Weckhuysen, B.M. The renaissance of the Sabatier reaction and its applications on Earth and in space. *Nat. Catal.* **2019**, *2*, 188–197. [CrossRef]
223. Reiter, G. Power-to-Gas. In *Fuel Cells: Data, Facts and Figures*; Wiley-VCH Verlag GmbH & Co. KGaA.: Weinheim, Germany, 2016; pp. 357–368. [CrossRef]
224. Gao, J.; Wang, Y.; Ping, Y.; Hu, D.; Xu, G.; Gu, F.; Su, F. A thermodynamic analysis of methanation reactions of carbon oxides for the production of synthetic natural gas. *RSC Adv.* **2012**, *2*, 2358–2368. [CrossRef]
225. Tichler, R.; Bauer, S. Chapter 18—Power-to-Gas. In *Storing Energy: With Special Reference to Renewable Energy Sources*; Elsevier Inc.: Amsterdam, The Netherlands, 2016; pp. 373–389. [CrossRef]
226. Ghaib, K.; Ben-Fares, F.-Z. Power-to-Methane: A state-of-the-art review. *Renew. Sustain. Energy Rev.* **2018**, *81*, 433–446. [CrossRef]
227. Boaro, M.; Colussi, S.; Trovarelli, A. Ceria-Based Materials in Hydrogenation and Reforming Reactions for CO_2 Valorization. *Front. Chem.* **2019**, *7*, 28. [CrossRef]
228. Lee, W.J.; Li, C.; Prajitno, H.; Yoo, J.; Patel, J.; Yang, Y.; Lim, S. Recent trend in thermal catalytic low temperature CO_2 methanation: A critical review. *Catal. Today* **2021**, *368*, 2–19. [CrossRef]
229. Jangam, A.; Das, S.; Dewangan, N.; Hongmanorom, P.; Hui, W.M.; Kawi, S. Conversion of CO_2 to C_1 chemicals: Catalyst design, kinetics and mechanism aspects of the reactions. *Catal. Today* **2020**, *358*, 3–29. [CrossRef]
230. Saeidi, S.; Najari, S.; Hessel, V.; Wilson, K.; Keil, F.J.; Concepción, P.; Suib, S.L.; Rodrigues, A.E. Recent advances in CO_2 hydrogenation to value-added products — Current challenges and future directions. *Prog. Energy Combust. Sci.* **2021**, *85*, 100905. [CrossRef]
231. Younas, M.; Loong Kong, L.; Bashir, M.J.K.; Nadeem, H.; Shehzad, A.; Sethupathi, S. Recent Advancements, Fundamental Challenges, and Opportunities in Catalytic Methanation of CO_2. *Energy Fuels* **2016**, *30*, 8815–8831. [CrossRef]
232. Frontera, P.; Macario, A.; Ferraro, M.; Antonucci, P.L. Supported catalysts for CO_2 methanation: A review. *Catalysts* **2017**, *7*, 59. [CrossRef]
233. Lv, C.; Xu, L.; Chen, M.; Cui, Y.; Wen, X.; Li, Y.; Wu, C.; Yang, B.; Miao, Z.; Hu, X.; et al. Recent Progresses in Constructing the Highly Efficient Ni Based Catalysts With Advanced Low-Temperature Activity Toward CO_2 Methanation. *Front. Chem.* **2020**, *8*, 269. [CrossRef]
234. De Leitenburg, C.; Trovarelli, A.; Kašpar, J. A Temperature-Programmed and Transient Kinetic Study of CO_2 Activation and Methanation over CeO_2 Supported Noble Metals. *J. Catal.* **1997**, *166*, 98–107. [CrossRef]
235. Dreyer, J.A.H.; Li, P.; Zhang, L.; Beh, G.K.; Zhang, R.; Sit, P.H.-L.; Teoh, W.Y. Influence of the oxide support reducibility on the CO_2 methanation over Ru-based catalysts. *Appl. Catal. B Environ.* **2017**, *219*, 715–726. [CrossRef]
236. Martin, N.M.; Hemmingsson, F.; Schaefer, A.; Ek, M.; Merte, L.R.; Hejral, U.; Gustafson, J.; Skoglundh, M.; Dippel, A.-C.; Gutowski, O.; et al. Structure–function relationship for CO_2 methanation over ceria supported Rh and Ni catalysts under atmospheric pressure conditions. *Catal. Sci. Technol.* **2019**, *9*, 1644–1653. [CrossRef]
237. Hatzisymeon, M.; Petala, A.; Panagiotopoulou, P. Carbon Dioxide Hydrogenation over Supported Ni and Ru Catalysts. *Catal. Lett.* **2021**, *151*, 888–900. [CrossRef]
238. Yu, Y.; Bian, Z.; Wang, J.; Wang, Z.; Tan, W.; Zhong, Q.; Kawi, S. CO_2 hydrogenation to CH_4 over hydrothermal prepared ceria-nickel catalysts: Performance and mechanism study. *Catal. Today* **2021**, *in press*. [CrossRef]
239. Zhang, J.; Yang, Y.; Liu, J.; Xiong, B. Mechanistic understanding of CO_2 hydrogenation to methane over Ni/CeO_2 catalyst. *Appl. Surf. Sci.* **2021**, *558*, 149866. [CrossRef]

240. Guo, Y.; Mei, S.; Yuan, K.; Wang, D.-J.; Liu, H.-C.; Yan, C.-H.; Zhang, Y.-W. Low-Temperature CO_2 Methanation over CeO_2-Supported Ru Single Atoms, Nanoclusters, and Nanoparticles Competitively Tuned by Strong Metal-Support Interactions and H-Spillover Effect. *ACS Catal.* **2018**, *8*, 6203–6215. [CrossRef]
241. Struijs, J.J.C.; Muravev, V.; Verheijen, M.A.; Hensen, E.J.M.; Kosinov, N. Ceria-Supported Cobalt Catalyst for Low-Temperature Methanation at Low Partial Pressures of CO_2. *Angew. Chem. Int. Ed.* **2022**, e202214864. [CrossRef]
242. Ye, R.-P.; Li, Q.; Gong, W.; Wang, T.; Razink, J.J.; Lin, L.; Qin, Y.-Y.; Zhou, Z.; Adidharma, H.; Tang, J.; et al. High-performance of nanostructured Ni/CeO_2 catalyst on CO_2 methanation. *Appl. Catal. B Environ.* **2020**, *268*, 118474. [CrossRef]
243. Liu, F.; Park, Y.S.; Diercks, D.; Kazempoor, P.; Duan, C. Enhanced CO_2 Methanation Activity of $Sm_{0.25}Ce_{0.75}O_{2-\delta}$–Ni by Modulating the Chelating Agents-to-Metal Cation Ratio and Tuning Metal–Support Interactions. *ACS Appl. Mater. Interfaces* **2022**, *14*, 13295–13304. [CrossRef]
244. Cárdenas-Arenas, A.; Quindimil, A.; Davó-Quiñonero, A.; Bailón-García, E.; Lozano-Castelló, D.; De-La-Torre, U.; Pereda-Ayo, B.; González-Marcos, J.A.; González-Velasco, J.R.; Bueno-López, A. Design of active sites in Ni/CeO_2 catalysts for the methanation of CO_2: Tailoring the Ni-CeO_2 contact. *Appl. Mater. Today* **2020**, *19*, 100591. [CrossRef]
245. Ratchahat, S.; Surathitimethakul, S.; Thamungkit, A.; Mala, P.; Sudoh, M.; Watanabe, R.; Fukuhara, C.; Chen, S.S.; Wu, K.C.-W.; Charinpanitkul, T. Catalytic performance of Ni/CeO_2 catalysts prepared from different routes for CO_2 methanation. *J. Taiwan Inst. Chem. Eng.* **2021**, *121*, 184–196. [CrossRef]
246. Lin, S.; Li, Z.; Li, M. Tailoring metal-support interactions via tuning CeO_2 particle size for enhancing CO_2 methanation activity over Ni/CeO_2 catalysts. *Fuel* **2023**, *333*, 126369. [CrossRef]
247. Hao, Z.; Shen, J.; Lin, S.; Han, X.; Chang, X.; Liu, J.; Li, M.; Ma, X. Decoupling the effect of Ni particle size and surface oxygen deficiencies in CO_2 methanation over ceria supported Ni. *Appl. Catal. B Environ.* **2021**, *286*, 119922. [CrossRef]
248. Varvoutis, G.; Lykaki, M.; Stefa, S.; Binas, V.; Marnellos, G.E.; Konsolakis, M. Deciphering the role of Ni particle size and nickel-ceria interfacial perimeter in the low-temperature CO_2 methanation reaction over remarkably active Ni/CeO_2 nanorods. *Appl. Catal. B Environ.* **2021**, *297*, 120401. [CrossRef]
249. Wang, F.; He, S.; Chen, H.; Wang, B.; Zheng, L.; Wei, M.; Evans, D.G.; Duan, X. Active Site Dependent Reaction Mechanism over Ru/CeO_2 Catalyst toward CO_2 Methanation. *J. Am. Chem. Soc.* **2016**, *138*, 6298–6305. [CrossRef]
250. Winter, L.R.; Chen, R.; Chen, X.; Chang, K.; Liu, Z.; Senanayake, S.D.; Ebrahim, A.M.; Chen, J.G. Elucidating the roles of metallic Ni and oxygen vacancies in CO_2 hydrogenation over Ni/CeO_2 using isotope exchange and in situ measurements. *Appl. Catal. B Environ.* **2019**, *245*, 360–366. [CrossRef]
251. Zheng, H.; Liao, W.; Ding, J.; Xu, F.; Jia, A.; Huang, W.; Zhang, Z. Unveiling the Key Factors in Determining the Activity and Selectivity of CO_2 Hydrogenation over Ni/CeO_2 Catalysts. *ACS Catal.* **2022**, *12*, 15451–15462. [CrossRef]
252. Zhang, Z.; Feng, K.; Yan, B. Enhanced Ni–Ce interactions to enable efficient low-temperature catalytic CO_2 methanation. *Catal. Sci. Technol.* **2022**, *12*, 4698–4708. [CrossRef]
253. Tada, S.; Nagase, H.; Fujiwara, N.; Kikuchi, R. What Are the Best Active Sites for CO_2 Methanation over Ni/CeO_2? *Energy Fuels* **2021**, *35*, 5241–5251. [CrossRef]
254. Pan, Q.; Peng, J.; Sun, T.; Gao, D.; Wang, S.; Wang, S. CO_2 methanation on Ni/$Ce_{0.5}Zr_{0.5}O_2$ catalysts for the production of synthetic natural gas. *Fuel Process. Technol.* **2014**, *123*, 166–171. [CrossRef]
255. Tang, R.; Ullah, N.; Hui, Y.; Li, X.; Li, Z. Enhanced CO_2 methanation activity over Ni/CeO_2 catalyst by one-pot method. *Mol. Catal.* **2021**, *508*, 111602. [CrossRef]
256. Torrente-Murciano, L.; Chapman, R.S.L.; Narvaez-Dinamarca, A.; Mattia, D.; Jones, M.D. Effect of nanostructured ceria as support for the iron catalysed hydrogenation of CO_2 into hydrocarbons. *Phys. Chem. Chem. Phys.* **2016**, *18*, 15496–15500. [CrossRef] [PubMed]
257. Sakpal, T.; Lefferts, L. Structure-dependent activity of CeO_2 supported Ru catalysts for CO_2 methanation. *J. Catal.* **2018**, *367*, 171–180. [CrossRef]
258. Ma, Y.; Liu, J.; Chu, M.; Yue, J.; Cui, Y.; Xu, G. Enhanced Low-Temperature Activity of CO_2 Methanation Over Ni/CeO_2 Catalyst. *Catal. Lett.* **2022**, *152*, 872–882. [CrossRef]
259. Bian, Z.; Chan, Y.M.; Yu, Y.; Kawi, S. Morphology dependence of catalytic properties of Ni/CeO_2 for CO_2 methanation: A kinetic and mechanism study. *Catal. Today* **2020**, *347*, 31–38. [CrossRef]
260. Xie, F.; Xu, S.; Deng, L.; Xie, H.; Zhou, G. CO_2 hydrogenation on Co/$CeO_{2-\delta}$ catalyst: Morphology effect from CeO_2 support. *Int. J. Hydrog. Energy* **2020**, *45*, 26938–26952. [CrossRef]
261. Wang, F.; Li, C.; Zhang, X.; Wei, M.; Evans, D.G.; Duan, X. Catalytic behavior of supported Ru nanoparticles on the {100}, {110}, and {111} facet of CeO_2. *J. Catal.* **2015**, *329*, 177–186. [CrossRef]
262. Xie, Y.; Chen, J.; Wu, X.; Wen, J.; Zhao, R.; Li, Z.; Tian, G.; Zhang, Q.; Ning, P.; Hao, J. Frustrated Lewis Pairs Boosting Low-Temperature CO_2 Methanation Performance over Ni/CeO_2 Nanocatalysts. *ACS Catal.* **2022**, *12*, 10587–10602. [CrossRef]
263. Yan, Y.; Wong, R.J.; Ma, Z.; Donat, F.; Xi, S.; Saqline, S.; Fan, Q.; Du, Y.; Borgna, A.; He, Q.; et al. CO_2 hydrogenation to methanol on tungsten-doped Cu/CeO_2 catalysts. *Appl. Catal. B Environ.* **2022**, *306*, 121098. [CrossRef]
264. Jomjaree, T.; Sintuya, P.; Srifa, A.; Koo-amornpattana, W.; Kiatphuengporn, S.; Assabumrungrat, S.; Sudoh, M.; Watanabe, R.; Fukuhara, C.; Ratchahat, S. Catalytic performance of Ni catalysts supported on CeO_2 with different morphologies for low-temperature CO_2 methanation. *Catal. Today* **2021**, *375*, 234–244. [CrossRef]

265. Fan, Q.; Li, S.; Zhang, L.; Wang, P.; Wang, S. Regulation of product distribution in CO_2 hydrogenation by modifying Ni/CeO_2 catalysts. *J. Catal.* **2022**, *414*, 53–63. [CrossRef]
266. Hasrack, G.; Bacariza, M.C.; Henriques, C.; Da Costa, P. On the effect of cobalt promotion over Ni/CeO_2 catalyst for CO_2 thermal and plasma assisted methanation. *Catalysts* **2022**, *12*, 36. [CrossRef]
267. Zhang, Z.; Yu, Z.; Feng, K.; Yan, B. Eu^{3+} doping-promoted Ni-CeO_2 interaction for efficient low-temperature CO_2 methanation. *Appl. Catal. B Environ.* **2022**, *317*, 121800. [CrossRef]
268. Zhang, T.; Wang, W.; Gu, F.; Xu, W.; Zhang, J.; Li, Z.; Zhu, T.; Xu, G.; Zhong, Z.; Su, F. Enhancing the low-temperature CO_2 methanation over Ni/La-CeO_2 catalyst: The effects of surface oxygen vacancy and basic site on the catalytic performance. *Appl. Catal. B Environ.* **2022**, *312*, 121385. [CrossRef]
269. Zhu, M.; Tian, P.; Cao, X.; Chen, J.; Pu, T.; Shi, B.; Xu, J.; Moon, J.; Wu, Z.; Han, Y.-F. Vacancy engineering of the nickel-based catalysts for enhanced CO_2 methanation. *Appl. Catal. B Environ.* **2021**, *282*, 119561. [CrossRef]
270. Zhang, Z.; Tong, Y.; Fang, X.; Xu, J.; Xu, X.; Wang, X. Interface-dependent activity and selectivity for CO_2 hydrogenation on Ni/CeO_2 and Ni/$Ce_{0.9}Sn_{0.1}O_x$. *Fuel* **2022**, *316*, 123191. [CrossRef]
271. Tada, S.; Ochieng, O.J.; Kikuchi, R.; Haneda, T.; Kameyama, H. Promotion of CO_2 methanation activity and CH_4 selectivity at low temperatures over Ru/CeO_2/Al_2O_3 catalysts. *Int. J. Hydrog. Energy* **2014**, *39*, 10090–10100. [CrossRef]
272. Shang, X.; Deng, D.; Wang, X.; Xuan, W.; Zou, X.; Ding, W.; Lu, X. Enhanced low-temperature activity for CO_2 methanation over Ru doped the Ni/$Ce_xZr_{(1-x)}O_2$ catalysts prepared by one-pot hydrolysis method. *Int. J. Hydrog. Energy* **2018**, *43*, 7179–7189. [CrossRef]
273. Tada, S.; Shimizu, T.; Kameyama, H.; Haneda, T.; Kikuchi, R. Ni/CeO_2 catalysts with high CO_2 methanation activity and high CH_4 selectivity at low temperatures. *Int. J. Hydrog. Energy* **2012**, *37*, 5527–5531. [CrossRef]
274. Zou, X.; Shen, Z.; Li, X.; Cao, Y.; Xia, Q.; Zhang, S.; Liu, Y.; Jiang, L.; Li, L.; Cui, L.; et al. Boosting CO_2 methanation on ceria supported transition metal catalysts via chelation coupled wetness impregnation. *J. Colloid Interface Sci.* **2022**, *620*, 77–85. [CrossRef]
275. Wang, X.; Zhu, L.; Liu, Y.; Wang, S. CO_2 methanation on the catalyst of Ni/MCM-41 promoted with CeO_2. *Sci. Total Environ.* **2018**, *625*, 686–695. [CrossRef] [PubMed]
276. Hu, F.; Tong, S.; Lu, K.; Chen, C.-M.; Su, F.-Y.; Zhou, J.; Lu, Z.-H.; Wang, X.; Feng, G.; Zhang, R. Reduced graphene oxide supported Ni-Ce catalysts for CO_2 methanation: The support and ceria promotion effects. *J. CO2 Util.* **2019**, *34*, 676–687. [CrossRef]
277. Zhou, G.; Liu, H.; Cui, K.; Xie, H.; Jiao, Z.; Zhang, G.; Xiong, K.; Zheng, X. Methanation of carbon dioxide over Ni/CeO_2 catalysts: Effects of support CeO_2 structure. *Int. J. Hydrog. Energy* **2017**, *42*, 16108–16117. [CrossRef]